Orientation Patterns of Bedding, Faults, and Veins in AND-1B Sedimentary Rock Core, McMurdo Ice Shelf Project: Significance for Terror Rift Evolution, Western Ross Sea, Antarctica

Senior Thesis

Submitted in partial fulfillment of the requirements for the

Bachelor of Science Degree

At The Ohio State University

By

Lauren Renee Baumgartner

The Ohio State University

2010

Approved by

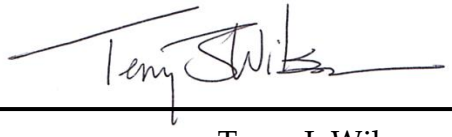

Terry J. Wilson, Advisor

School of Earth Sciences

Abstract

The McMurdo Ice Shelf project recovered 1285 m of Neogene sedimentary rock core from the Victoria Land rift basin, Antarctica. The core contains over 1475 natural fractures of faults, veins, and clastic dikes. This study measured and mapped the attitudes and locations of bedding and natural fractures in select intact core intervals of AND-1B core to determine structure orientation. Whole-core scanned images were loaded into DMT CoreBase® software and manipulated to create digital intact intervals of core, joining core run breaks and correcting misfits that occurred during scanning. CoreBase® was used make independent orientation measurements of bedding and natural fractures within the core by drawing a 'best fit' sinusoid to each structure. Stereoplots were made for each intact interval to show whether there were systematic orientations of bedding and of each fracture type. The digital measurements were then compared with hand-measured orientations of the same structural features made during core logging. Twenty-four intact core intervals were analyzed and compared. Analysis of bedding orientation revealed that dip angle steepens with depth. Bedding within oriented intervals may be used to orient more core segments in the future. Results of comparing the two structural measurement methods indicate that both have strengths and weaknesses. Measurements during core logging can be made on fractures that are small and lack visible vein fill. These fracture types are not observable on digital images in the CoreBase® software. However, core logging methods can not measure the overall attitude of irregular veins and measurements on fractures exposed on the blue-scribed side of the core were commonly in error. Using the CoreBase® software, measurements are made viewing the whole core surface, giving a better overall attitude measurement. Weaknesses in CoreBase® methods are associated with the low resolution of the digital images once they are loaded into the software. This results in a smaller fracture population, missing many of the faults in particular, because they are not visible and therefore can't be measured within CoreBase®. This comparison will help to guide future core-based fracture logging studies.

Acknowledgments

I would like to thank my advisor, Dr. Terry Wilson for the opportunity to work on this project and for her continued support and advice throughout this study. Special thanks to Cristina Millan for her guidance, I would have been lost countless times over the past year and a half without her.

I would especially like to thank my parents, Karen and Bob. Their love and encouragement has meant more to me than they will ever know.

And to Zak, thank you for all of your love and support. You have had to put up with my frustrations and bad attitude one too many times and without you, I would not be where I am today.

Table of Contents

Introduction

The ANDRILL Project

The ANDRILL (ANtarctic geological DRILLing) Project is a multinational collaboration of over 200 scientists, students and educators from Antarctic programs in Germany, Italy, New Zealand, and the United States. ANDRILL uses drilling technology to recover a stratigraphic record of the Antarctic margins. The chief objective is to drill back in time to recover a history of paleoenvironmental changes that will guide our understanding of the speed, size, and frequency of glacial and interglacial changes in the Antarctica region. The goal of the McMurdo Ice Shelf (MIS) Project was to drill approximately ~1200 meters (m) of continuous Neogene sediment core through glacimarine, terrigenous, volcanic, and biogenic sediment deposited in a region currently beneath the McMurdo Ice Shelf within the Windless Bight region (Naish et al., 2007). During the 2006-2007 austral season, the MIS Science team recovered a single 1285 m-deep core (AND-1B) from the northwest part of the Ross Ice Shelf at Windless Bight.

Study Objectives

This project is part of a research program designed to document the neotectonic fault and volcanic history of the Terror Rift in the western Ross Sea, including the Terror Rift Project and structural studies of ANDRILL rock cores. The goal of this project is to measure and map the attitudes of both natural fractures and bedding

contained within selected intact core intervals from the AND-1B drill core. The approach here is to identify and measure structural features on scanned images of the whole-round rock core using the commercial CoreBase® software. These independent digital measurements are compared with the hand-measured structural features identified during core logging. This comparison establishes the differences, strengths and weaknesses between the two approaches in order to guide future core-based fracture logging studies. Specifically, the abundance of fracture numbers and types that can be identified on the scanned core images and the reliability of core-based structural measurements are evaluated. Where intact intervals can be oriented by a feature-matching procedure, true *in situ* coordinates of core structures are mapped and structural dip directions of bedding are mapped. The orientation patterns of measured bedding and fracture planes are assessed using stereographic analyses, to help determine if the attitudes within the AND-1B core are consistent with Terror Rift faulting or if the fractures are the result of other processes such as subglacial deformation.

Geologic Setting

The AND-1B sedimentary rock core was recovered from the Windless Bight region of the McMurdo Ice Shelf, south of Ross Island in the western Ross Sea, Antarctica (Figures 1 & 2). Ross Island is situated within the southern part of the Victoria Land Basin (VLB), an elongated north-south trending extensional basin within the West Antarctic Rift System (Figure 3). The VLB is a structural half-graben approximately 350 km long and runs along the border of the Transantarctic Mountain (TAM) front. Major rifting occurred in the latest Eocene-Oligocene, but possibly initiated in the Cretaceous, providing space for accumulation of 10 km of sediment in the VLB (Naish et al., 2007). The oldest post-Paleozoic sedimentary rocks within the VLB are Eocene in age and were recovered by stratigraphic drilling by the Cape Roberts Project. The Eocene strata are located along the western margin of the basin and overlie Devonian sedimentary rocks correlated with the Taylor Group of the Beacon Supergroup (Henrys et al., 2000, Fielding et al., 2001). Since the latest Eocene, sedimentation along the western margin of the VLB has resulted in a 1.5 to 2 km –thick sedimentary wedge that thickens seaward to 7km underneath Ross Island. The western portion of the wedge is comprised of glacimarine conglomerate, diamicts, and sandstone interbedded with mudstones. Numerous unconformities occur within the Oligocene and lower Miocene strata forming this wedge, a number of which have been correlated with erosion surfaces in regional seismic lines (Henrys et al., 2000, Fielding et

al., 2001). These erosion surfaces are interpreted to indicate widespread grounding of the ice sheet on the continental shelf during glacial periods. Interglacial-glacial periods are recorded by sedimentary sequences that display cyclical facies associated with ice advance and retreat (Naish et al., 2007). Younger Neogene strata mapped in southern McMurdo Sound show a thickening and eastward-dipping succession that extends under Ross Island in the vicinity of the MIS project drill site (Fielding et al., 2008).

Late Cenozoic igneous intrusions and extrusive volcanism in the Ross Island region is associated with extension in the Terror Rift, which developed within the VLB (Cooper et al., 1987). The drill site for the MIS project was situated above a flexural moat basin that had formed in response to volcanic loading of the crust by volcanoes localized along the Terror Rift. (Naish et al, 2007). Ross Island is built by the Mount Bird, Mount Terror, and Mount Erebus volcanoes and includes the elongate Hut Point Peninsula. The radial arrangement of volcanoes has been interpreted to represent crustal doming as a result of mantle upwelling (Naish et al., 2007). The Ross Island volcanic pile has caused loading of the crust and produced up to 1 km net subsidence beneath Ross Island resulting in the development of an enclosing moat (Stern et al., 1991). Localized accommodation space created by the subsidence is superimposed on the rift basin. The depositional accommodation space associated with the rift basin and flexural moat basin, formed adjacent to Pliocene and Pleistocene volcanoes, provided an

opportunity to recover stratigraphic records with high-resolution chronology (Naish et al., 2007).

The Terror Rift consists of two parts, the Discovery Graben and the Lee Arch. Faults associated with the Terror Rift reach the seafloor, indicating that the rift represents the youngest episode of faulting within the West Antarctic Rift System (Cooper et al., 1987). Both north and south of Ross Island, the Lee Arch has been intruded by Cenozoic volcanic rocks, obscuring the structural geometry of the area. When projected southward, the graben and arch structures trend beneath the Windless Bight region (Naish et al., 2007).

Multichannel seismic reflection data of the area reveals the stratigraphic architecture of the moat-fill on the southeast side of Ross Island (Figure 4). Three seismic stratigraphic units are identified that generally thicken and dip towards Ross Island and are bounded by unconformities (Naish et al., 2007). The seismic lines reveal an eastward dipping and thickening package of strata that has been dislocated by north-south trending high-angle normal faults. The sediment package is bounded to the east by a north-south zone of volcanic bodies. Volcanism in the region is coeval with late Miocene/early Pliocene to more recent extension in the Terror Rift and seems to be associated with major west-dipping normal faults that form the eastern margin of the half-graben extending northward to Drygalski Ice Tongue (Hall et al., 2006).

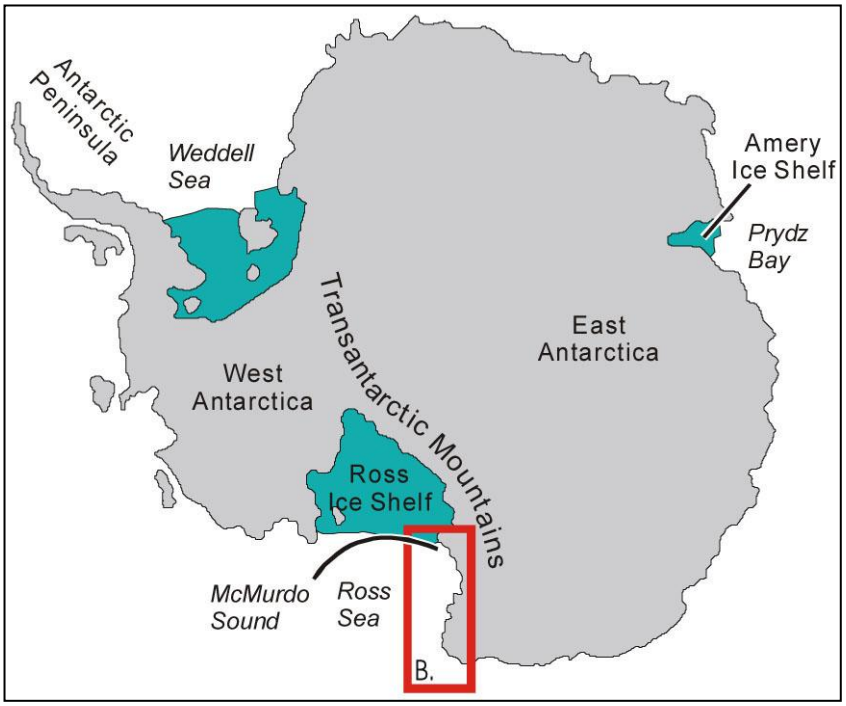

Figure 1. The general location of McMurdo Sound in western Ross Sea adjacent to the north western corner of the Ross Ice Shelf and the Transantarctic Mountains (Naish et al., 2007)

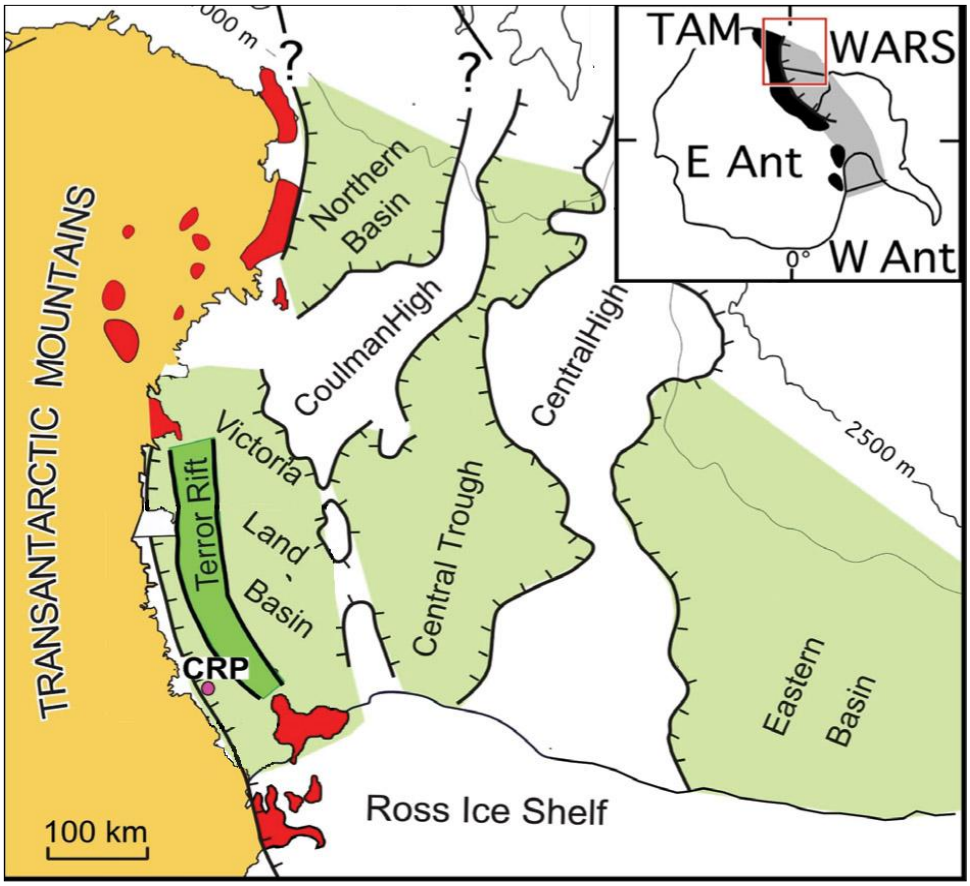

Figure 2. The regional tectonic setting of the study area (Naish et al., 2007).

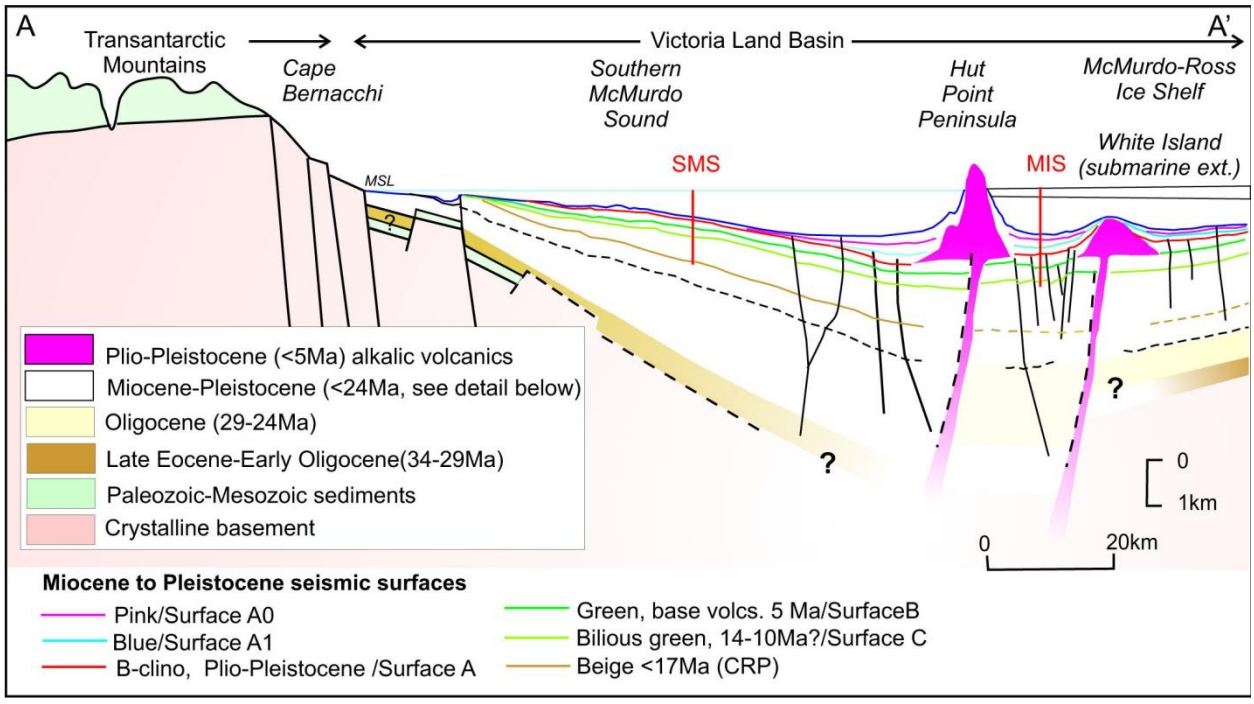

Figure 3. Schematic of the structural-stratigraphic cross section across the VLB shows the stratigraphic context of the MIS drill site with respect to previous and future drilling sites in Southern McMurdo Sound. (Cooper et al., 1987; Fielding et al., 2005; Wilson et al., in press).

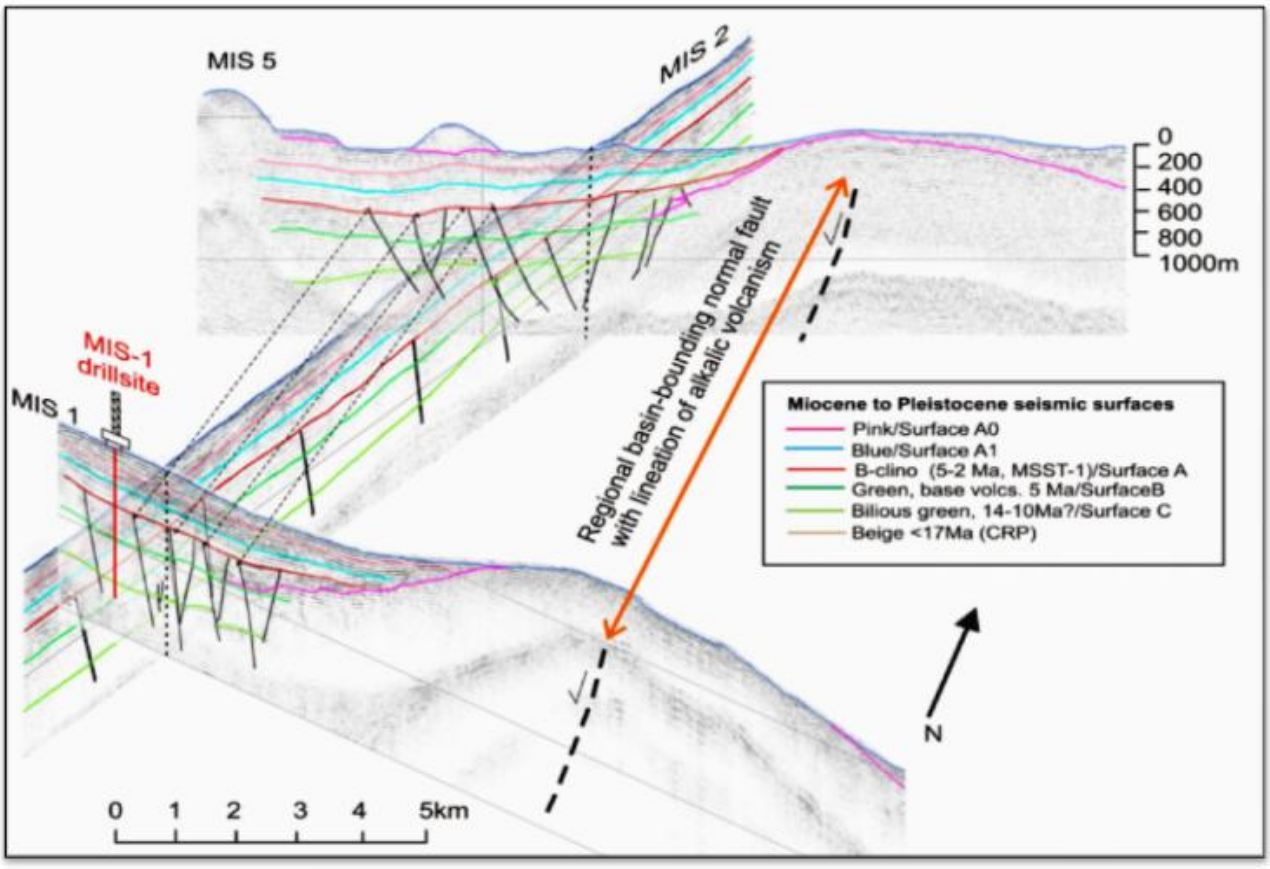

Figure 4. A 3-D fence diagram of the stratigraphic architecture of the Ross Island moat near the MIS drill site (Horgan et al., 2005).

Lithology and Depositional Environment of Strata Cored in AND-1B

The AND-1B core was divided into eight lithostratigraphic units and 25 subunits based on lithologic abundance within a given length of core (Figure 5). Eleven lithofacies have being recognized on the basis of lithologies, bed contacts and thickness, sediment texture, sedimentary structures, and in some cases color. The 1285 m long sediment core that was recovered from the MIS project contained a variety of lithologies, including siliciclastics, sandstone, mudstone, and one phonolitic lava flow. The majority of the core was composed of diatomite, diamictite, and volcanics with the depositional environments of these lithologies varying throughout the core (Krissek et al., 2007).

Diatomite is soft, friable, and often light colored siliceous rock that is composed of opaline frustules of diatoms or unicellular aquatic algae (Boggs, 2006). Found throughout the AND-1B core in various lithostratigraphic units, diatomite makes up Facies 1 of the sediment core. Described as massive to weakly stratified diatomite, Facies 1 diatomite is defined by color changes or laminations of sandstone and gravel. The pelagic sedimentation of Facies 1 is consistent with a marine depositional environment, with occasional periods of iceberg rafting have been recorded as well (Krissek et al., 2007).

Diamictite is a non-sorted to poorly sorted conglomerate that contains a wide range of particle sizes and is matrix supported (Boggs, 2006). In the AND-1B core, two separate lithofacies have been recognized as diamictite. Facies 9 is described as stratified diamictite with layers that can be recognized based on color, clast concentration, or particle size. The lithofacies ranges from clast-poor to clast-rich, with clasts from of a wide range of lithologies, including volcanic, metasedimentary, sedimentary, granite, dolerite, marble, and mudstone interclasts (Krissek et al., 2007). The environment of deposition of the stratified diamictite is diverse. Thinner beds are often associated with marine facies likely originating from ice rafting or debris flows. For units associated with ice contact, deposition may have resulted from rainout of basal glacial debris or reworking by marine outwash. Facies 9 is often interbedded with Facies 10, a massive diamictite. The compositional characteristics of the Facies 10 are identical to that of the stratified diamictite. Facies 10 is likely a result of subglacial deposition. However, rainout from floating ice and mass-flow processes may have occurred as well (Krissek et al., 2007).

Volcanics within the AND-1B core are localized between 511.18 meters below seafloor (mbsf) and 759.32 mbsf and are associated with the nearby volcanism of Mount Erebus and/or White Island. Facies 11 is described as volcanic rocks and sediments and consists of primary to near-primary volcanic deposits. Volcanic diamictites, lapilli tuffs,

and one phonolitic lava flow make up the diverse sediments of Facies 11, and all but the phonolitic lava have undergone redeposition.

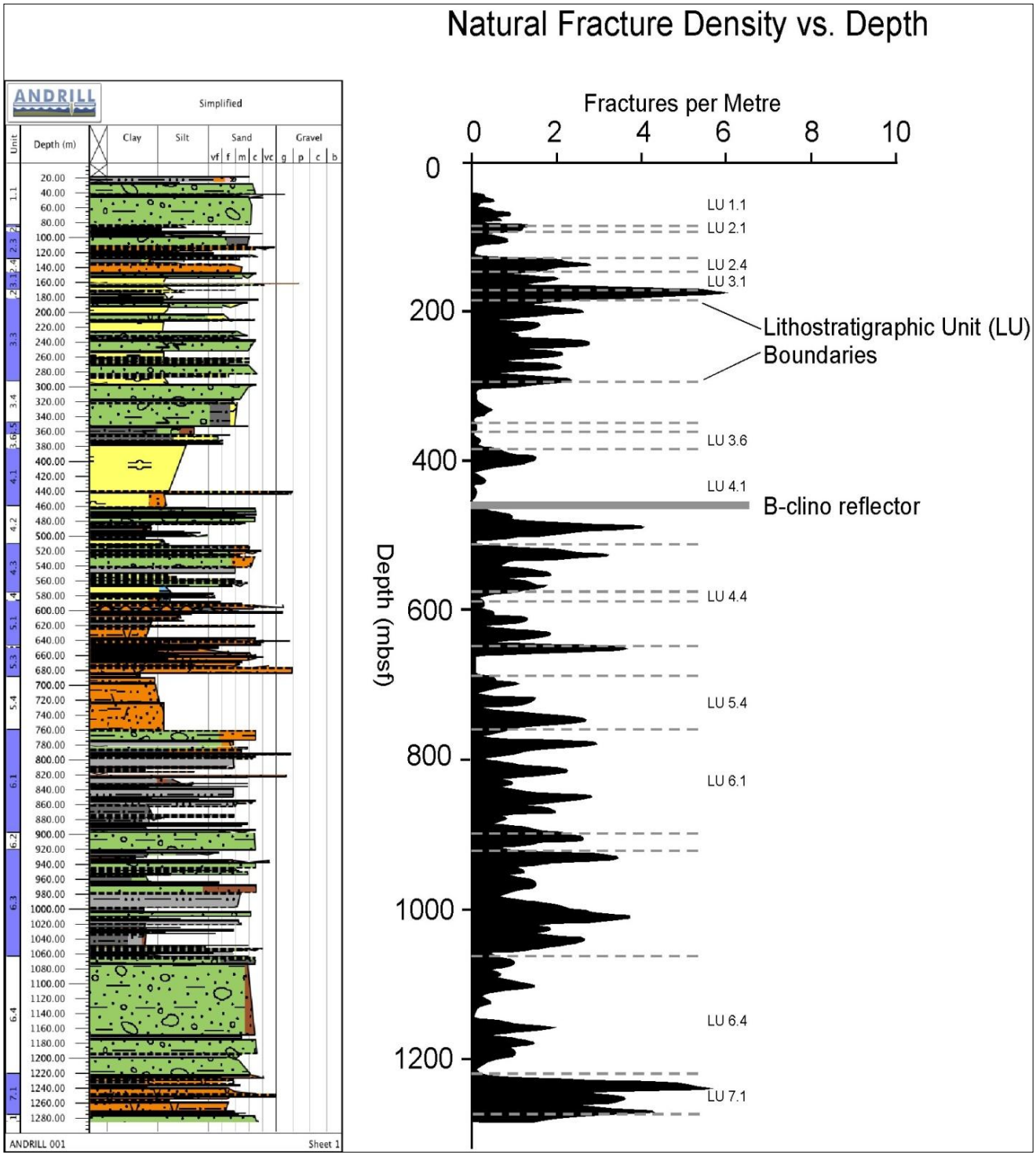

Figure 5. Fracture density plot showing the number of natural fractures (faults and veins) per meter of core with relation to depth, lithology, and lithostratigraphic unit boundaries within the AND-1B core (Wilson et al., 2007).

Structures in AND-1B Core

Bedding

Bedding is the primary layering or stratification in sedimentary rock that is formed during deposition. Bedding is commonly defined by changes in color, grain size, texture, or composition. Bedding in the AND-1B core was noted in the sedimentology log of the core. That log was used to identify depths of bedding occurrence within intact intervals of core examined in this study. If bedding is characterized by a homogeneous dip angle and/or dip direction, it may prove possible to use stratified sections of the core to orient core intervals to original *in situ* coordinates.

Induced fractures

Fractures that form during the drilling, coring, or handling of the core are known as induced fractures. The AND-1B core contained 410 petal, petal-centerline, and core edge fractures which are steeply dipping, generally curviplanar extensional fractures that occur just below the drill bit and propagate downward during drilling. These fractures occurred mainly in mudstone, where drilling was more difficult and required a higher pump pressure, and were more uncommon in the diatomites and diamictite lithologies. Sub-horizontal drilling- and handling-induced fractures were identified throughout the core as well. Induced fractures may be used to provide orientation

angles to intact intervals, returning core to *in situ* coordinates (Wilson et al., 2007). The induced fractures in the AND-1B core are not a focus of this study.

Natural Fractures

Natural fractures are fractures that existed within a rock body prior to drilling that are intersected during coring. The AND-1B core contained 1475 natural fractures with the average fracture density of 1.2 fractures per meter and reaching as many as 6 fractures per meter in the upper and lower portions of the core. Natural fractures include veins, faults and sedimentary intrusions (clastic dikes) and can have a variety of geometries and characteristics. Overall the natural fractures found in core will provide new information on the paleostress and strain regime that occurs with deposition of the Neogene strata and deformation within the Terror Rift (Wilson et al., 2007).

In general, a vein is a fracture that has filled with a crystallized mineral that precipitated from a fluid solution (Figure 6). Veins can typically initiate from joints and faults and come in all sizes ranging from no wider that a strand of a hair to massive tabular veins that are tens of meters long (Van der Pluijm & Marshak, 2004). The veins within the AND-1B core are extremely abundant and range from 1 mm to 2 cm in thickness. Microscopic analyses by Cristina Millan at the Ohio State University reveal that vein fill materials include calcite, pyrite, chlorite, and minor zeolite. Veins within the core commonly contain fibers that run either perpendicular or parallel to vein

margins. Many veins are closely associated with fault planes and have dips between 55° and 75°. Complex vein webs occur in the core as branching networks associated with fault planes. The AND-1B core contains a large number of very steeply dipping (>75°) calcite veins in the lower section of the core. These veins are typically microfolded, indicating that they formed early before the rocks had fully lithified. Evidence of vein development during compaction and vertical loading can be seen as vertical fibrous veins in pressure shadows on the margins of clasts (Wilson et al. 2007).

A fault is any surface or zone within the earth where measurable slip has occurred (Figure 7). Near the earth's surface, a fault is defined as a fracture on which slip develops primarily due to brittle deformation processes. The term fault zone is used for brittle structures where loss of cohesion and slip occur on several fault planes within a limited area. Faults occur on all scales and within all lithologies (Van der Pluijm & Marshak, 2004). The AND-1B core contains a large population of faults exposed as open fractures with highly polished slickensided and striated surfaces (Figure 6). Present in all lithologies recognized in the core, faults are particularly abundant in intervals consisting of mudrock. Identified mineral fill along faults includes calcite and pyrite, along with an unidentified dark green mineral that is likely chlorite. Nearly all faults have striae parallel or close to the dip direction, whereas oblique slip lineations that deviate more that 20° from the dip direction are extremely rare. Faults that are

recognized to offset bedding typically display normal-sense displacement of a few millimeters up to 3 cm and have dip angles ranging from 50°-70° (Wilson et al., 2007).

Sedimentary intrusions, or clastic dikes, are sedimentary structures that occur when liquefied sand is forcefully injected into a cohesive host as a response to loading and/or tectonic stresses (Figure 6). The intrusions most likely come from below, however some clastic dikes are injected laterally. In all sedimentary intrusions, the source of the liquefied sand or mud must have been buried by less permeable cohesive sediment (Collinson, 1994). Several sandstone dikes that intruded downward along fractures from the base of beds were observed in the AND-1B core, along with many closed fractures with steep dips that were filled with granular material of clastic or cataclastic origin. A few intervals contained brecciated core with a sedimentary matrix that intruded into coherent material in a "ladder" pattern. The presence of sedimentary dikes and intrusions of clastic material in breccia zones gives evidence that deformation was occurring prior to complete lithification (Wilson et al., 2007).

Natural fractures in AND-1B core could have formed in a variety of ways. Given the glacially-influenced environment and evidence for numerous episodes of over-riding of the depositional site by grounded ice (Naish et al., 2007), the faults, veins and clastic dikes could have been induced by glaciotectonic deformation. Faults defining the Terror Rift pass through the Windless Bight area, so that the natural fractures in the

core could also be formed during tectonic rifting. Orientation patterns in intact intervals in the AND-1B core, examined in this study, will help to determine the origin of the structures.

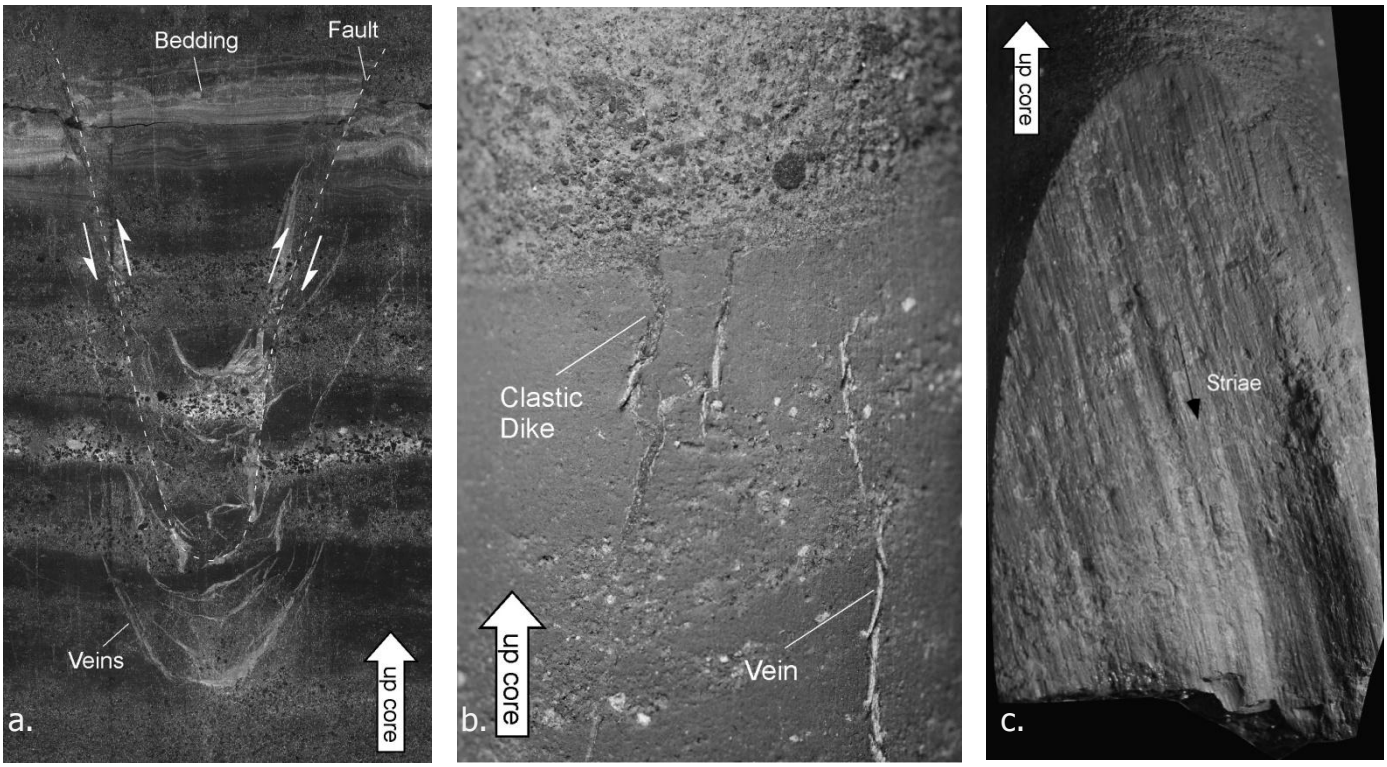

Figure 6. (a) Photograph showing bedding planes, veins with calcite fill, and a fault displaying reverse offset. (b) Sandstone clastic dike intruded downward into finer grained material and a calcite vein. (c) A high angle-fault with down-dip striae in the AND-1B core (Wilson et al., 2007).

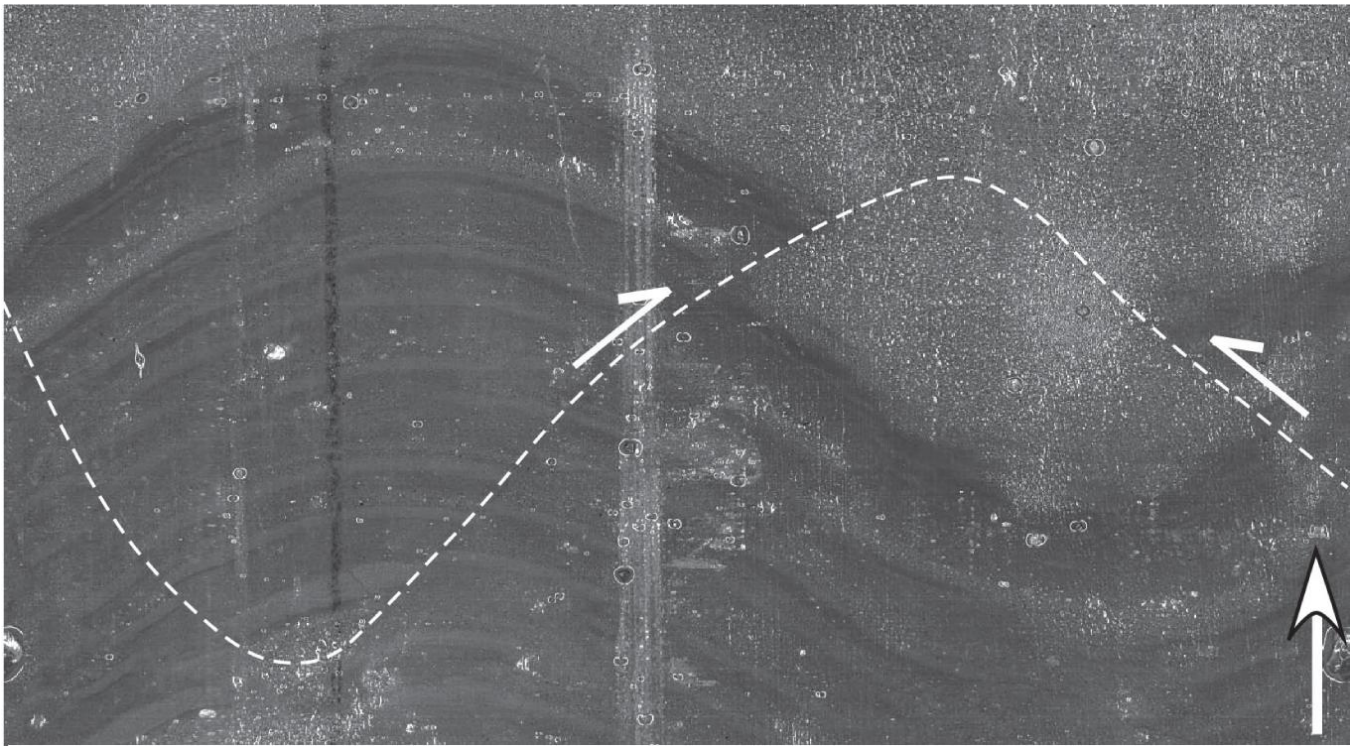

Figure 7. – A whole-round image of a reverse fault offsetting bedding planes (Wilson et al., 2007)

Methods

Drilling

Drilling for the AND-1B core took place during the 2006-2007 austral summer from October, 31st to December, 26th. The custom built drilling system consisted of a UDR-1200 drill rig, jack-up platform, hot water drill, sea riser, and a diamond-bit wireline coring string. The system was designed to handle the 85 m-thick moving ice shelf 'platform' which the rig sat upon (Falconer et al., 2007).

There were three separate drill rod sizes used during the AND-1B coring operation: PQ, HQ, and NQ (Falconer et al., 2007). The PQ-rod had a borehole diameter of 120 millimeters (mm), a core diameter of 83 mm and was used from 0-238.04 mbsf. The HQ-rod had a borehole diameter of 90 mm, a core diameter of 61 mm, and was used in the drilling interval 238.04-702.64 mbsf. The final and smallest size was the NQ-rod with a borehole diameter of 65 mm, a core diameter of 45 mm and was used in the drilling interval 708.63-1284.87 mbsf. During NQ drilling, large tidal and sub-ice shelf currents acting on the increased length of the drill string caused drilling problems and resulted in under-sized and variable core diameter (Falconer et al., 2007).

Fracture Logging

Each core size was recovered from the ground in 3 and 6 m runs and transferred from the drill rig to the drill-site laboratory complex where a two-person processing

team cleaned and scribed the core with a red and blue line approximately 180 degrees apart (Figure 8). This created a core reference frame, with the red scribe line designated as arbitrary 'north', from which all core measurements were recorded.

Measurements taken from the core were recorded on log sheets that provided descriptions of structures found in the core. Top and bottom depths were recorded for each fracture in meters below seafloor (mbsf). Both the dip angle and dip direction azimuth were recorded relative to the red scribe line. These measurements were made using clear template sheets created to fit around each of the three core diameters (Figure 9). Fracture characteristics were recorded on the log sheets, including fracture fill type and texture and any features documenting shear and extensional sense of the fractures. Structures within the core were documented with photographs. When fracture logging was complete, over 4300 fractures of all types were documented within the AND-1B core.

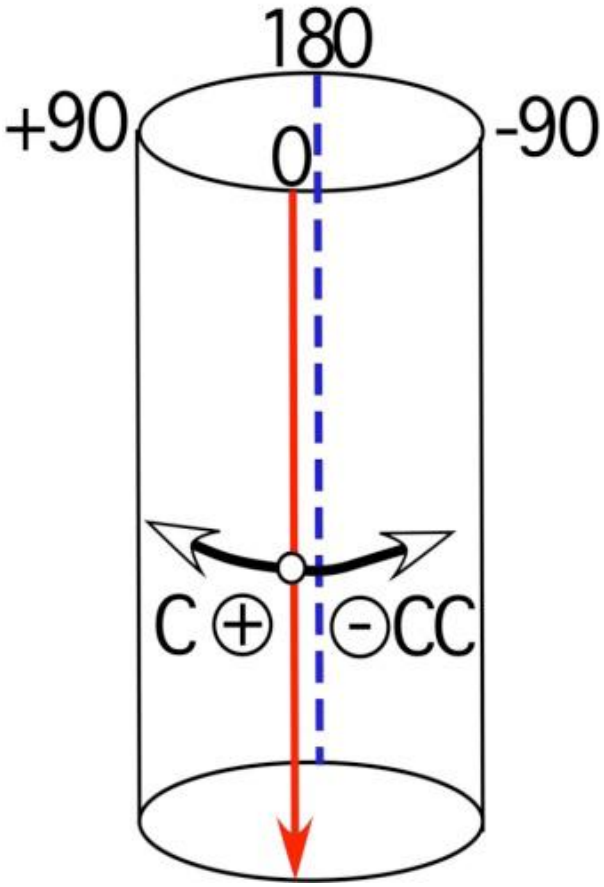

Figure 8. The core was scribed with a red line and a blue line separated by 180 degrees. The red line acted as an arbitrary north from which all hand measurements were made during core logging (Paulsen et al., 2008).

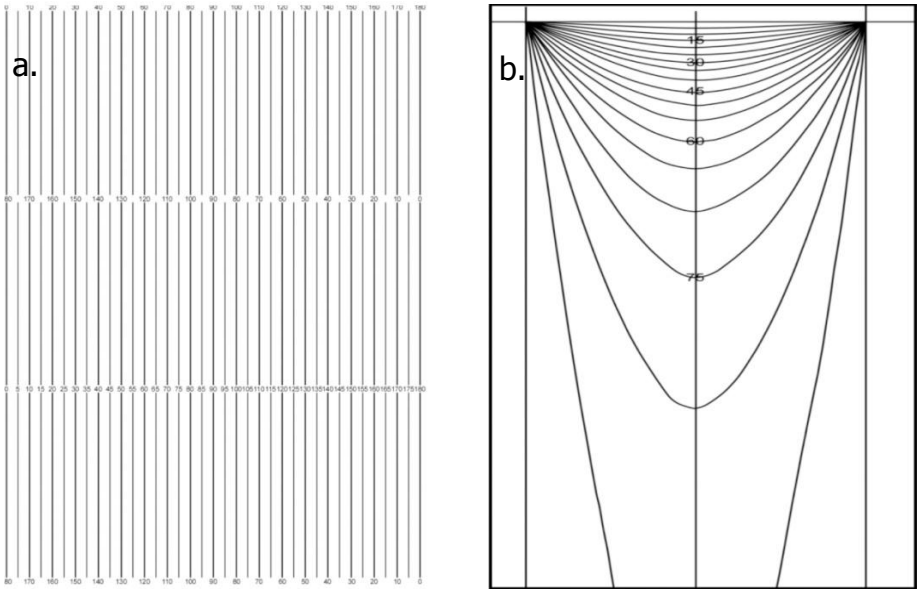

Figure 9. (a). Template used to measure best fit dip direction with respect to the red scribe line during core logging (b) Template was used to measure a best fit dip angle during core logging (Wilson, unpublished).

Whole-Core Scanning

After fracture logging, the core was cut into one-meter segments and was scanned using the DMT CoreScan II® to provide a digital record of the drilled core. Whole-round core segments up to 1 meter in length were scanned by revolving the cut core on rollers as a digital line scanner captured the image of the core from above. This provides a 360 degree unrolled image of the core (Figure 10). Each of the scanned whole-core image files were then named based on the depth in meters below seafloor of the top of the core segment. Segments of core that were soft or highly fractured could not be scanned because the integrity of the core would not be maintained on the rollers of the CoreScan II®. Due to the soft and fractured core condition, the PQ core that was collected between the seafloor and 41.88 (mbsf) was not scanned. Whole-core image scans of 56% of the PQ3 core (between the depths of 41.88 and 283.04 mbsf), 89% of HQ core (between 238.04 and 702.64 mbsf), and 90% of the NQ core (between 702.64 and 1284.87 mbsf) were obtained at the drill-site lab (Wilson et al., 2007).

Once reviewed, the core scans revealed that the red and blue orientation lines scribed on the core were not straight and parallel to the long axis of the image (Figure 11). An average 'drift' of the scribe lines of 6.7 degrees from top to bottom of a one meter core scan was calculated. Although the cause of the 'drift' was uncertain at the time, it was determined in the following drilling season that it was due to a

misalignment of the line-scanning camera with respect to the rollers rotating the core during scanning. If left uncorrected, the drift would cause errors in core orienting as well as any analysis of fractures thereafter. Under the direction of project collaborator Richard Jarrard, Anastasia Yatsenko, a master's student at the University of Utah, corrected the scanning error. To remove the scribe line drift, the red line position was measured at both the top and the bottom of every image using Paint software. With this information, the images were then uploaded and corrected in Matlab® software using linear interpolation: the red line was aligned in the same position and orientation in all images.

Figure 10. (a) Picture of the core prior to scanning. (b) Unrolled image of the core after it has been digitally scanned using the DMT CoreScan II®.

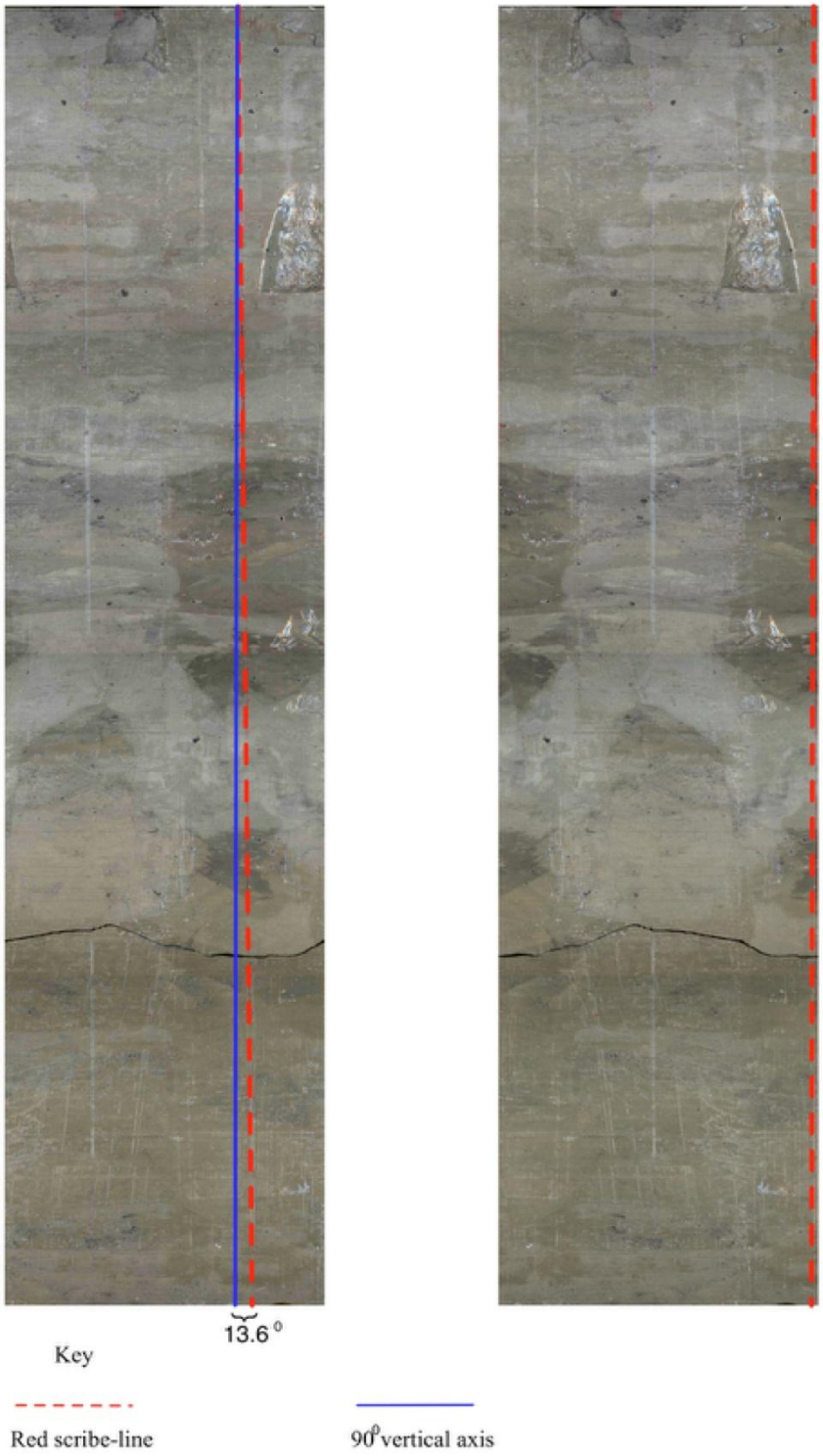

Figure 11. A one meter core segment before (left) with a 13.6 degree 'drift', and after (right) the red scribe-line was corrected for drift. The average 'drift' of the scribe lines in the AND-1B core was 6.7 degrees from top to bottom of a one meter core. Once corrected, the red line was placed to the right side of every image prior to stitching (Yatsenko, 2008).

Digital Stitching of Core Images

"Intact intervals" are continuous segments of core that have not had internal relative rotation during coring (Figure 12). Boundaries between intact intervals can be the breaks between core runs that did not fit end-to-end, or fractures within a core logged as 'spins' where rotation occurred during drilling. Using the DMT CoreBase® software, intact intervals of core were reconstructed from the individual core-scan images. This process is referred to as 'stitching'. The digitally 'stitched' intact-interval images are used in the process of core orientation and to measure the orientation of fractures in the core.

The initial step in the process was loading core images into AdobePhotoshopCS2 where color adjustments were made to all core scans. By manipulating red saturation levels of the images, I was able to improve the clarity of the red scribe line, allowing for better detection of the red scribe line in the CoreBase® software. I imported the adjusted, red-saturated images for a given intact interval, along with their corresponding DMT text files that provide depth information, into the DMT CoreBase® software. CoreBase® allows images to be shifted up and down as well as rotated clockwise or counterclockwise to align them into a continuous core interval. The individual cut images were realigned based on the red scribe line that acted as the arbitrary north direction. In instances where a fractured core moved during scanning

and the red line became misaligned, the core image was digitally cut and rotated to proper alignment (Figure 13). The "fit angles" between matching ends of adjacent core runs were inserted using the recorded rotation angles on the drill-site logging sheets. The complete 'stitched' intact intervals of core were saved and exported.

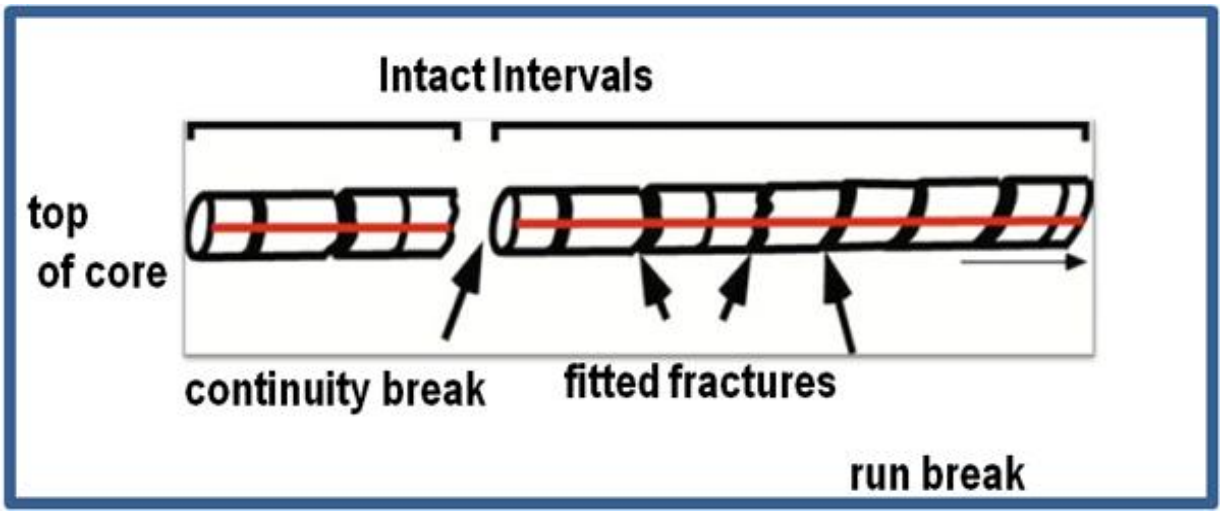

Figure 12. Diagram showing 'intact intervals'. Boundaries are either ends of core runs that could be fit together, or drilling induced fractures that spun during coring process (Paulsen and Wilson, 1998).

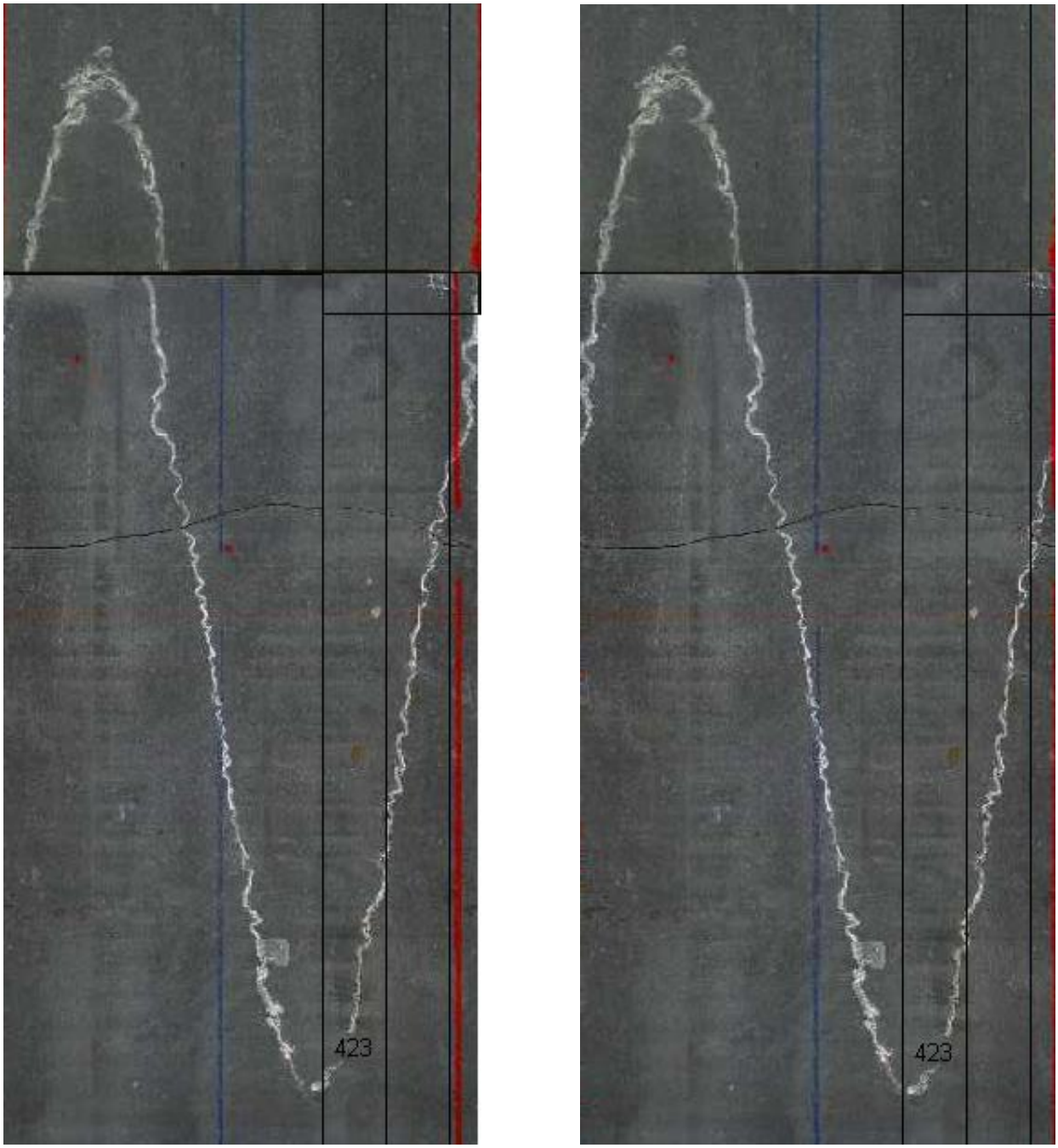

Figure 13. (a) Whole round core scan loaded in DMT CoreBase® software prior to stitching. (b) Whole round core scan after it has been stitched, corrected for misfits, and the red scribe line has been aligned.

Core Orienting

Core orientation was completed by Richard Jarrard at the University of Utah. Intact intervals were oriented using a direct side-by-side comparison of the stitched core scan image to oriented borehole televiewer (BHTV) imagery of the borehole walls for matching depth intervals (Figure 14). Features that could be matched included natural fractures, bedding, and clasts. The set of 'feature matches' allowed the orientation of the red scribe line relative to the true *in situ* north direction to be calculated. This 'rotation angle' was used to reorient the red scribe line in the whole-core image of the intact interval to true north in CoreBase®, which allowed structures in the core to be measured with respect to *in situ* coordinates, as if the core were repositioned in the ground.

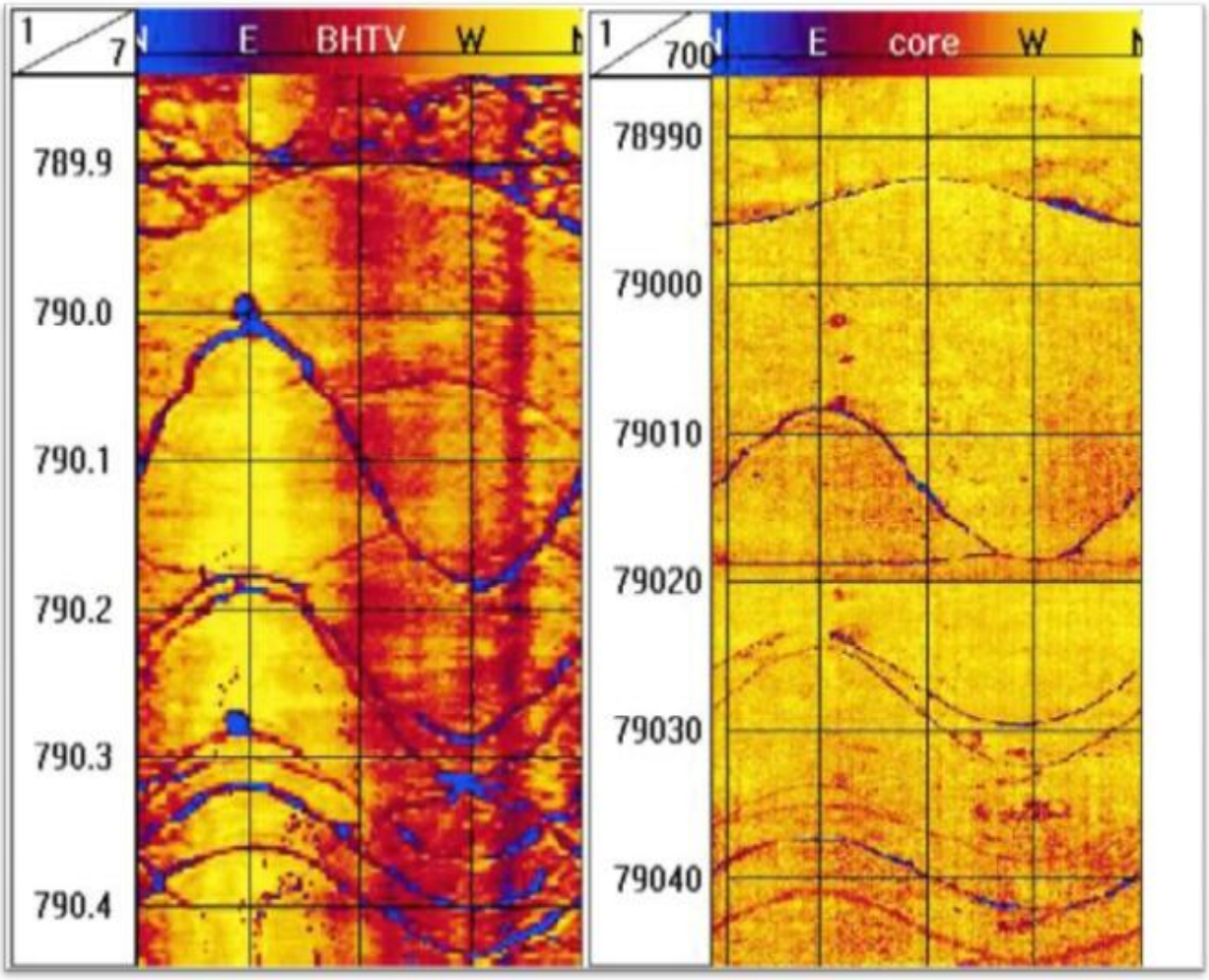

Figure 14. BHTV imaging is used to orient core to original *in situ* coordinates by feature matching (Jarrard et al., 2001).

Fracture Analysis

The CoreBase® software can be used to measure the dip angle and dip direction of fractures in the core by drawing a 'best fit' sinusoid to each structure. This process of fracture analysis is known as 'picking' structures. Measurements within each intact interval are made with respect to the red scribe line, aligned to 'CoreBase® north' position. Each intact interval of core was 'picked' two separate times. The first was a blind pick, with each visible structure in the core image selected and measured. The second pick involved searching for structures recorded on the fracture log sheet for the intact interval using the original core scan images, which have enhanced resolution relative to the stitched core image, and then identifying and picking them on the stitched core image. Bedding was picked by comparing the high-resolution images with the 1m sedimentary log description of the core recorded by members of the sediment logging team on ice. Fractures were assigned as veins, faults, or clastic dikes, where type could be identified. CoreBase® assigned a different color for each fracture category and bedding (Figure 15). Once all of the structures had been measured, I exported the dip angle and dip direction data from CoreBase® into Excel.

In order to determine if the AND-1B core contains systematic orientations of bedding and fractures, Rick Allmendinger's Stereonet® v. 6.0.2 for Mac was used to analyze the orientation of picked structures. For each intact interval, separate text files

were created based on the exported data of picked structures from CoreBase®. Separate files were created for confirmed veins, faults, clastic dikes, and bedding, as well as for 'possible' veins, faults, clastic dikes, and bedding. Possible fractures were logged on ice and represent fractures that were questionable. Files were loaded into the stereonet software where separate plots were created for each category of veins, faults, bedding, and clastic dikes. In cases where an intact interval contained both confirmed and 'possible' veins the planes were plotted on the same stereonet with the confirmed planes in black and the possible planes in blue. Intact intervals that had both confirmed and possible faults were also plotted on the same stereonet with confirmed planes in black and possible planes in red. Contour plots were created for those intervals that displayed clear sets of subparallel fractures. Using 1% area contour, clustered poles were contoured and an average great circle was picked based on the center point of each contour 'bulls-eye'.

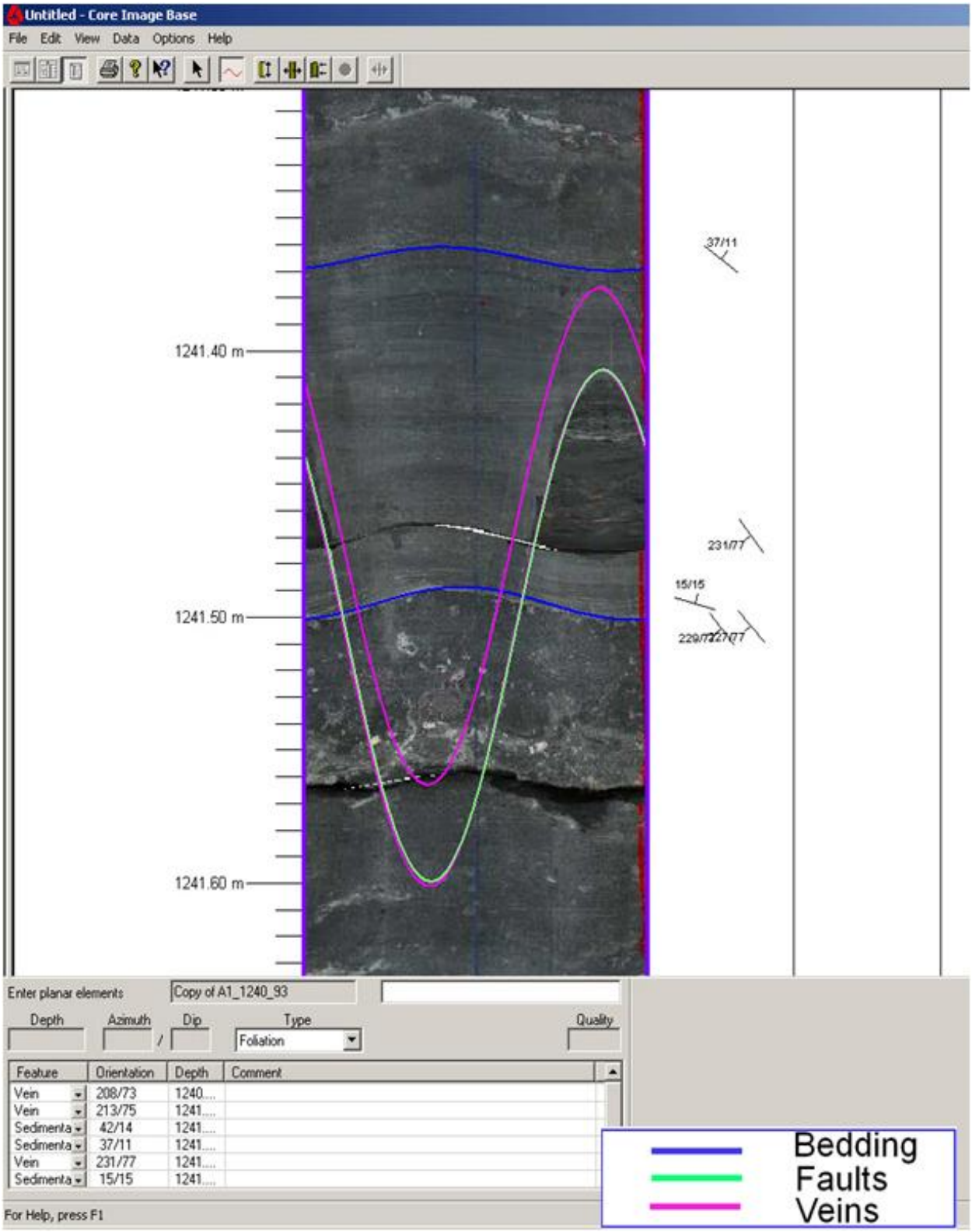

Figure 15. Picking structures based on fracture type within CoreBase® Software. Fracture types and bedding are distinguished by color. All faults are picked using a green sinusoid, all veins are picked using a fuchsia sinusoid, clastic dikes were picked using a yellow sinusoid, and bedding was picked with a blue sinusoid.

Results

For this project, twenty four intact intervals totaling 212.59 meters of the AND-1B core were digitally stitched at the Ohio State University. Of the intact intervals used for this study, five intervals were oriented to their original *in situ* coordinates at the University of Utah using the feature matching method. 363 measurements of natural fractures were made from the digitally-stitched scanned images of the whole round rock core using the commercial CoreBase® software, including 215 veins, 91 faults, and 8 clastic dikes. These independent measurements were then compared with the 267 veins, 126 faults and 11 clastic dikes, totaling 403 hand-measured natural fractures that were measured during core logging at the drill-site laboratory in Antarctica.

Table A shows a comparison of the natural fractures of all types identified on the scanned whole-core images in CoreBase® to the natural fractures identified during core logging. Table B presents the number of natural fractures of specific structural types identified in each intact interval during the CoreBase® measurements, compared with the number of hand-measured structural features of each type identified during core logging. Appendix A compares the orientation of natural fractures from measurements recorded during core logging and measurements using the CoreBase® method for the same fractures. The results are presented separately for each fracture type: veins, faults, and clastic dikes. Appendix B presents graphical stereoplots of the orientations of veins,

faults, and clastic dikes in each intact interval as measured during core logging. Appendix C contains stereoplots of the orientations of natural fractures generated from the independent CoreBase® measurements taken from intact intervals of digitally-stitched whole-round rock core. For both appendices B and C, definite natural fractures are recorded in black, possible veins are recorded in blue, possible faults are recorded in red, and possible clastic dikes are recorded in green. Appendix D presents the bedding measurements that were made using the CoreBase® software. Definite bedding planes are recorded in black, whereas possible bedding planes are recorded in fuchsia. For each appendix, contour plots were created for intervals containing clustered fractures that represent fracture sets or subparallel bedding planes that could be averaged.

The following sections summarize the results of comparing the independent measurements of natural fractures and bedding found using the CoreBase® software with the natural fractures that were found within the AND-1B rock core during core logging. Intact intervals are identified by the topmost depth and orientation trends are given with respect to the arbitrary north scribed on the rock core during core logging. This comparison will determine the differences, strengths and weaknesses between the two approaches and help to guide future core-based fracture logging studies.

Comparison of Fracture Populations Mapped in CoreBase® and by Core Logging

Natural fractures were identified and measured (referred to here as 'picks') using the CoreBase® method in two sequential analyses. The first analysis used only the scanned whole-core images digitally stitched into intact core intervals using the CoreBase® Software to locate natural fractures. The second analysis used the same intervals of whole-core scanned images in the CoreBase® software, but involved an attempt to identify the same fractures recorded on log sheets from the on-ice fracture logging with the aid of the original high-resolution scanned images viewed in Photoshop®. The log sheets provided dip and dip direction measurements, top and bottom depth, and identifying information for each logged fracture. This information was used as a guide to identify and measure the same fractures on the whole-core scans. Table A shows the number of logged natural fractures, the number of fractures located during the first and second 'picks' in CoreBase®, the number of logged fractures that could not be located in CoreBase®, and the number fractures that were found in CoreBase® but unlogged on the ice. A comparison was made to determine the percentage of fractures not logged on ice but found using CoreBase®, and fractures not located in CoreBase®, but logged on ice, relative to the total fracture population recorded in both CoreBase® and core logging methods.

The first pick, based on viewing only the scanned whole-core images in the CoreBase® software, identified sixty-three definite fractures and two questionable

fractures for a total of sixty-five natural fractures. The natural fracture population retrieved during this first CoreBase® pick was only 16% of the total natural fracture population. Fractures identified in the first pick were predominantly veins with mineral fill. The second pick, using the logged fractures to guide identification, yielded 258 definite fractures and forty-five questionable fractures for a total of 303 natural fractures. The natural fracture population retrieved from the second pick was 75% of the total natural fracture population logged directly from the core.

Table B records the total population of veins, faults, and clastic dikes from both picks, located in CoreBase® and during core logging. The percent of recovery of each fracture type from CoreBase® is calculated and reported below. Core logging methods identified 267 veins. CoreBase® methods were able to retrieve 215 of the originally logged veins. Total vein population recovery from CoreBase® was 80.5%. During core logging, 126 faults were identified and recorded, whereas 91 of the originally logged faults were located and measured using the unrolled core images in the CoreBase® software. The total fault population recovery from CoreBase® was 72.2%. 11 total clastic dikes were identified during core logging and 8 clastic dikes were measured independently using CoreBase®. Total clastic dike population recovery in CoreBase® was 72.7%.

Comparison of Fracture Orientations from CoreBase® and Core Logging

Appendix A presents the orientation of natural fractures from core logging measurements compared with the independent measurements recorded from CoreBase®.

Of the total vein population, orientations of 192 fractures were compared for both methods of the study. Dip angle comparison revealed that 49% of the recorded measurements differed by less than or equal to 2 degrees, 30% differed by greater than 2 degrees but less than or equal to 5 degrees, 14% differed by greater than five percent but less than or equal to 10 degrees, and 12% exceeded a ten degree difference in dip between methods. Of the compared vein dip angles, 94% of the population was within ten degrees difference between core logging measurements and measurements recorded from CoreBase®. Comparison of dip direction azimuth of veins recorded from core logging with measurements of the same veins taken in CoreBase® revealed that 14% of the population measurements differed by less than or equal to two degrees, 45% differed by greater than two degrees but less than or equal to five degrees, 12% differed by greater than five degrees but less than or equal to ten degrees, 2% differed by greater than ten degrees but less than or equal to twenty degrees, and 34% exceeded twenty degrees difference in dip direction azimuth measurements between methods.

71% of the compared vein population was within a ten degree difference of dip direction azimuth orientation.

The orientation of eighty-two faults were compared from core logging and CoreBase® measurement methods. Of the fault population, 40% of measured dip angles differed by less than or equal to two degrees, 29% differed by greater than two degrees but less than or equal to five degrees, 9% differed by greater than five degrees but less than or equal to ten degrees, and 22% differed by greater than ten degrees but less than or equal to twenty degrees. Of the compared fault dip angles, 78% of the population was within ten degrees difference between the measurements made during core logging and the measurements recorded from CoreBase®. Dip direction azimuth comparison between core logging and CoreBase® measurement methods showed that 15% of the measurements differed by less than or equal to two degrees, 21% differed by greater than two degrees but less than or equal to five degrees, 10% differed by greater than five degrees but less than or equal to ten degrees, 13% differed by greater than ten degrees but less than or equal to twenty degrees, and 41% exceeded twenty degrees difference in dip direction azimuth between measurement methods. The fault orientation comparison revealed that 45% of the compared fault population was within a ten degree difference in dip direction azimuth orientation.

A total of eight clastic dikes were compared between core logging and CoreBase® measurement methods for dip angle and dip direction azimuth. Of the total clastic dike population compared, 63% differed by less than or equal to two degrees, and 38% differend by greater than two degrees but less than or equal to five degrees. This resulted in 100% of the compared clastic dike population falling within a ten degree difference of dip angle measurements. Dip direction azimuth comparison of clastic dikes measured in core logging and by CoreBase® methods found that 13% of the populations measurements differed by less than or equal to two degrees, 38% differed by greater than two degrees but less than or equal to five degrees, 0% differed by greater than five degrees but less than or equal to ten degrees, 50% differed by greater than ten degrees but less than or equal to twenty degrees, and 38% exceeded twenty degrees difference in dip direction azimuth measurements between methods. The clastic dike comparison revealed that 50% of the compared population of clastic dikes was within a ten degree difference of dip direction azimuth.

Fracture Patterns in MIS Core

Interval 516.49 contains veins and faults. Measurements of the interval during core logging recorded three veins and eleven faults. Veins are scattered in orientation. Faults form conjugate sets with west-northwest strikes and have similar dip angles of fifty-nine degrees northeast and fifty-eight degrees southwest. Three veins and four

faults were measured in CoreBase® with veins and faults exhibiting scattered trends. Four identified bedding planes with a northeast strike and an average dip angle of eight degrees southeast were picked in CoreBase®.

Interval 535.56 has been oriented to original *in situ* coordination and contains only faults. Four faults were logged on ice and display dispersed northwest strikes and dips to the southwest. CoreBase® identified two of the originally logged faults and yielded northwest strikes. Bedding found within the interval is averaged with a northwest strike and has a dip angle of twenty-six degrees south; this is the steepest dip angle for any interval containing bedding.

Interval 614.71 contains veins and faults. A total of eight veins and twenty one faults were measured during core logging and neither population shows a consistent orientation. CoreBase® was able to measure four veins and thirteen faults with veins exhibiting scattered trend and faults having apparent conjugate sets striking north-west. Fifty five bedding planes were identified having roughly north-south strikes and dips both to the east and to the west. The averaged orientation yields a northwest strike and a low dip angle of four degrees east.

Interval 644.47 contains veins and faults. Thirty six veins were logged on ice and exhibit three separate sets; one with a northeast strike and a twenty- one degree dip to the east, another with a strike of northwest and a fifty-four degree north dip, and the

final set with a northeast strike and a dip angle of sixty-nine degree west. Thirty four of the veins that were documented on the log sheets were identified in CoreBase® along with another thirty-one unlogged veins. The veins found in CoreBase® showed three separate sets as well; the first with a northeast strike and a twenty- six degree dip to the east, another averaged northwest strike and a thirty-four degree dip, and the final strike with a northwest dip direction and a low dip angle of six degree south. Five faults were found using both the core logging and CoreBase® method and have an averaged northeast strike. The dip measured during core logging is a twenty-seven degree east dip; whereas the CoreBase® measured dip was averaged at twenty-four degrees east. Five bedding planes were 'picked' in CoreBase® and have a northwest strike and a low dip angle of six degrees south.

Interval 674.40 contains only veins. Core logging on ice identified eight veins and CoreBase® was able to identify four of these veins on the scanned core images. The majority of core logging measurements display a northeast strike with a steep dip of eighty-seven degrees east. The CoreBase® measurements have a more scattered strike and were not averaged.

Interval 874.74 has been oriented to original *in situ* coordinates using feature matching and contains veins and faults. Core logging recorded four veins and one fault but neither type of fracture displayed sets. The CoreBase® method was unable to

identify any veins or faults within the interval. Six bedding planes were identified but show opposing dips.

Interval 900.8 is one of the five oriented intervals and contains veins, faults and one clastic dike. Core logging recorded ten veins, five faults, and one clastic dike. The identified veins form a possible conjugate set with northeast and north strikes and dip angles at sixty- five degrees west and sixty-four degrees east. The faults and the clastic dike do not show clear sets. Using the CoreBase® software, ten veins, five faults and one clastic dike were identified. Although the faults and the clastic dikes recorded from CoreBase® were scattered and do not display sets, the veins measured in CoreBase® present a conjugate set with northeast to north strikes and dip angles at sixty-two degrees west and sixty-five degrees east. Three bedding planes were identified and display an averaged northeast strike and a dip angle of eleven degrees north.

Interval 939.48 has been oriented to original *in situ* coordinates and contains veins, faults and one clastic dike. Core logging identified seven veins, two faults and one clastic dike and all fracture types show scattered orientation. CoreBase® identified the seven veins, two faults, and the one clastic dike that were documented on the log sheets along with one unlogged vein that was found in CoreBase®. The independent vein measurements show a set with northwest strike and steep southwest dip, while the few faults and clastic dikes do not form sets.

Using feature matching, interval 1008.1 has been returned to *in situ* orientation and contains veins and faults. During core logging five veins and three faults were recorded, whereas four veins and three faults were located using the CoreBase® software. Veins and faults that were measured independently with CoreBase® or measured during core logging, show northeast strikes and steep northwest dips, possibly representing a fracture set.

Interval 1047.01 contains veins and one clastic dike. During core logging, two veins and one clastic dike were observed, whereas one vein and one clastic dike were located in the whole round core images in CoreBase®. All fracture types show northwest to north strikes and steep dips. Eleven bedding planes were 'picked' with a northeast strike and an averaged dip of eleven degrees east.

Interval 1082.35 contains veins and faults. Twelve veins and twelve faults were identified on ice during core logging. Veins form a possible conjugate set striking northeast, while faults are more scattered. Seven veins and nine faults that were logged on ice were located using the CoreBase® software along with five unlogged veins; however they do not display oriented sets when plotted.

Interval 1111.42 contains veins and faults. Core logging recorded five veins and one fault. CoreBase® located only the five veins. The majority of veins in both methods display a northeast strike with respect to arbitrary north.

Interval 1138.33 is the longest of the intact intervals in this study. Using bedding dip, this interval was oriented to original *in situ* coordinates and contains veins, faults and clastic dikes. Core logging identified thirty-eight veins, nineteen faults, and three clastic dikes. Veins have three observable strikes; one striking northeast, and the other two striking northwest. Dips are averaged at seventy-two degrees south, seventy-five degrees northeast, and seventy-nine degrees northeast. Faults from core logging are more scattered in orientation, but appear to have similarly oriented sets as the veins display. The majority of clastic dikes show a northwest strike. Thirty-two veins, sixteen faults and two clastic dikes that were originally logged on ice were observed using the CoreBase® software along with one unlogged vein. Veins form two sets, one with northeast orientation and a eighty degree east dip and the other with a northwest orientation with a eighty degree north dip. Faults are more scattered and have northeast and northwest strikes. The two clastic dikes have a northwest strike. Fifteen bedding planes were observed and have an averaged orientation striking northeast and an averaged dip of sixteen degrees northwest.

Interval 1192.715 contains veins and faults. Both core logging and CoreBase® methods recorded four veins and one fault. However, no consistent orientation is present in either plotted veins or faults.

Interval 1203.36 contains only veins. During core logging, two veins were recorded and one vein was identified using the CoreBase® software. Seven bedding planes were identified using CoreBase® and have an averaged east-northeast strike and a nine degree north dip.

Interval 1230.02 contains veins and faults. Core logging documented eleven veins and eight faults. The majority of the veins display a northeast strike while the faults show a northwest strike. CoreBase® was able to identify ten veins and eight faults. The veins are scattered in orientation, whereas the faults strike northwest.

Interval 1233.46 contains veins and faults and one clastic dike. Twenty-four veins, five faults, and one clastic dike were documented during core logging. Faults and the clastic dike have scattered northerly strikes. The veins are also scattered in orientation, but also yield two sets, one in the northwest direction with a thirty-six degree east dip angle and the other striking west-east with an averaged dip angle of ninety degrees north. Along with three unlogged veins, twenty-two originally logged veins and one fault were located using the CoreBase® software. Veins form two sets, one with northwest strike and a dip angle of twenty-eight degrees east and the other strike being west-east with a dip angle of eighty nine degrees south.

Interval 1237.05 contains veins and faults. Six veins and one fault were observed during core logging. CoreBase® software was able to identify three veins and one fault.

Veins strike dominantly to the northwest. Fifteen bedding planes were observed and 'picked' in CoreBase®. The averaged orientation strikes to the northeast with a dip angle of sixteen degrees north.

Interval 1239.34 contains veins, one fault, and one clastic dike. Core logging yielded sixteen veins, one fault, and one clastic dike. The veins cluster and strike northeast with an averaged dip angle of seventy-two degrees southeast. Using the CoreBase® software, sixteen veins, one fault and one clastic dike were recovered from the originally logged fractures along with twelve unlogged veins. The veins cluster well, and strike northeast with an averaged dip angle of seventy-three degrees south. Fourteen bedding planes were observed with averaged dip angle of fifteen degrees north and strike northeast.

Interval 1247.61 contains veins and faults. Core logging recorded ten veins and two faults. Veins have steep dips and form two general strikes, one being north-south, and the other striking west-east. Eight veins and one fault were measured independently with the CoreBase® software. Two sets are visible in the vein measurements, one striking northeast with a dip of seventy one degrees north, and the other striking northwest with a dip of seventy-five degrees west.

Interval 1255.84 contains veins, faults, and one clastic dike. Core logging identified twenty veins, three faults, and one clastic dike. The veins logged form two

sets, with a northeast strike and an eighty nine degree east dip and another striking west-east with an averaged eighty-three degree south dip. Fifteen veins and two faults that were originally logged on ice were observed using the CoreBase® method, along with four other unlogged veins. Two visible sets are observed from the vein measurements, one with a northeast strike and seventy-seven degree east dip angle, and the other striking northwest with an averaged dip angle of eighty-four degrees south. Fifty five bedding planes were measured using CoreBase® and have an averaged northeast strike and a twelve degree west dip.

Interval 1264.63 contains veins and faults. Core logging recorded eight veins and three faults. CoreBase® identified four originally logged veins, three unlogged veins and three faults. Fractures recorded by both methods are scattered. Two bedding planes were identified in CoreBase® and have an averaged northeast strike and a thirteen degree north dip.

Interval 1267.71 contains veins, faults, and clastic dikes. Ten veins, two faults, and three clastic dikes were observed during core logging. CoreBase® identified twelve veins, eight faults and two clastic dikes. The dominant strike direction is east-west to northwest-southeast, but there is considerable scatter in orientation and no clear sets. Three bedding planes were identified with an averaged orientation striking northwest with dip angle of nineteen degrees east.

Interval 1272.94 contains veins and faults. Core logging identifies twelve veins, and eight faults. The majority of veins and faults strike northwest and have steep dip angles. CoreBase® measured nine logged and one unlogged vein as well as six faults. Faults strike northeast with steep dip angles. Veins strike northeast with an averaged dip angle of eighty-eight degrees. Six bedding planes were identified with two orientations; one striking northeast with an averaged dip angle of twenty-five degrees east, and the other striking northwest and having a dip angle of sixteen degrees south.

Table A

	Number of fractures located using CoreBase®-first pick			Number of fractures located using CoreBase®-second pick			Number of fractures located in CoreBase®	Fractures located during core logged			Logged on ice, but never located in CoreBase®	Found in CoreBase®, but never logged on ice
Interval Depth	**Definite**	**Questionable**	**Total**	**Definite**	**Questionable**	**Total**	**Total**	**Definite**	**Questionable**	**Total**	**Total**	**Total**
516.49-522.55	0	0	0	6	1	7	7	13	1	14	**7**	**0**
535.56-540.55	0	0	0	0	2	2	2	0	4	4	**2**	**0**
614.71-638.95	4	1	5	7	5	12	17	19	10	29	**12**	**0**
644.47-650.47	17	0	17	53	0	53	70	39	2	41	**5**	**31**
674.40-692.40	0	0	0	4	0	4	4	8	0	8	**4**	**0**
874.74-876.28	0	0	0	0	0	0	0	2	2	4	**4**	**0**
900.8-906.44	4	0	4	10	1	11	15	14	1	15	**0**	**0**
939.48-944.12	0	0	0	10	1	11	11	8	2	10	**1**	**1**
1008.1-1009.37	0	0	0	7	0	7	7	8	0	8	**1**	**0**
1047.01-1052.15	0	0	0	2	0	2	2	3	0	3	**1**	**0**
1082.35-1098.44	0	0	0	19	2	21	21	21	3	24	**8**	**5**
1111.42-1125.75	5	0	5	0	0	0	5	5	0	5	**0**	**0**
1138.33-1192.715	0	0	0	42	9	51	51	49	12	61	**9**	**1**
1192.715-1197.19	0	0	0	4	1	5	5	4	1	5	**0**	**0**
1203.36-1217.66	0	0	0	1	0	1	1	2	0	2	**1**	**0**
1230.02-1233.46	0	0	0	11	7	18	18	11	8	19	**1**	**0**
1233.46-1236.83	3	0	3	21	1	22	25	24	11	35	**9**	**3**
1237.05-1239.34	2	0	2	1	1	2	4	6	1	7	**3**	**0**
1239.34-1245.24	22	0	22	6	1	7	29	17	1	18	**0**	**12**
1247.61-1249.84	2	0	2	7	0	7	9	12	0	12	**3**	**0**
1255.84-1264.14	4	1	5	14	2	16	21	17	6	23	**5**	**4**
1264.63-1267.25	0	0	0	9	1	10	10	8	3	11	**3**	**3**
1267.71-1272.77	0	0	0	14	4	18	18	22	4	26	**8**	**0**
1272.94-1284.87	0	0	0	10	6	16	16	12	7	19	**3**	**1**
Total	**63**	**2**	**65**	**258**	**45**	**303**	**368**	**324**	**79**	**403**	**90**	**61**

% of total fracture population retrieved from CoreBase® first pick 16
% of total fracture population retrieved from CoreBase® second pick 75

% of logged fractures located in CoreBase® 84
% of logged fractures not located in CoreBase® 22

% of total fracture population logged on ice 87
% of fractures not logged on ice but located using CoreBase® 13

Table B

Interval Depth	Corebase			Core logging			Difference in methods		
	Number of Veins	Number of Faults	Number of Clastic Dikes	Number of Veins	Number of Faults	Number of Clastic Dikes	Number of Veins	Number of Faults	Number of Clastic Dikes
516.49-522.55	3	4	0	3	11	0	0	7	0
536.56-540.55	0	2	0	0	4	0	0	2	0
614.71-638.95	4	13	0	8	21	0	4	8	0
644.47-650.47	34	5	0	36	5	0	2	0	0
674.40-692.40	4	0	0	8	0	0	4	0	0
874.74-876.28	0	0	0	4	1	0	4	1	0
900.8-906.44	10	5	1	10	5	1	0	0	0
939.48-944.12	7	2	1	7	2	1	0	0	0
1008.1-1009.37	4	3	0	5	3	0	1	0	0
1047.01-1052.15	1	0	1	2	0	1	1	0	0
1082.35-1098.44	7	9	0	12	12	0	5	3	0
1111.42-1125.75	5	0	0	5	1	0	0	1	0
1138.33-1192.715	32	16	2	38	19	3	6	3	1
1192.715-1197.19	4	1	0	4	1	0	0	0	0
1203.36-1217.66	1	0	0	2	0	0	1	0	0
1230.02-1233.46	10	8	0	11	8	0	1	0	0
1233.46-1236.83	22	1	0	24	5	1	2	4	1
1237.05-1239.34	3	1	0	6	1	0	3	0	0
1239.34-1245.24	16	1	1	16	1	1	0	0	0
1247.61-1249.84	8	1	0	10	2	0	2	1	0
1255.84-1264.14	15	2	0	20	3	1	5	1	1
1264.63-1267.25	4	3	0	8	3	0	4	0	0
1267.71-1272.77	12	8	2	15	10	2	3	2	0
1272.94-1284.87	9	6	0	12	8	0	3	2	0
Totals	**215**	**91**	**8**	**266**	**126**	**11**	**51**	**35**	**3**

Total vein population from CoreBase®	215
Total vein population from core logging	266
% of recovered veins in CoreBase®=	81
Total fault population from CoreBase®	91
Total fault population from core logging	126
% of recovered faults in CoreBase®=	72
Total clastic dike population from CoreBase®	8
Total clastic dike population from core logging	11
% of recovered clastic dikes in CoreBase®=	73

Discussion

Fracture Populations Identified by Logging vs. by Core Image Analysis

The first pick in CoreBase® recovered only 16% of the total natural fracture population that was identified during core logging. Fractures identified during this analysis are predominantly veins with mineral fill that is visible on the low resolution images in CoreBase®. The second pick from CoreBase® recovered 75% of the total natural fracture population logged on ice. Using CoreBase®, it was possible to identify 80% of veins, 72% faults, and 72% of clastic dikes when compared with core logging methods.

Images loaded into CoreBase® lose resolution relative to the original whole-core scanned images. The low resolution of the images in CoreBase® makes it more difficult to locate fractures; this was most evident with faults. Veins are visible because they are typically filled with light-colored material, making the fracture stand out on the core image despite the low resolution. Faults however, may not have any vein fill and require that some amount of offset of bedding is visible in order to identify the fault in CoreBase®. During core logging, faults were identified by offset of bedding, but also by the presence of slickenlines and slickenfibers on open fracture surfaces in the core. Fracture surface features are not visible on the whole-core surface scans that are loaded into CoreBase®. The material injected into clastic dikes often has contrasting colors to the surrounding material, making them more visible and thus more easily located.

The 'first pick' of fractures in CoreBase® was less reliable then the 'second pick', which relied on the log sheet data and higher resolution scanned images in identifying fractures. The first pick relied solely on the visibility of the structures on the imported scanned images in CoreBase®. When using CoreBase® to identify fractures and take measurements, a large proportion of the fracture population can be missed. The use of log sheet data and higher resolution scanned images greatly improves the ability to record an accurate population for different fracture types.

Fracture Orientations Measured by Logging vs. by Core Image Analysis

According to the comparative analysis in this study, the majority of the dip angles measured directly on the core are within ten degrees of the measurements made in CoreBase®. More dip angles of veins and clastic dikes measured from CoreBase® were within ten degrees of the core logging measurements than those of measured faults. 94% of veins and 100% of clastic dikes measured in CoreBase® were within ten degrees of core logging measurements, whereas only 78% of the compared faults were within ten degrees.

Comparison of CoreBase® and logging-derived measurements revealed that fewer dip azimuths are within a ten degree range. Dip azimuths of veins are more closely comparable, with 71% being within ten degrees, than those of recorded faults and clastic dikes, with 45% and 50% within ten degrees, respectively.

Large discrepancies in orientation between core logging and CoreBase® measurement methods are linked to many different factors. Orientation measurement difference is related to the irregularity of fractures. Fracture irregularity can cause a large error during core logging. The templates used to measure fractures during core logging are used on only one side of the whole core, and may not be able to measure the 'total trend' of the fracture, whereas CoreBase® is able to estimate the overall orientation of the fracture from the entire unrolled surface of the core shown on the core scan. CoreBase® allows for a better representation of the overall fracture orientation. Orientation discrepancies due to fracture irregularities are most common for veins and clastic dikes. Faults commonly follow a clear planar path, whereas veins and clastic dikes that were identified on the core were commonly folded or had changes in orientation, making the measurement much more difficult with templates during core logging.

Differences in orientation between CoreBase® methods and core logging methods frequently occurred when fractures were identified and measured on the side of the core where the blue line was scribed during core fracture logging. In general, fracture measurements were consistently made relative to the red scribe line, which was marked on the core before it was rolled over. The blue scribe line was marked after the core was rolled 180 degrees, which could result in relative rotations of segments within the core. It is possible that the blue scribe line was not consistently drawn at 180

degrees to the red scribe line, skewing measurements. CoreBase® on the other hand is able to pick fractures based on the whole round unrolled core scan, and measurements were always made with respect to the red scribe line.

The strengths behind the core logging method include the fact that the measurements are taken directly from the core, allowing for more fine detail to be recorded and measured. In the case of faults, fracture surface characteristics such as slickenlines and slickenfibers can be identified and measured when the core is in hand. Small and therefore less visible veins are more easily measured as well when one can examine the core up close. A weakness of the direct core fracture logging arises due to the irregular diameter of the core. Fractures recorded on ice during core logging used a set of premade templates scaled to a specific core diameter to measure dip and dip direction azimuth with respect to the 'arbitrary north' red scribe line. These templates cannot provide accurate measurements for undersized core. Another weakness associated with core-based fracture measurement comes when fractures are measured with respect to the less accurate blue scribe line, after the core has been flipped over and possibly disturbed.

The strengths associated with the independent measurements made on scanned whole-core images in this study are based on the fact that the CoreBase® software enables one to see the full fracture around the whole core, allowing the measurement to

be taken from an overall representation of the fracture. This is most evident when picking fractures that are irregular or change orientation through the length of the core. Another advantage of CoreBase® analysis of core images is the fact that the blue side is more visible when the core is scanned and unrolled. Because of this, many fractures that are clustered on the blue side can be located in CoreBase®, but not identified during core logging. Disadvantages associated with measurements taken from CoreBase® are linked to the poor visibility of the scanned images once imported into the software. The low resolution of CoreBase® makes it more difficult to locate fractures that are small, or fractures that lack vein fill material which would make it stand out on the core. Another weakness within the CoreBase® method is the error that can occur in measuring fractures on such a small core diameter. This error can result in a ten plus degree difference in orientation due to only a few millimeters in difference when picking the fracture. In this way it is very easy to accumulate error when picking fracture orientations in CoreBase®.

Orientation Patterns in Analyzed Intervals of AND-1B Core

Overall, where intact intervals had sufficient numbers of natural fractures present, oriented fracture sets could be identified. Multiple fracture sets were present in intact intervals with large natural fracture populations. Most commonly, fault sets and vein sets in the same intact interval had similar orientations. Typically the vein populations were larger and showed a larger number of sets than the fault population

in the same interval. In the 5 oriented intervals of core, both northeast- and northwest-striking fracture sets were present. No systematic change in orientation from upper to lower levels of the core is indicated by the sets in these oriented intervals. The sets with the largest populations and most consistent orientation in the lower core intervals strike northeast. Further work is required to compare these core fracture orientations to seismically-mapped faults around the MIS coring location.

Bedding Orientation and Potential for Core Orientation

Bedding planes picked from CoreBase® were analyzed and revealed that among all intact intervals, bedding dip seems to increase with depth of the core. Another observation made from the study was the similarities in bedding planes among oriented intervals. Intervals 874.74, 900.8, and 1138.33 have all been oriented to *in situ* orientation using feature matching. The bedding planes within these intervals are consistent in an averaged dip direction ranging from 241 degrees to 245 degrees. Dip increases with depth, as with un-oriented intervals, from ten degrees in interval 874.74, eleven degrees in interval 900.8, and sixteen degrees in interval 1138.33. The analysis of the bedding planes in the AND-1B core that were identified using the CoreBase® software suggest that bedding dip and dip direction from oriented core may be used to orient more intact intervals in the future. This would involve rotating the average bedding dip direction in an unoriented intact interval to match the average dip direction in oriented intervals,

simultaneously rotating the fractures in the interval to this new orientation. Stereoplot test are required to determine the reliability of this orientation method.

Conclusions

This study measured and mapped the attitudes of bedding and natural fractures in select intact intervals from the AND-1B core. The comparison of the core logging and CoreBase® methods found that more fractures can be identified by direct core logging. However, CoreBase® can identify fractures on the blue-scribed side of the core that were not measured and recorded on ice. Many more veins, than faults and clastic dikes, are recorded in CoreBase® because the veins often contain mineral fill that is visible on the low resolution imagery in CoreBase®. Small natural fractures with little to no mineral fill that are logged on ice are not easily identified using the CoreBase® software.

When the independent measurements from CoreBase® are compared to the hand-measured structural features recorded during core logging, it is determined that both methods have measurement errors and more accurate orientation records of the structural features in the core would be obtained by systematically using both methods on the same fractures. Natural fractures picked in CoreBase® allow the measurement to be taken from an overall representation of the fracture. Measurements are acquired from a larger population of fractures using direct core logging, resulting in better identification of oriented sets and more significant averaging of set orientations using stereographic analysis.

The stereographic analysis of bedding planes picked in CoreBase® shows that dip increases with depth. The consistent orientation of bedding plane dip direction azimuth from intervals oriented from feature matching suggests that more intact intervals can be oriented to original *in situ* coordinates by rotating the core so that all bedding dip directions match. Fracture analysis using both core logging measurements and independent measurements from CoreBase® showed that oriented natural fracture sets are present in the AND-1B core. Analysis of more oriented intact intervals will determine if attitudes of structures within the AND-1B core are consistent with Terror rift faulting or other processes.

References:

Allmendinger, R. W. (2002). Stereonet for Macintosh. http://www.geo.cornell.edu/geology/faculty/RWA/programs.html. Ithaca, NY: Dept. of Earth and Atmospheric Sciences, Cornell University.

Barrett, P., (2008). A History of Antarctic Cenozoic Glaciation – View from the Margin. In: Florindo, F., and Siegert M., (eds.), *Developments in Earth & Environmental Sciences*, v. 8, 33-83.

Boggs, Jr. S., (2006). *Principles of Sedimentology and Stratigraphy*. Upper Saddle River, NJ: Pearson Prentice Hall, p. 137, 209.

Collinson, J. (1994). Sedimentary Deformation Structures. In: Maltman, A. (ed), The geological deformation of sediments. London, UK: Chapman and Hall, 362.

Cooper, A.K., Davey, F.J., Behrendt, J.C., 1987. Seismic stratigraphy and structure of the Victoria Land Basin, Western Ross Sea, Antarctica. In: Cooper, A.K. and Davey, F.J. (eds.), *The Antarctic Continental Margin: Geology and Geophysics of the Western Ross Sea.* CPCEMR, 5b, Houston, Texas: 27–77.

Falconer, T., A. Pyne, R. Levy, M. Olney, M. Curren, and the ANDRILL-MIS Science Team (2007). *Operations overview for the ANDRILL McMurdo Ice Shelf Project, Antarctica.* Terra Antartica. 14 (3), 131-140.

Fielding C.R., Naish, T.R., Woolfe, K.J. (2001). Facies Architecture of the CRP-3 Drillhole, Victoria Land Basin, Antarctica. Studies from the Cape Roberts Project, Ross Sea, Antarctica; scientific report of CRP-3; Part I, Sedimentary environments for CRP-3 Terra Antartica, 8, 217-224.

Fielding, C., Whittaker J., Henrys S.A., Wilson T.J., & Naish, T. R., (2007). Seismic facies and stratigraphy of the Cenozoic succession in McMurdo Sound, Antarctica; implications for tectonic, climatic and glacial history. In: Cooper, A., Raymond, C., and the 10th ISAES Editorial Team Antarctica; A Keystone in a Changing World–Online Proceedings for the 10th International Symposium on Antarctic Earth Sciences: U.S. Geological Survey Open-File Report 2007-1047 [http://pubs.usgs.gov/of/2007/1047/srp/srp090/]

Hall, J.M., (2006). *Structural Evolution of the Terror Rift, Western Ross Sea, Antarctica: Interpretation from 2-D Seismic Reflection Data*. Unpublished M.Sc. Thesis, Ohio State University, Columbus, Ohio.

Henrys, S.A., Bucker, C.J., Bartek, L., Bannister, S., Niessen, F., Wonik, T. (2000). Correlation of Seismic Reflections with CRP-2/2A, Terra Antartica, 7, 221-230.

Horgan, H., Naish, T., Bannister, S., Balfour, N., and Wilson, G., (2005). *Seismic Stratigraphy of the Ross Island Flexural Moat under the McMurdo-Ross Ice Shelf, Antarctica, and a Prognosis for Stratigraphic Drilling*. Glob. Planet. Changes, 45, 83-97

Naish, T., R. Powell, R. Levy, and the ANDRILL Science Team (2007). *Back-ground to the ANDRILL McMurdo Ice Shelf Project (Antarctica) and initial science volume.* Terra Antartica, 14 (3), 121-130.

Krissek, L., Browne, G., Carter, L., Cowan, E., Dunbar, G., McKay, R., Naish, T., Powell, R., Reed, J., Wilch, T., and the ANDRILL-MIS Science Team (2007). *Sedimentology and Stratigraphy of the AND-1B Core, ANDRILL McMurdo Ice Shelf Project, Antarctica.* Terra Antartica, *14 (3), 185-222.*

Paulsen, T.S., & Wilson, G.S. (1998). Orientation of the CRP−1 core. *Terra Antarctica*, *5*(3), 319−325.

Paulsen T., Millan C., Pierdominici S., Wilson T., Drew S. & the ANDRIL−SMS Science Team, (2008). Fracture Logging of the AND−2A Core, ANDRILL Southern McMurdo Sound Project, Antarctica. Terra Antarctica, 15(1), 69−76.

Stern, T.A., Davey, F.J., Delisle, G. (1991). Lithospheric Flexure Induced by the Load of the Ross Archipelago, Southern Victoria Land Basin, Antarctica. In Thomas, M.R.A., Crame, A., Thomas, J.W. (eds.), *Geological Evolution of Antarctica*. Cambridge University Press, Cambridge, UK, 323-328.

Van der Pluijm, B.A., & Marshak, S. (2004). *Earth Structure: an introduction to structural geology and tectonics*. New York City, NY: W. W. Norton and Company, Inc.

Yatsenko, Anastasia. (2008). *Tectonic implications of the AND-1B and AND-2A borehole data, McMurdo Sound region, Antarctica.* . Unpublished M.Sc. Thesis, The University of Utah, Salt Lake City, Utah.

Wilson, T. J., T. S. Paulsen, A. L. Laufer, and C. Millan (2007). *Fracture logging of the AND-1B core, McMurdo Ice Shelf Project, Antarctica.* Terra Antartica. 14 (3), 175-184.

Appendix A:
Comparison of natural fracture orientation

Appendix A

Veins	Core logging		CoreBase®		Difference	
Fracture #	Dip	DD	Dip	DD	Dip	Azimuth
516.49-522.55						
1509	55	53	50	40	5	13
1510	65	98	56	95	9	3
1526	55	328	63	314	8	14
535.56-540.55						Oriented
none	none	none	none	none	none	none
614.71-638.95						
1825a	89	170	85	116	4	54
1843	30	340	17	10	13	30
1856	55	172	29	153	26	19
644.47-650.47						
1887	70	285	75	302	5	17
1889	30	125	27	124	3	1
1890	20	128	21	121	1	7
1891	25	117	25	112	0	5
1892	24	118	28	123	4	5
1893	21	117	22	125	1	8
1894	16	110	19	114	3	4
1895	20	118	19	117	1	1
1897	45	22	51	26	6	4
1898	40	25	33	38	7	13
1899	44	17	33	325	11	52
1900	44	20	42	17	2	3
1901	36	21	40	18	4	3
1902	45	8	34	11	11	3
1904	30	10	28	364	2	6
1905	67	233	64	228	3	5
1907	63	290	65	314	2	24
1908	35	10	31	9	4	1
1909	66	195	64	201	2	6
1910	35	13	33	13	2	0
1911	73	290	79	349	6	59
1913	60	215	59	203	1	12
1924	86	233	87	221	1	12
1925	72	210	76	278	4	68
674.40-692.40						
1963	90	263	90	267	0	4
1974	85	317	88	280	3	37
1991	78	157	83	187	5	30
1993	79	168	77	185	2	17
900.8-906.44						Oriented
2911	64	79	65	90	1	11
2912	65	97	60	97	5	0
2915	43	277	35	307	8	30
2916	72	340	67	31	5	51
2919	64	240	60	254	4	14
2920	62	232	65	78	3	154
2921	65	234	63	82	2	152
2929	41	154	47	148	6	6
939.48-944.12						Oriented
3086	60	105	54	111	6	6
3087	45	72	45	74	0	2
3088	70	60	61	74	9	14
3089	88	90	82	90	6	0
3092	85	90	86	101	1	11

Faults	Core logging		CoreBase®		Difference	
Fracture #	Dip	DD	Dip	DD	dip	Azimuth
516.49-522.55						
1509	55	53	50	37	5	16
1510	55	98	56	93	1	5
1524	68	170	64	174	4	4
1526	65	328	63	314	2	14
535.56-540.55						Oriented
1577	30	93	24	112	6	19
1578	89	89	27	114	62	25
614.71-638.95						
1840	61	85	38	75	23	10
1841	16	130	19	50	12	80
1843	30	340	28	59	11	79
1844	60	0	39	8	21	8
1845	43	5	24	71	19	66
1848	64	0	52	350	12	10
1849	63	91	35	350	28	101
1851	66	327	70	13	4	46
1853	51	180	49	175	2	5
1861	48	179	32	28	16	151
1866	25	176	27	183	2	7
1831a	35	175	36	186	1	11
1831b	30	8	27	16	3	8
644.47-650.47						
1884	63	102	68	100	5	2
1885	75	124	70	129	5	5
1888	30	125	25	122	5	3
1889	30	128	27	124	3	4
1890	20	117	21	121	1	4
674.40-692.40						
none	none	none	none	none	none	none
900.8-906.44						Oriented
2912	65	97	60	96	5	1
2916	72	340	67	30	5	50
2918	50	195	42	195	8	0
2929	41	154	46	152	5	2
2930	38	134	33	121	5	13
939.48-944.12						Oriented
3090	40	126	42	131	2	5
3087	45	72	45	75	0	3

Clastic Dikes	Core Logging		CoreBase®		Difference	
Fracture #	Dip	DD	Dip	DD	dip	Azimuth
516.49-522.55						
none	none	none	none	none	none	none
535.56-540.55						Oriented
none	none	none	none	none	none	none
614.71-638.95						
none	none	none	none	none	none	none
644.47-650.47						
none	none	none	none	none	none	none
674.40-692.40						
none	none	none	none	none	none	none
900.8-906.44						Oriented
2913	15	190	18	329	3	139
939.48-944.12						Oriented
3087	45	208	45	211	0	3

Appendix A

Veins	Core logging		CoreBase®		Difference	
Fracture #	Dip	DD	Dip	DD	Dip	Azimuth
1008.1-1009.37						Oriented
3335	58	55	58	55	0	0
3337	74	72	71	74	3	2
3338	60	105	64	112	4	7
3339	61	72	47	91	14	19
1047.01-1052.15						
3507	85	68	87	271	2	157
1082.3-1098.44						
3608	76	258	71	240	5	18
3614	71	325	68	322	3	3
3620	65	89	83	177	18	88
3621	66	98	81	220	15	122
3633	75	272	74	246	1	26
3638	78	150	70	165	8	15
3655	90	222	90	354	0	132
1111.42-1125.75						
3691	88	121	88	130	0	9
3692	85	130	86	94	1	36
3696	82	65	83	63	1	2
3702	82	10	83	7	1	3
3708	75	80	75	75	0	5
1138.33-1192.715						Oriented
3748	81	325	84	328	3	3
3751	75	265	77	268	2	3
3752	74	275	73	238	1	37
3756	81	178	82	177	1	1
3759	76	222	67	244	9	22
3760	84	258	80	257	4	1
3761	85	260	87	279	2	19
3762	80	70	83	91	3	21
3766	81	350	81	352	0	2
3768	63	255	61	298	2	43
3769	65	280	70	285	5	5
3771	79	191	80	192	1	1
3776	70	180	67	177	3	3
3777	75	185	77	216	2	31
3794	77	6	77	14	0	8
3795	73	61	75	76	2	15
3796	80	10	81	19	1	9
3798	70	50	70	67	0	17
3802	58	118	54	125	4	7
3806	79	6	78	16	1	10
3813	75	338	74	333	1	5
	90	309	90	126	0	183
3815	77	332	83	319	6	13
3818	62	347	61	4	1	17
3819	78	329	78	348	0	19
3820	81	309	79	310	2	1
3823	74	334	81	298	7	36
3836	65	233	66	228	1	5
3837	81	30	80	34	1	4
3838	87	4	86	15	1	11
1192.715-1197.19						
3864	88	52	88	46	0	6
3866	85	85	85	290	0	205
3865	81	349	79	353	2	4
3867	83	338	82	314	1	24
1203.36-1217.66						
3887	75	186	73	101	2	85
1230.02-1233.46						
3962	85	255	82	259	3	4
3979	89	138	82	199	7	61
3984	76	100	72	101	4	1
3985	63	282	66	279	3	3
3966	44	315	59	287	15	28

Faults	Core logging		CoreBase®		Difference	
Fracture #	Dip	DD	Dip	DD	dip	Azimuth
1008.1-1009.37						Oriented
3335	58	55	58	55	0	0
3337	74	72	70	70	4	2
3339	61	72	46	86	15	14
1047.01-1052.15						
none	none	none	none	none	none	none
1082.3-1098.44						
3608	76	258	71	235	5	23
3614	71	325	68	311	3	14
3619	71	247	66	114	5	133
3620	65	89	82	182	17	93
3621	66	98	80	227	14	129
3631	54	60	52	126	2	66
3642	68	205	68	141	0	64
3644	15	292	17	228	2	64
3645	20	330	19	266	1	64
1111.42-1125.75						
none	none	none	none	none	none	none
1138.33-1192.715						Oriented
3751	**75**	**265**	77	269	2	4
3761	85	260	86	281	1	21
3762	80	70	83	92	3	22
3766	81	350	80	349	1	1
3768	63	255	61	298	2	43
3769	65	280	69	284	4	4
3803	80	2	80	52	0	50
3807	63	340	54	352	9	12
3814	90	309	3	126	87	183
3829	13	153	42	240	29	87
3836	65	233	66	227	1	6
3837	81	30	80	34	1	4
3842	72	307	79	321	7	14
3843	79	317	73	309	6	8
1192.715-1197.19			Dip			
3866	85	85	85	290	0	155
1203.36-1217.66						
none	none	none	none	none	none	none
1230.02-1233.46			Dip			
3962	85	255	82	258	3	3
3971	33	86	29	88	4	2
3973	33	76	32	74	1	2
3974	33	68	30	71	3	3
3975	33	67	33	65	0	2

Clastic Dikes	Core Logging		CoreBase®		Difference	
Fracture #	Dip	DD	Dip	DD	dip	Azimuth
1008.1-1009.37						Oriented
none	none	none	none	none	none	none
1047.01-1052.15						
3507	85	68	87	270	2	158
1082.3-1098.44						
none	none	none	none	none	none	none
1111.42-1125.75						
none	none	none	none	none	none	none
1138.33-1192.715						Oriented
3843	79	66	79	65	0	1
3842	72	56	73	52	1	4
1192.715-1197.19			Dip			
none	none	none	none	none	none	none
1203.36-1217.66						
none	none	none	none	none	none	none
1230.02-1233.46			Dip			
none	none	none	none	none	none	none

Appendix A

Veins	Core logging		CoreBase®		Difference	
Fracture #	Dip	DD	Dip	DD	Dip	Azimuth
1233.46-1236.83						
3989	80	182	84	173	4	9
3991	40	65	40	60	0	5
3992	65	198	66	231	1	33
3994	74	307	72	312	2	5
3995	30	71	25	76	5	5
3996	30	73	29	69	1	4
3997	32	60	33	57	1	3
3998	65	285	68	284	3	1
3999	35	60	28	63	7	3
4000	32	70	29	83	3	13
4001	58	313	64	197	6	116
4002	79	13	61	317	18	56
4003	61	233	55	241	6	8
4004	85	84	84	252	1	168
4005	81	259	82	250	1	9
4006	85	10	83	9	2	1
4007	88	18	88	357	0	21
4008	82	182	81	182	1	0
4030	89	180	89	186	0	6
4031	75	234	72	233	3	1
1237.05-1239.34						
4028	80	230	78	252	2	22
4029	67	235	67	239	0	4
1239.34-1245.24						
4035	80	125	80	135	0	10
4036	79	120	78	122	1	2
4037	75	130	71	150	4	20
4039	71	158	73	155	2	3
4039	71	158	72	139	1	19
4041	69	131	75	133	6	2
4042	71	135	76	131	5	4
4044	70	138	78	189	8	51
4046	75	163	71	158	4	5
4049	75	157	71	149	4	8
4050	78	125	77	125	1	0
4052	74	130	71	126	3	4
4053	68	147	71	114	3	33
4054	81	110	76	109	5	1
4061	75	140	75	136	0	4
4062	74	190	71	164	3	26
1247.61-1249.84						
4078	81	358	79	352	2	6
4080	81	328	83	333	2	5
4083	83	273	81	251	2	22
4084	75	260	61	256	14	4
4085	75	270	74	249	1	21
4086	70	358	68	351	2	7
4087	75	175	69	350	6	175
4090	82	68	82	286	0	142
1255.84-1264.14						
4127	75	121	67	210	8	89
4128	65	235	72	121	7	114
4130	78	278	79	290	1	12
4132	84	180	82	193	2	13
4133	83	189	81	194	2	5
4134	80	180	77	196	3	16
4137	90	126	88	234	2	108
4139	90	306	87	256	3	50
4143	83	200	80	197	3	3
4147	76	35	68	38	8	3
4149	85	175	87	342	2	167
4154	81	31	78	328	3	63
4155	82	215	82	62	0	153
4156	78	165	81	271	3	106
4157	86	30	82	26	4	4
1264.63-1267.25						
4158	84	152	81	165	3	13
4161	86	225	81	234	5	9
4174	86	315	87	286	1	29
4175	86	115	88	11	2	104
4177	85	140	88	230	3	90

Faults	Core logging		CoreBase®		Difference	
Fracture #	Dip	DD	Dip	DD	dip	Azimuth
1233.46-1236.83						
3988	84	303	66	277	18	26
1237.05-1239.34						
4021	85	15	87	358	2	17
1239.34-1245.24						
4042	71	135	76	130	5	5
1247.61-1249.84						
4083	83	278	82	249	1	29
1255.84-1264.14						
4127	75	121	73	120	2	1
4128	65	235	67	213	2	22
1264.63-1267.25						
4159	78	135	80	140	2	5
4164	62	236	47	81	15	155

Clastic Dikes	Core Logging		CoreBase®		Difference	
Fracture #	Dip	DD	Dip	DD	dip	Azimuth
1233.46-1236.83			Dip			
none	none	none	none	none	none	none
1237.05-1239.34			Dip			
none	none	none	none	none	none	none
1239.34-1245.24						
4042	71	135	76	130	5	5
1247.61-1249.84			Dip			
none	none	none	none	none	none	none
1255.84-1264.14			Dip			
none	none	none	none	none	none	none
1264.63-1267.25			Dip			
none	none	none	none	none	none	none

Appendix A

Veins	Core logging		CoreBase®		Difference	
Fracture #	Dip	DD	Dip	DD	Dip	Azimuth
1267.71-1272.77						
4191	69	221	77	217	8	4
4192	81	238	85	255	4	17
4194	87	90	79	7	8	83
4197	90	9	86	314	4	55
4204	74	182	75	182	1	0
4208	30	350	25	3	5	13
4209	90	12	89	11	1	1
4210	70	255	71	260	1	5
4211	45	160	43	178	2	18
4212	80	185	80	180	0	5
4214	80	30	82	31	2	1
4201	69	298	72	302	3	4
1272.94-1284.87						
4221	88	70	86	111	2	41
4228	85	255	86	115	1	140
4230	75	215	77	267	2	52
4231	84	111	79	170	5	59
4232	90	87	83	304	7	143
4237	79	85	74	135	5	50
4238	73	172	86	322	13	150
4241	75	295	86	323	11	28
4247	80	75	81	142	1	67

ALL VEINS	N=192	% of total viens	% 10 Difference
N dip diff <= 2 degrees	95	49	
N dip diff >2 & <= 5 degrees	58	30	
N dip diff >5 & <= 10 degrees	27	14	94
N dip diff exceeds 10 degrees	12	6	
N az diff <= 2 degrees	26	14	
N az diff >2 & <=5 degrees	8	45	
N az diff >5 & <=10 degrees	23	12	71
N within 10-20 degrees	4	2	
N az diff exceeds 20 degrees	65	34	

Faults	Core logging		CoreBase®		Difference	
Fracture #	Dip	DD	Dip	DD	dip	Azimuth
1267.71-1272.77						
4194	87	90	22	319	65	131
4213	65	0	65	351	0	9
4201	69	298	72	302	3	4
4195	20	302	79	9	59	67
1272.94-1284.87						
4220	60	56	66	276	6	140
4221	88	70	86	111	2	41
4233	72	330	74	128	2	158
4237	79	300	86	110	7	170
4238	73	27	74	321	1	66

ALL FAULTS	N=82	% of toal faults	% 10 Difference
N dip diff <= 2 degrees	33	40	
N dip diff >2 & <= 5 degrees	24	29	
N dip diff >5 & <= 10 degrees	7	9	78
N dip diff exceeds 10 degrees	18	22	
N az diff <= 2 degrees	12	15	
N az diff >2 & <=5 degrees	17	21	
N az diff >5 & <=10 degrees	8	10	45
N within 10-20 degrees	11	13	
N az diff exceeds 20 degrees	34	41	

Clastic Dikes	Core Logging		CoreBase®		Difference	
Fracture #	Dip	DD	Dip	DD	dip	Azimuth
1267.71-1272.77						
4211	45	160	43	178	2	18
4208	30	350	25	364	5	14
1272.94-1284.87			Dip			
none	none	none	none	none	none	none

ALL CLASTIC DIKES	N=8	% of total CD	% 10 Difference
N dip diff <= 2 degrees	5	63	
N dip diff >2 & <= 5 degrees	3	38	
N dip diff >5 & <= 10 degrees	0	0	100
N dip diff exceeds 10 degrees	0	0	
N az diff <= 2 degrees	1	13	
N az diff >2 & <=5 degrees	3	38	
N az diff >5 & <=10 degrees	0	0	50
N within 10-20 degrees	4	50	
N az diff exceeds 20 degrees	3	38	

Appendix B:

Stereoplots of natural fractures measured during core logging. Definite fractures are labeled as Nd, whereas possible fracture types are labeled Np. All definite fractures are plotted in black. Possible veins are plotted in blue, possible faults are plotted in red, and possible clastic dikes are plotted in green

Interval: 516.49-522.55

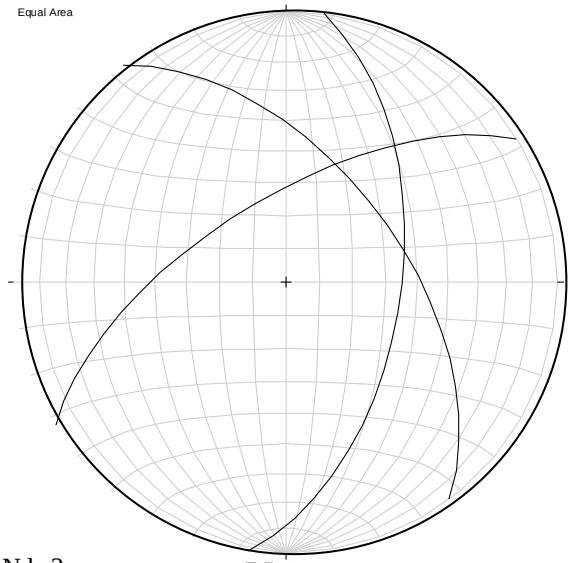

Nd=3

Veins

Veins Averaged

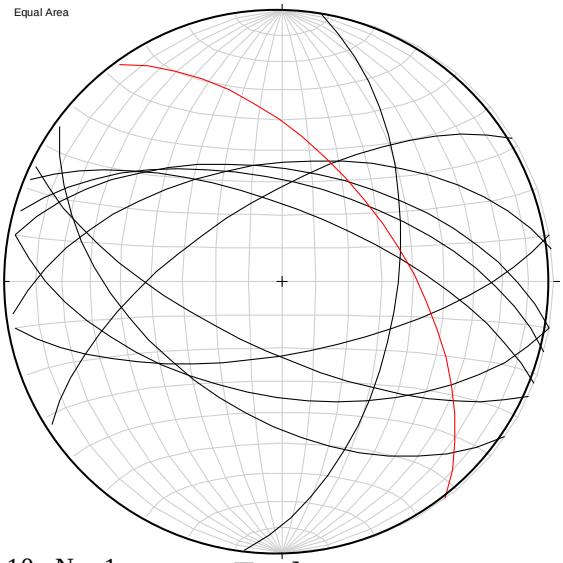

Nd=10 Np=1

Faults

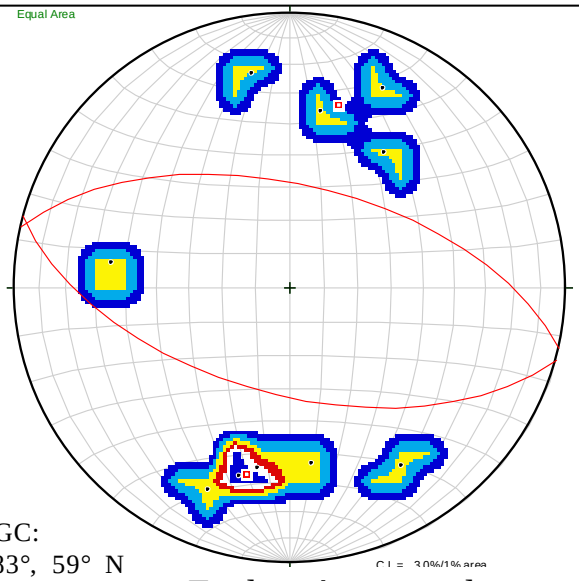

PGC:
283°, 59° N
105°, 58° E

Faults Averaged

Clastic Dikes

Clastic Dikes Averaged

Veins

Veins Averaged

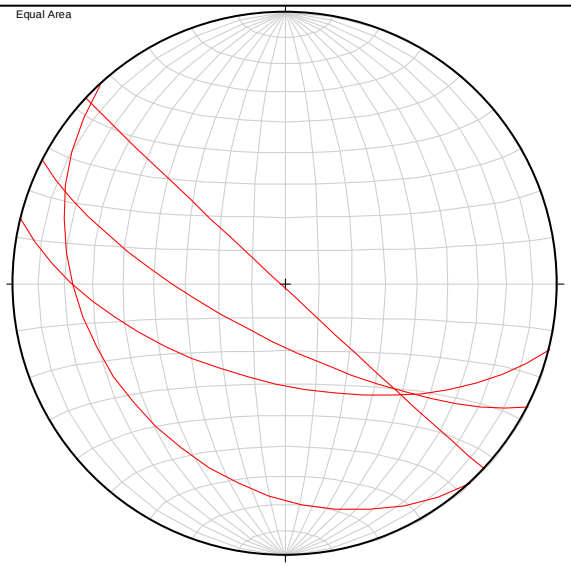

Np=4

Faults

Faults Averaged

Clastic Dikes

Clastic Dikes Averaged

Interval: 614.71-638.95 Oriented

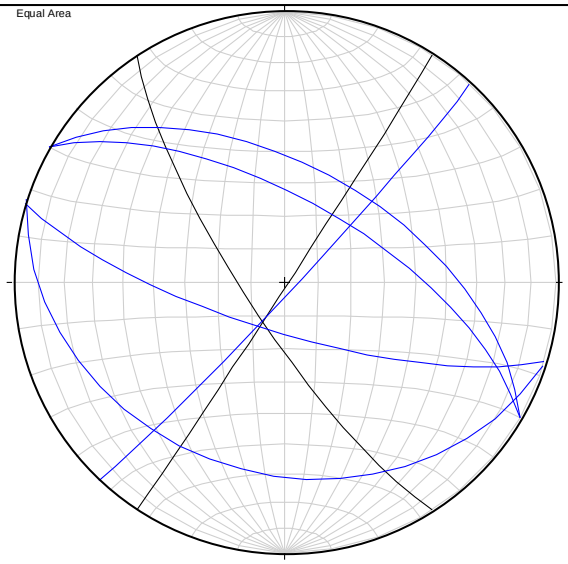

Nd=2 Np=4

Veins

Veins Averaged

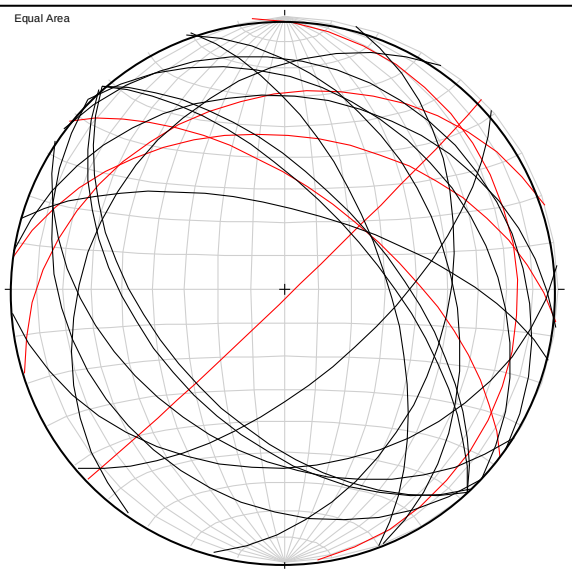

Nd=16 Np=5

Faults

Faults Averaged

Clastic Dikes

Clastic Dikes Averaged

Interval:644.47-650.47

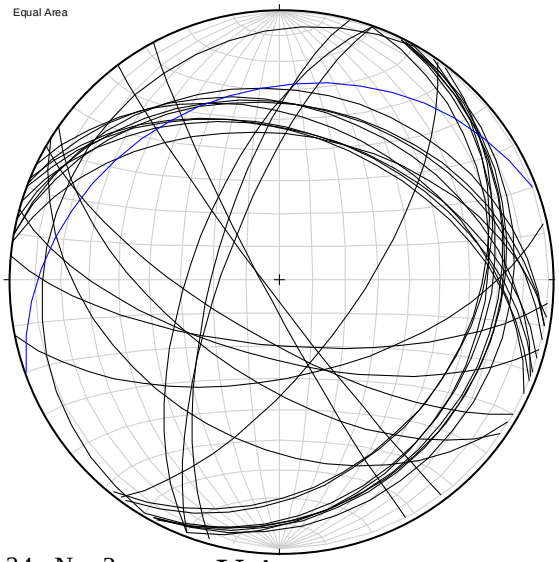

Nd=34 Np=2

Veins

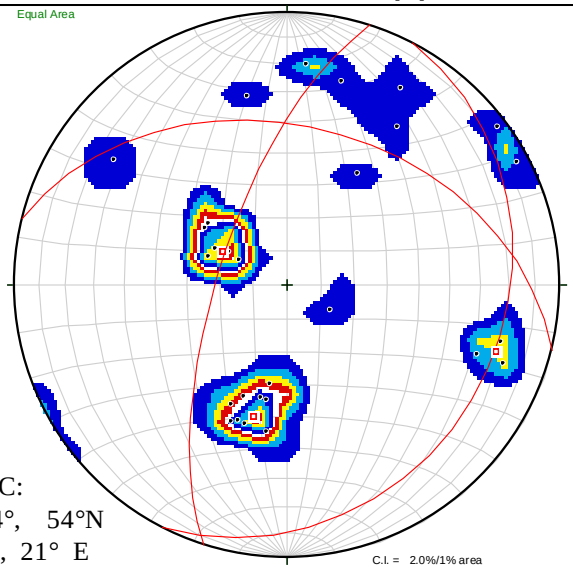

PGC:
284°, 54°N
28°, 21° E
198°, 69° W

Veins Averaged

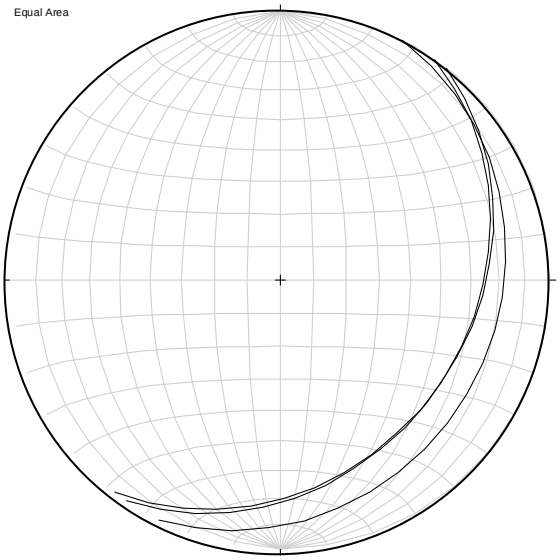

Nd=3

Faults

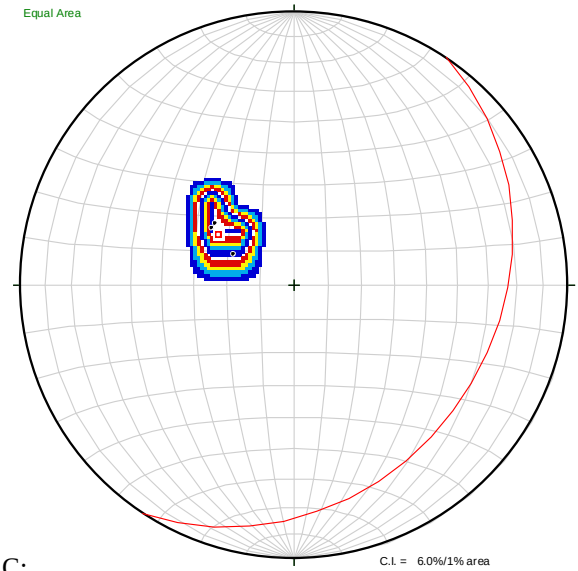

PGC:
34°, 27° E

Faults Averaged

Clastic Dikes

Clastic Dikes Averaged

Interval: 674.40-876.28

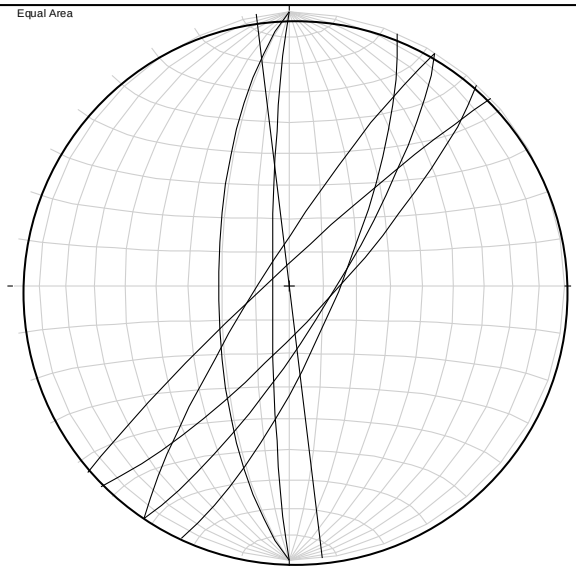

Nd=8

Veins

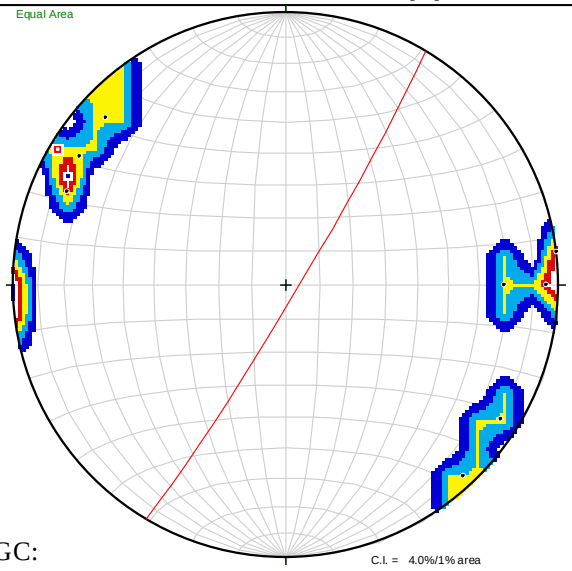

PGC:
31°, 87° E

Veins Averaged

Faults

Faults Averaged

Clastic Dikes

Clastic Dikes Averaged

Interval: 874.74-876.28

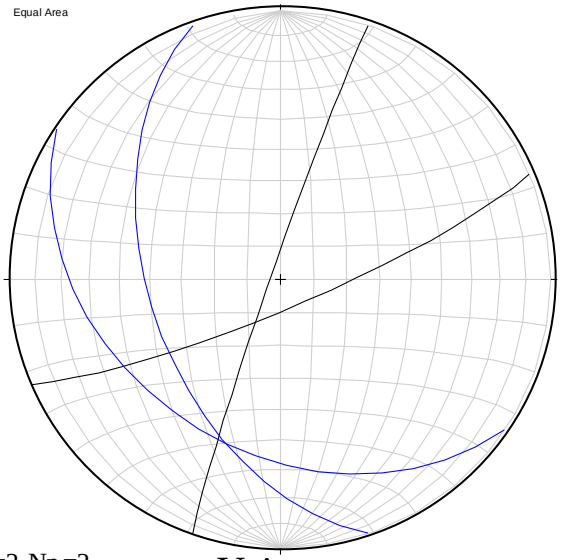

Nd=2 Np=2

Veins

Veins Averaged

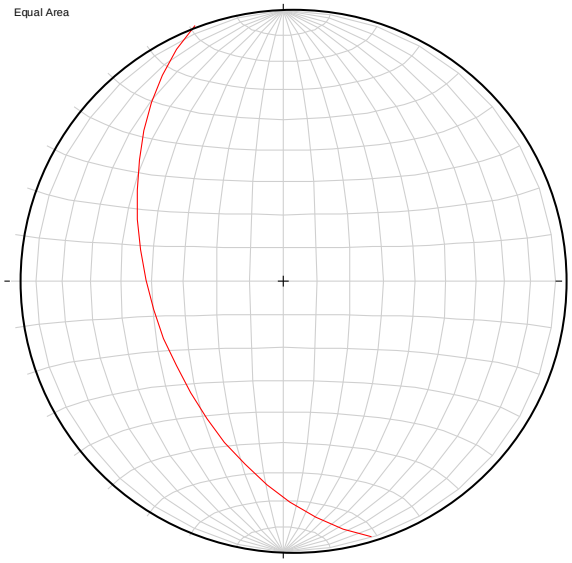

Np=1

Faults

Faults Averaged

Clastic Dikes

Clastic Dikes Averaged

Interval: 900.8-906.44 Oriented Appendix B

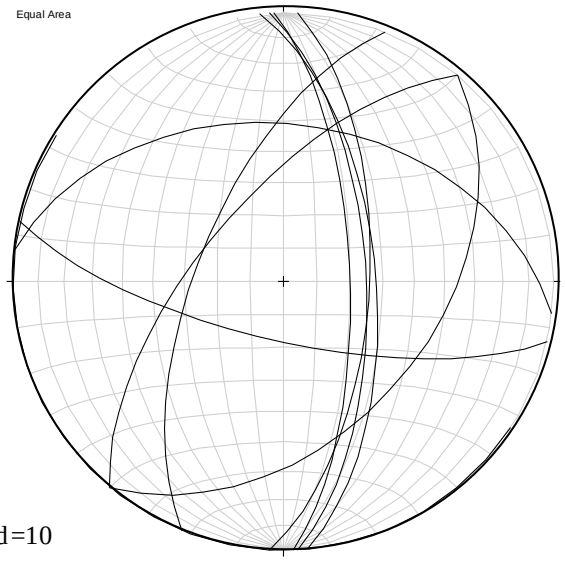

Nd=10

Veins

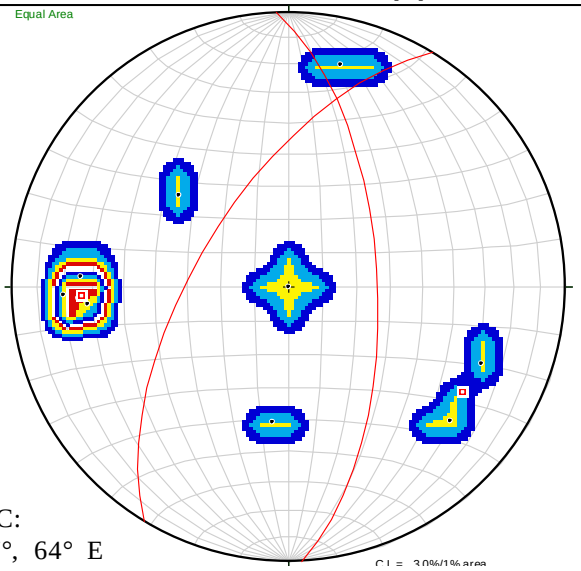

PGC:
357°, 64° E
211°, 63° W

Veins Averaged

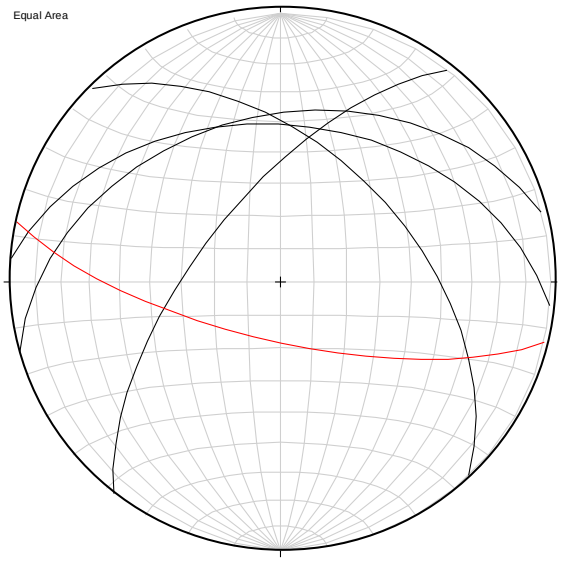

Nd=4 Np=1

Faults

Faults Averaged

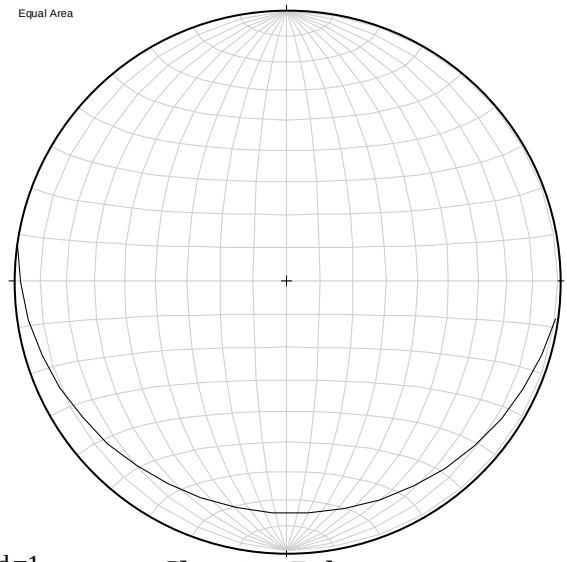

Nd=1

Clastic Dikes

Clastic Dikes Averaged

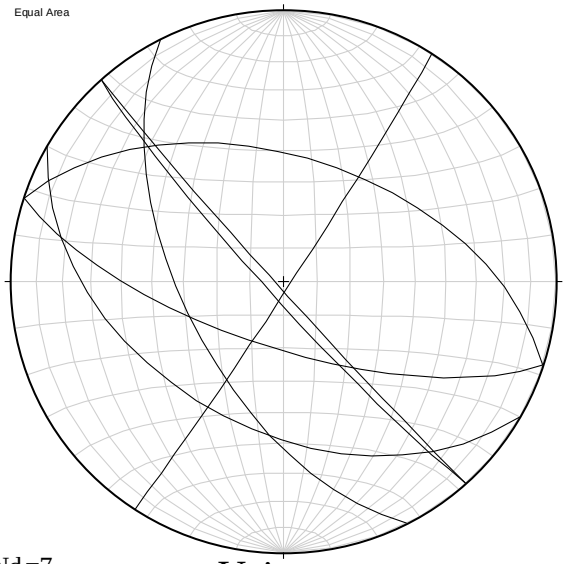

Nd=7

Veins

Veins Averaged

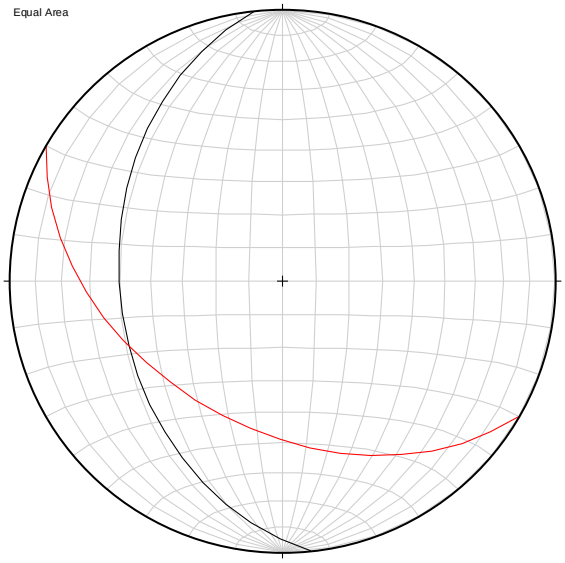

Nd=1 Np=1

Faults

Faults Averaged

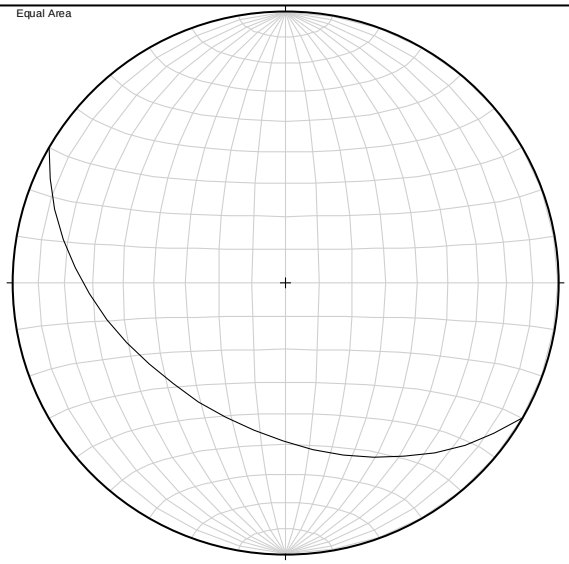

Nd=1

Clastic Dikes

Clastic Dikes Averaged

Interval: 1008.1-1009.97 Oriented

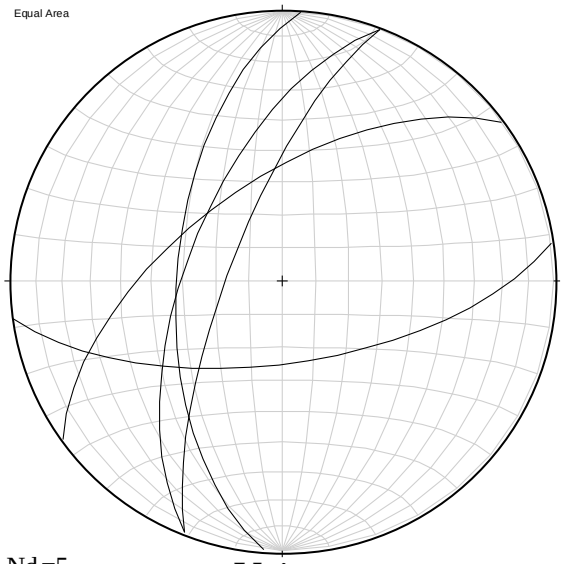

Nd=5

Veins

Veins Averaged

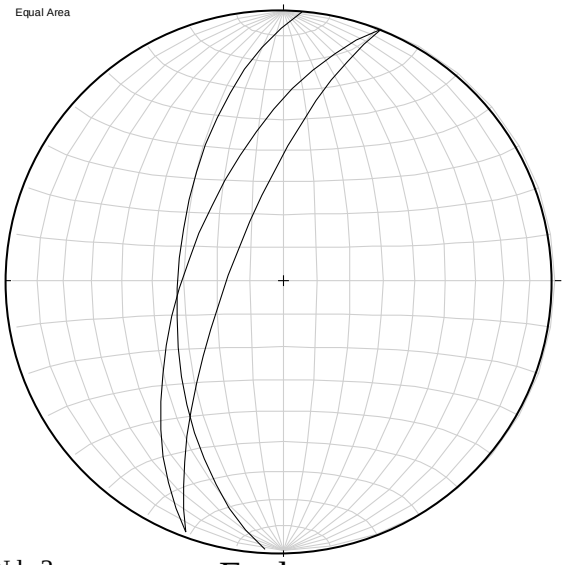

Nd=3

Faults

Faults Averaged

Nd=1

Clastic Dikes

Clastic Dikes Averaged

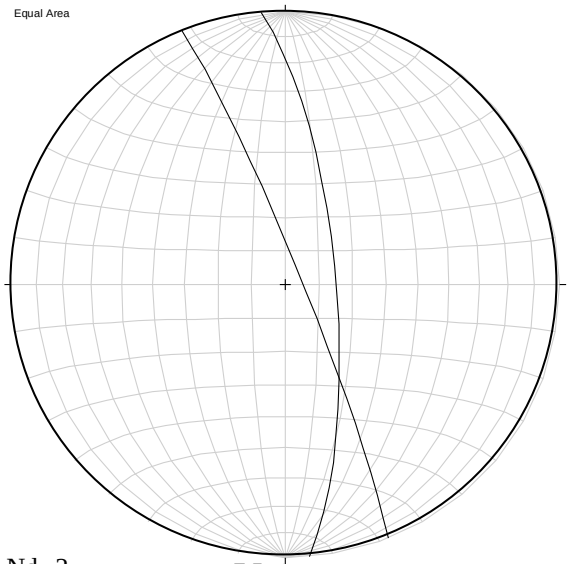

Nd=2

Veins

Veins Averaged

Faults

Faults Averaged

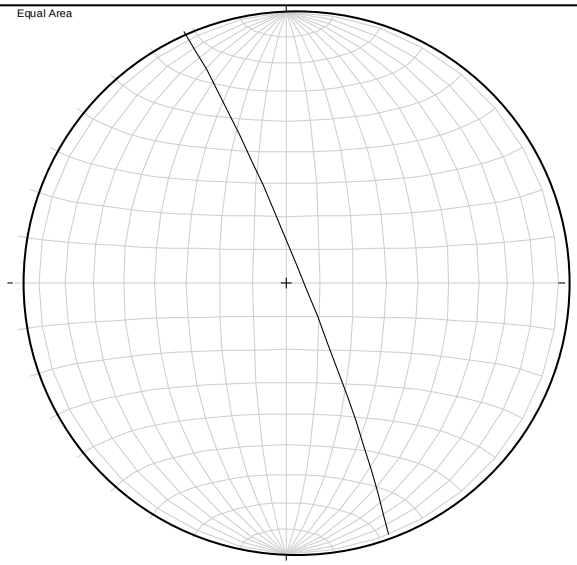

Nd=1

Clastic Dikes

Clastic Dikes Averaged

Interval: 1082.35-1098.44

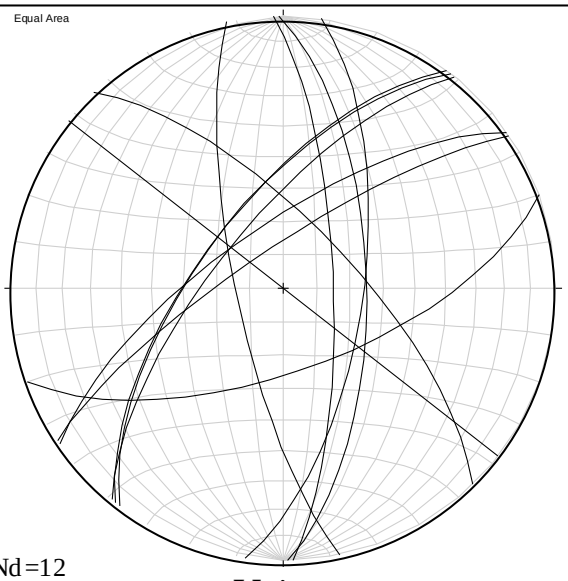

Nd=12

Veins

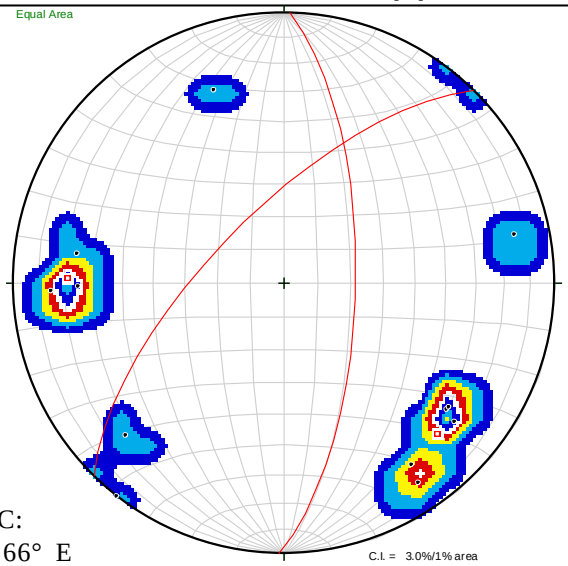

PGC:
1°, 66° E
225°, 66 °W

Veins Averaged

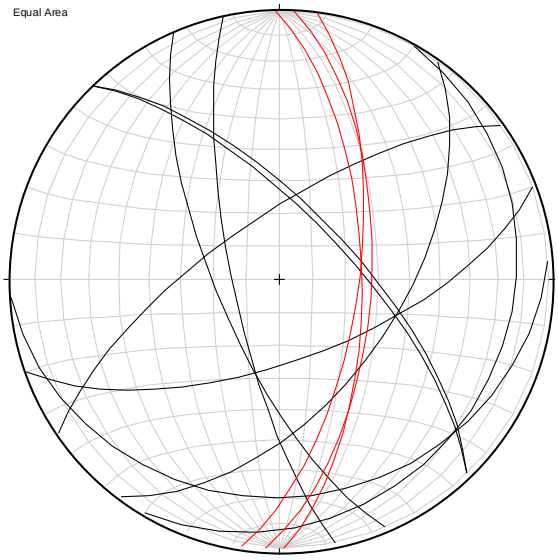

Nd=9 Np=3

Faults

Faults Averaged

Clastic Dikes

Clastic Dikes Averaged

Interval: 1111.42-1125.75

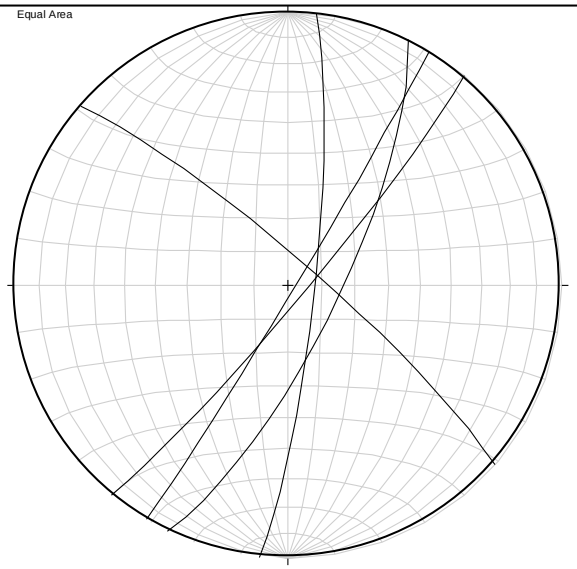

Nd=5

Veins

Veins Averaged

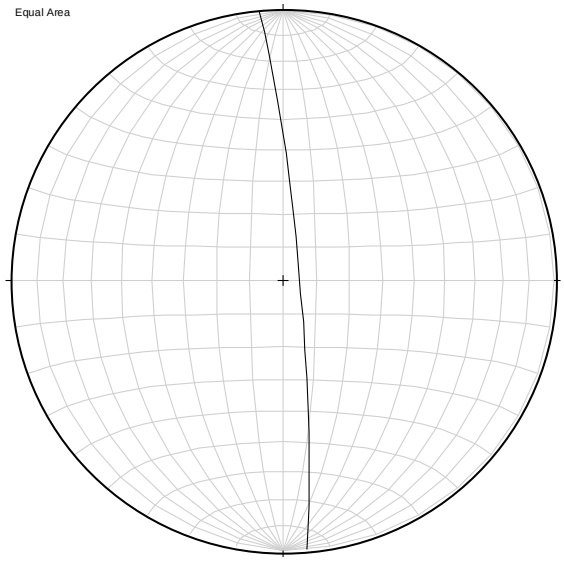

Np=1

Faults

Faults Averaged

Clastic Dikes

Clastic Dikes Averaged

Interval: 1138.33-1192.71 Oriented

Appendix B

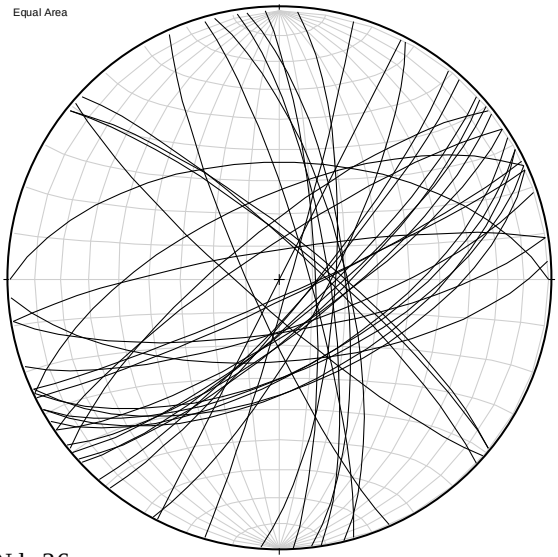

Nd=36

Veins

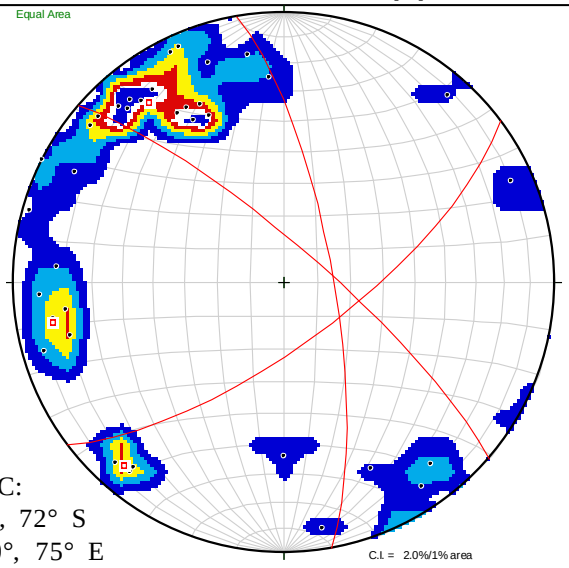

PGC:
52°, 72° S
350°, 75° E
311°, 79° N

Veins Averaged

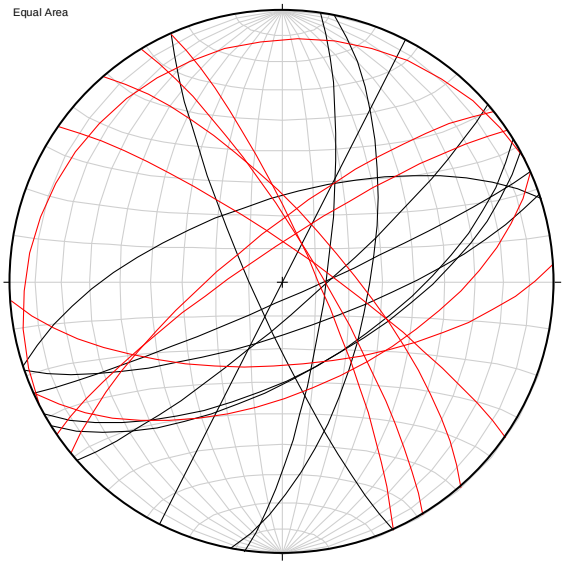

Nd=10 Np=9

Faults

Faults Averaged

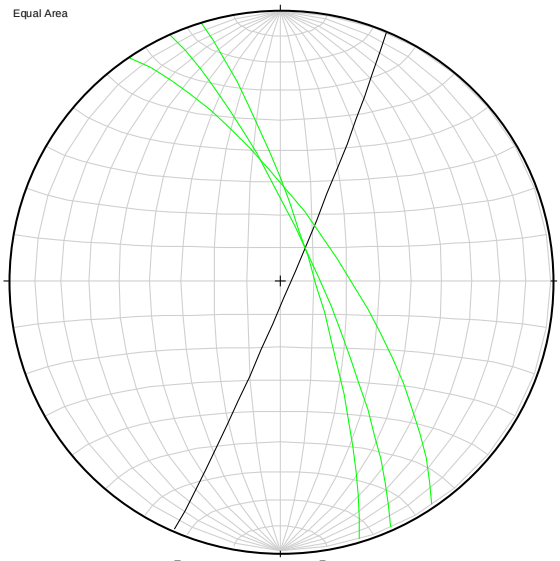

Nd=1 Np=3

Clastic Dikes

Clastic Dikes Averaged

Interval: 1192.71-1197.19

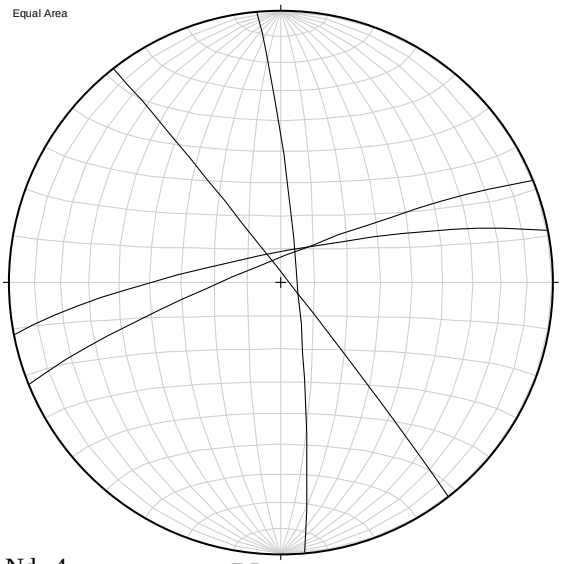

Nd=4

Veins

Veins Averaged

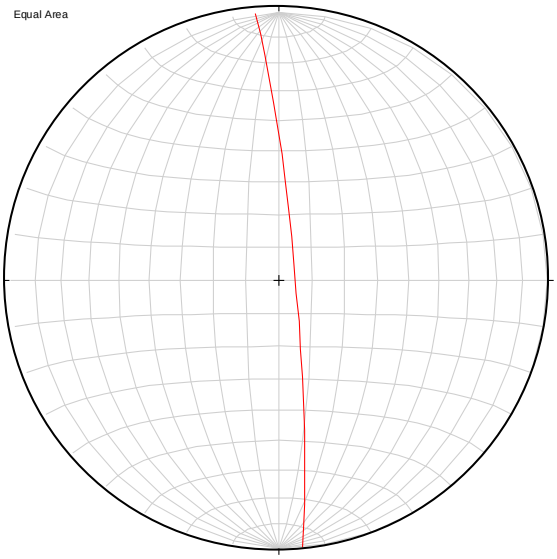

Np=1

Faults

Faults Averaged

Clastic Dikes

Clastic Dikes Averaged

Interval: 1203.36-1217.19

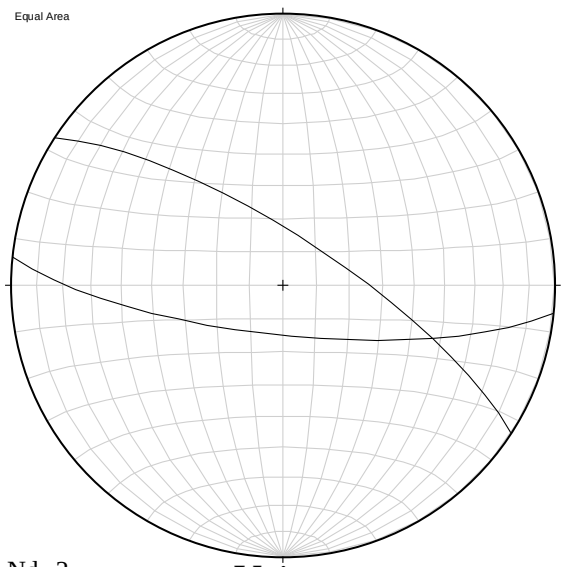

Nd=2

Veins

Veins Averaged

Faults

Faults Averaged

Clastic Dikes

Clastic Dikes Averaged

Interval: 1230.02-1233.46

Appendix B

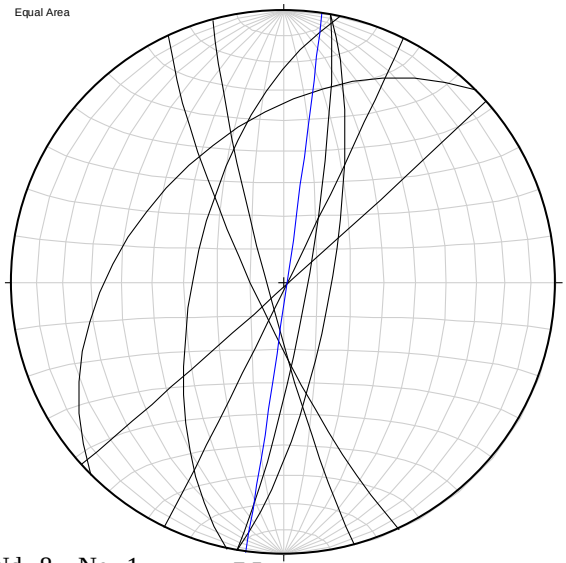

Nd=8 Np=1

Veins

Veins Averaged

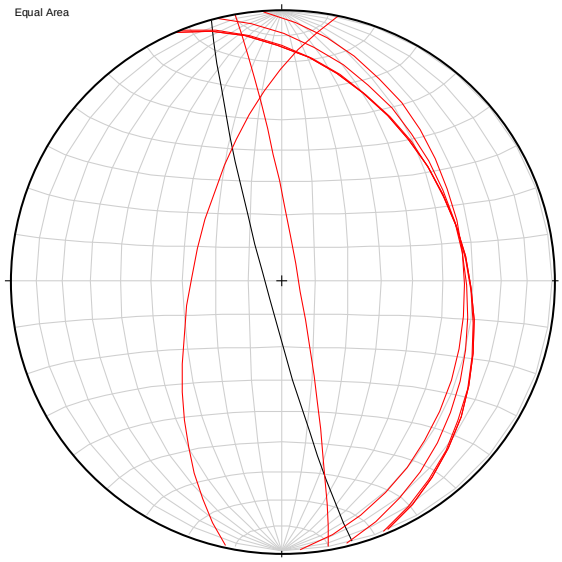

Nd=1 Np=6

Faults

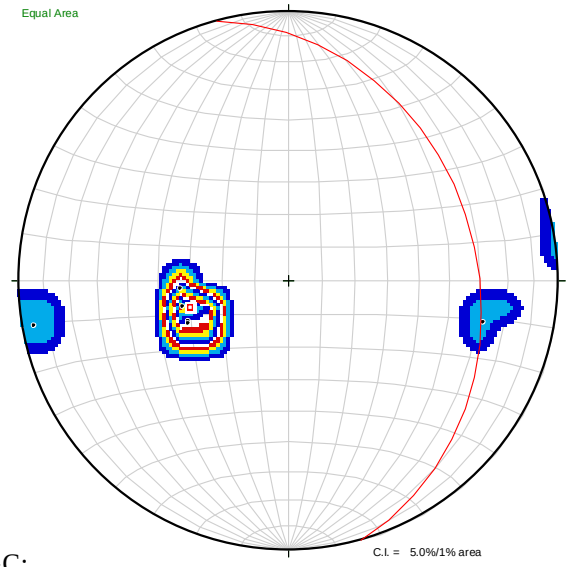

PGC:
345°, 31° E

Faults Averaged

Clastic Dikes

Clastic Dikes Averaged

Interval: 1233.46- 1236.83

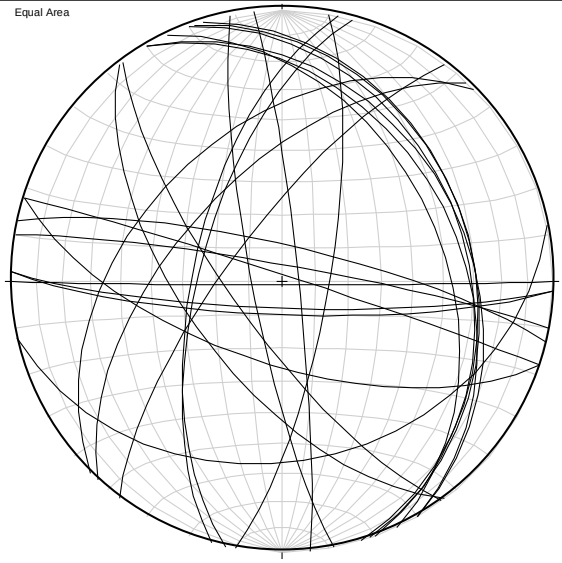

Nd=24

Veins

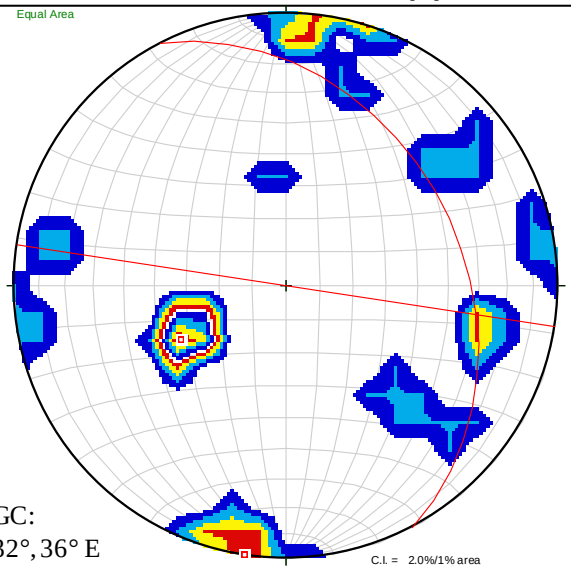

PGC:
332°, 36° E
279°, 90° N

Veins Averaged

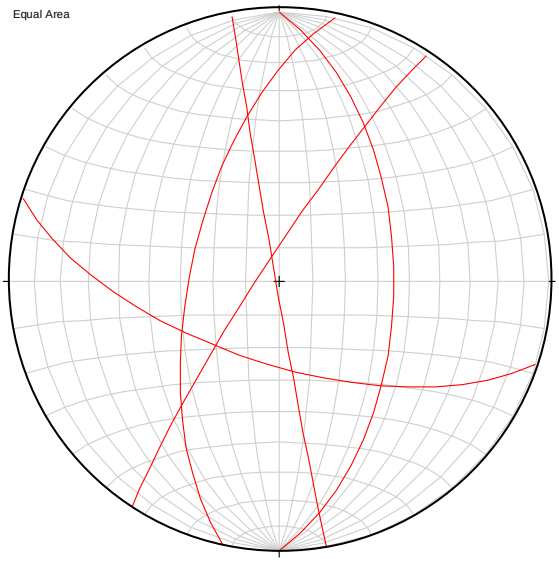

Np=5

Faults

Faults Averaged

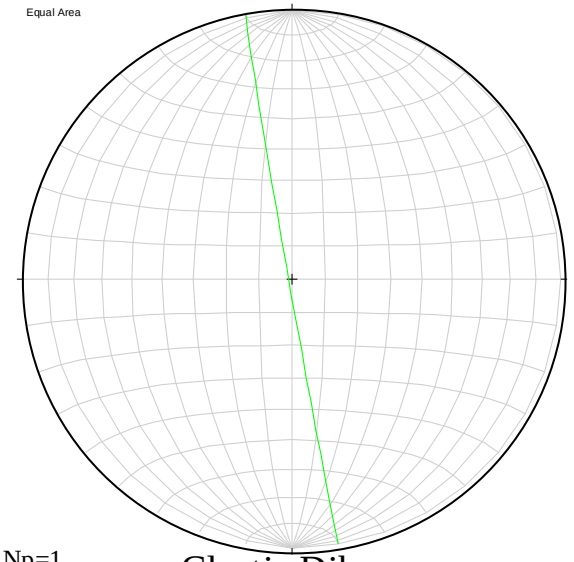

Np=1

Clastic Dikes

Clastic Dikes Averaged

Interval:1237.05- 1239.34

Appendix B

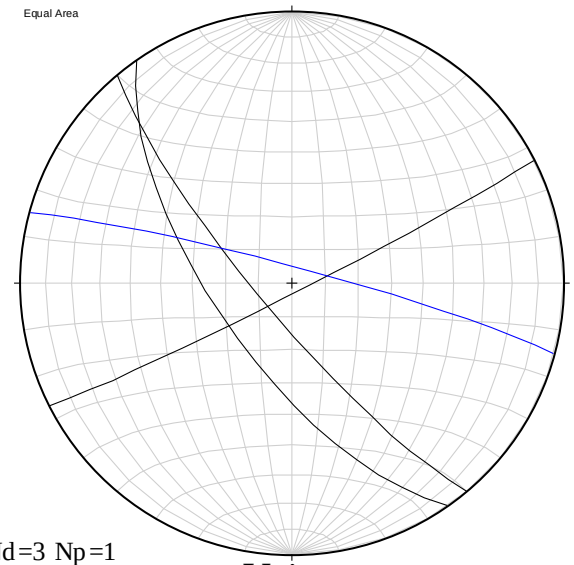

Nd=3 Np=1

Veins

Veins Averaged

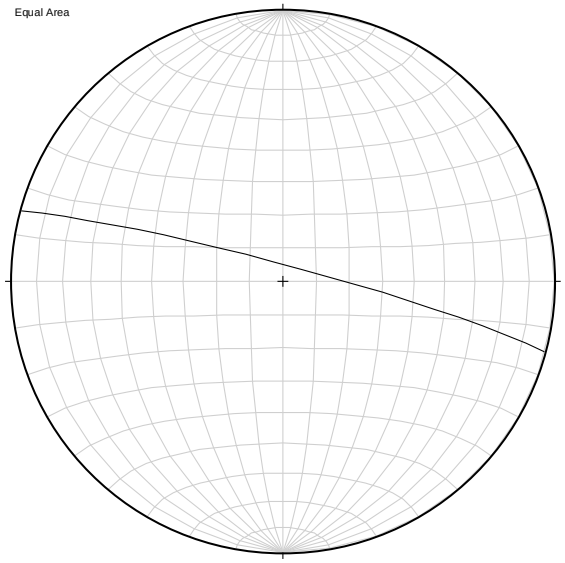

Np=1

Faults

Faults Averaged

Clastic Dikes

Clastic Dikes Averaged

Interval: 1239.34-1245.24

Appendix B

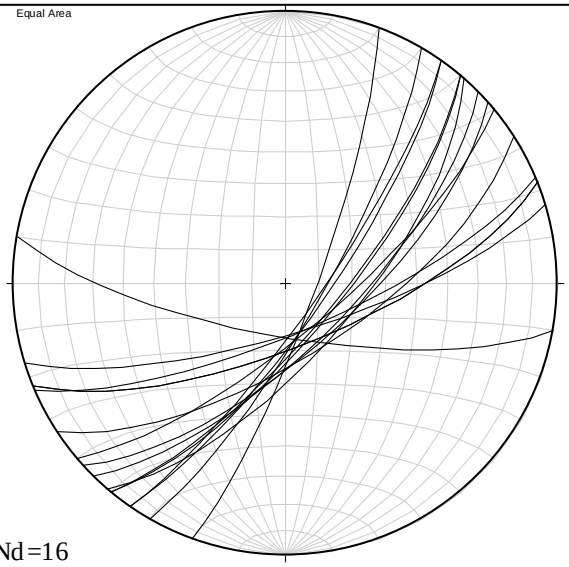

Nd=16

Veins

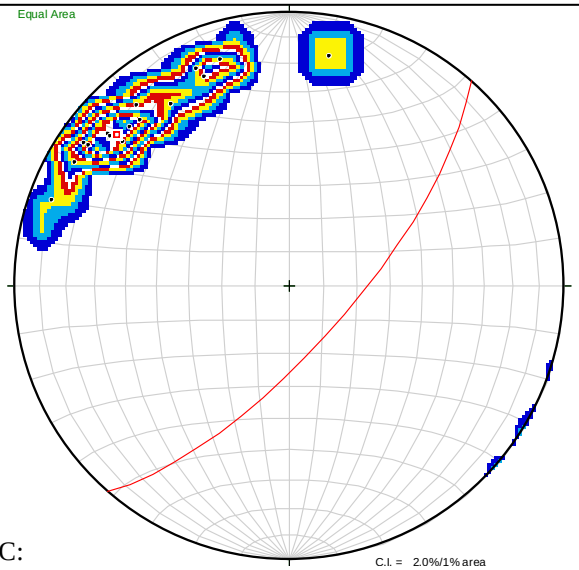

PGC:
41°, 72° E

Veins Averaged

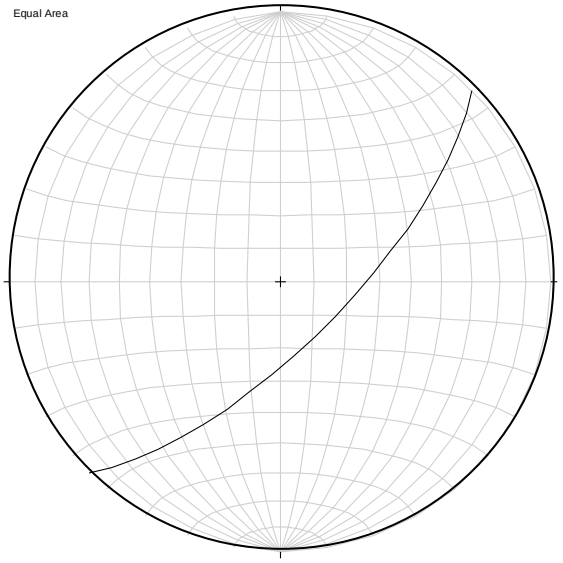

Nd=1

Faults

Faults Averaged

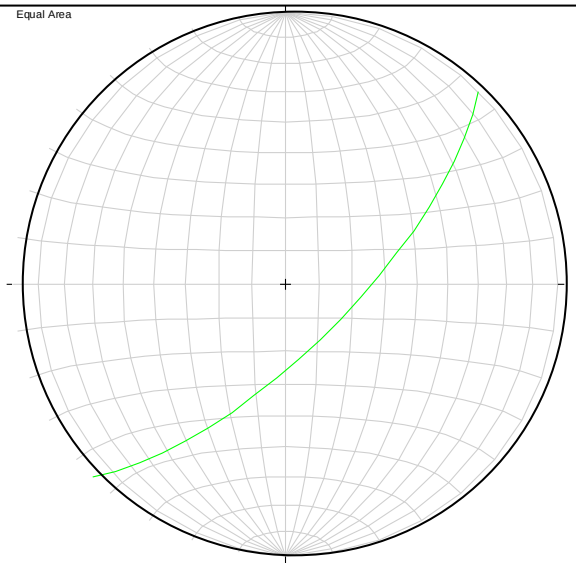

Np=1

Clastic Dikes

Clastic Dikes Averaged

Interval: 1247.61-1249.84

Appendix B

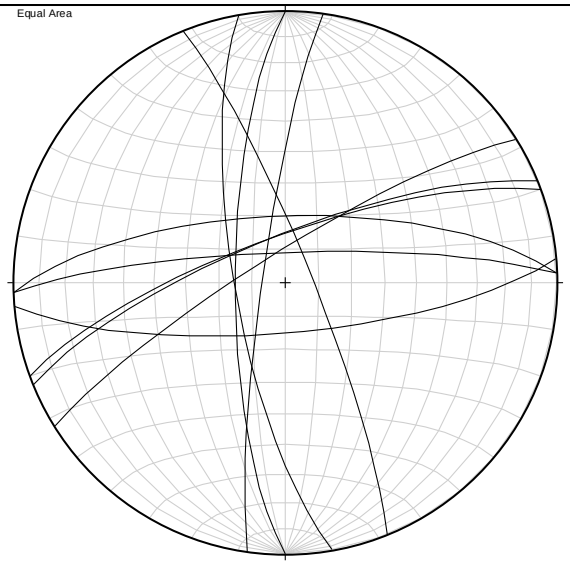

Nd=10

Veins

Veins Averaged

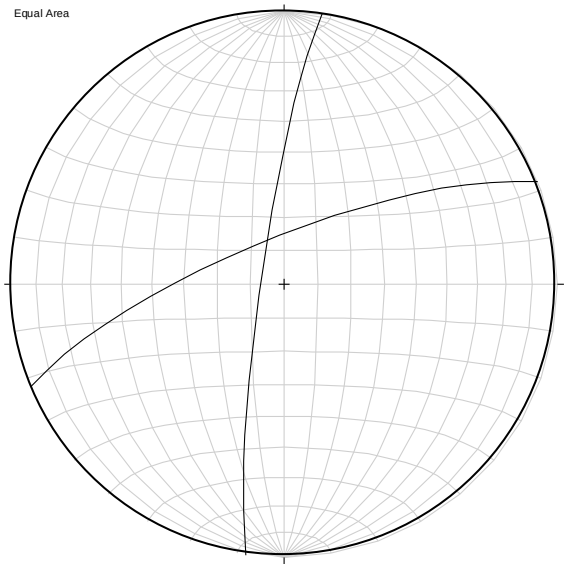

Nd=2

Faults

Faults Averaged

Clastic Dikes

Clastic Dikes Averaged

Interval:1255.84-1264.14

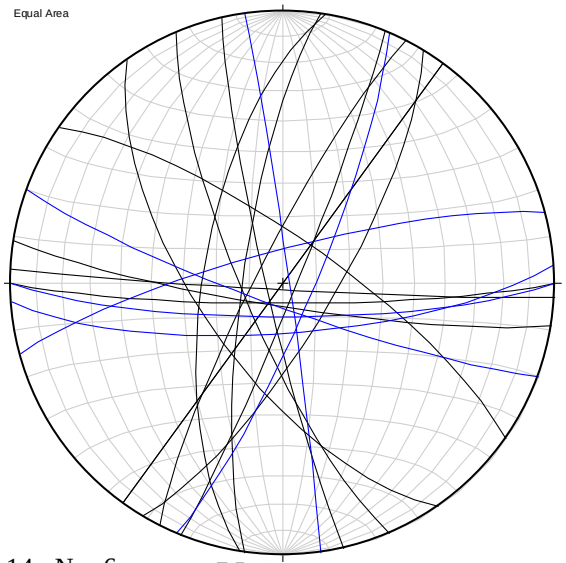

Nd=14 Np=6

Veins

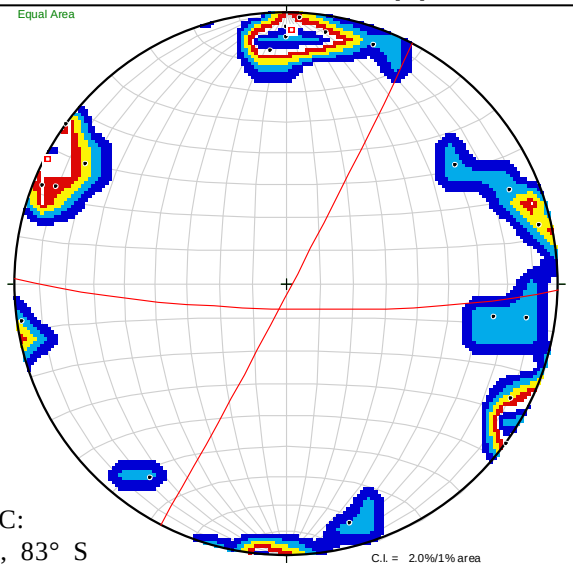

PGC:
91°, 83° S
28°, 89° E

Veins Averaged

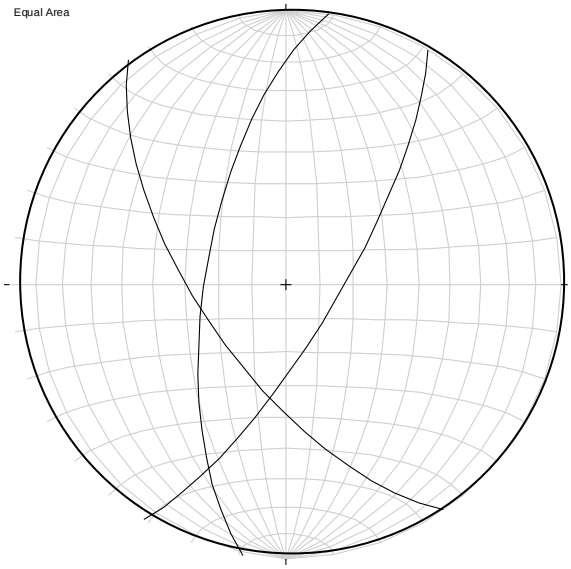

Nd=3

Faults

Faults Averaged

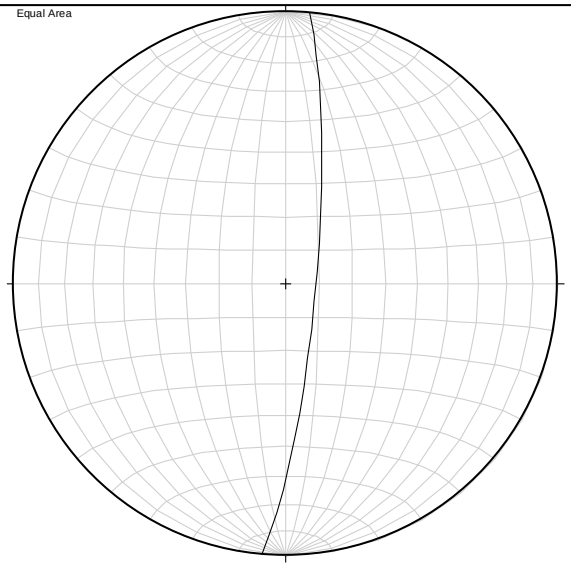

Np=1

Clastic Dikes

Clastic Dikes Averaged

Interval: 1264.63-1267.25

Appendix B

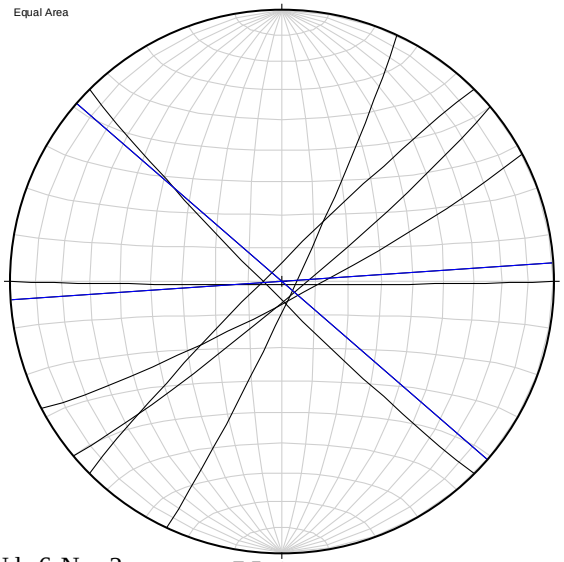

Nd=6 Np=2

Veins

Veins Averaged

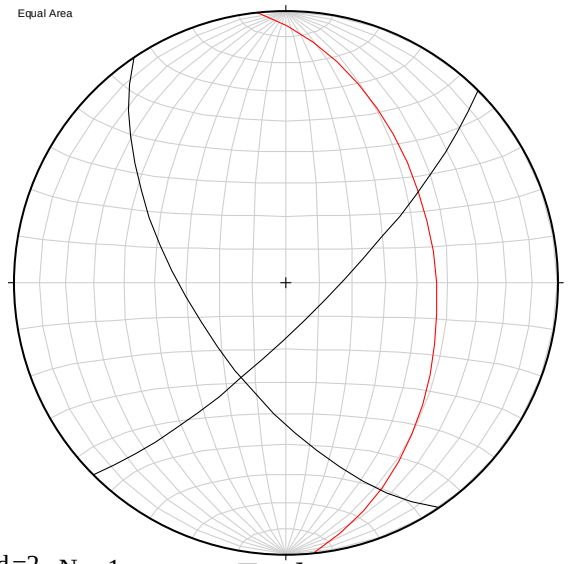

Nd=2 Np=1

Faults

Faults Averaged

Clastic Dikes

Clastic Dikes Averaged

Interval: 1267.71-1272.77

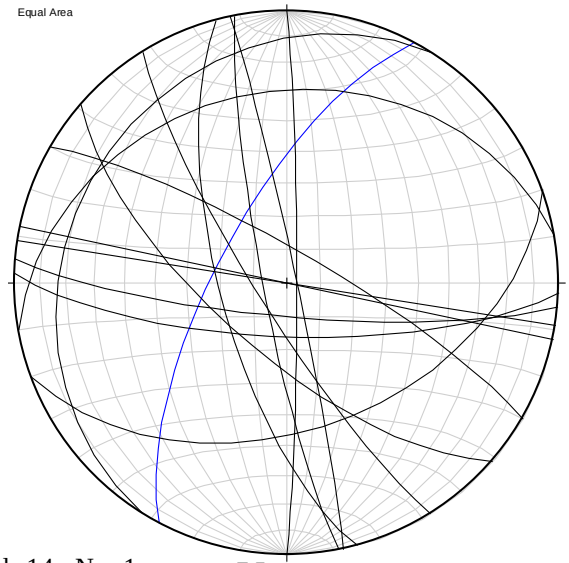

Nd=14 Np=1 Veins

Veins Averaged

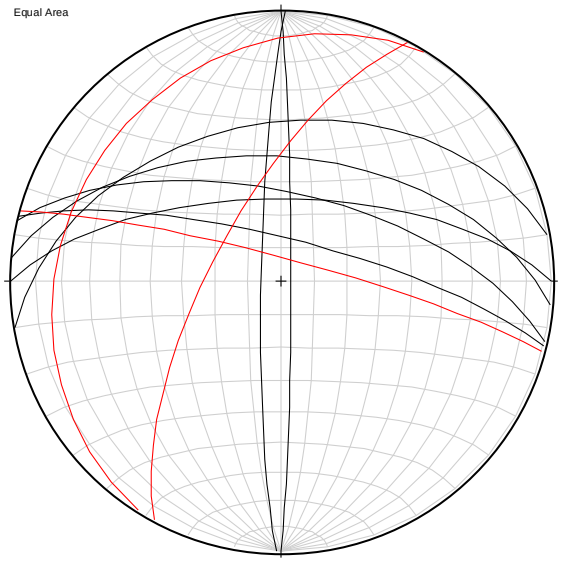

Nd=7 Np=3 Faults

Faults Averaged

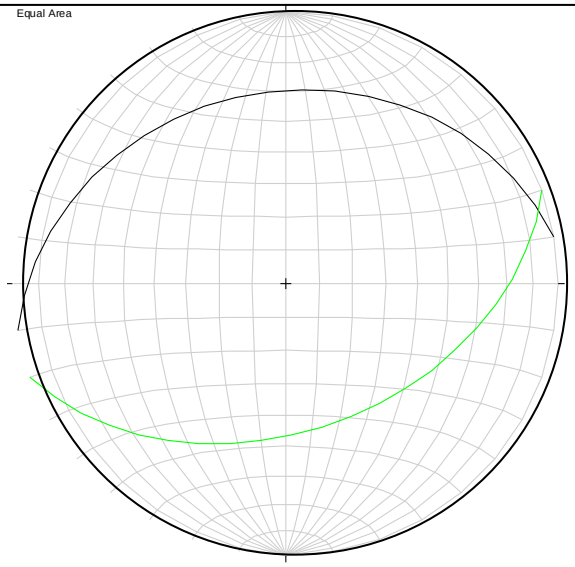

Nd=1 Np=1 Clastic Dikes

Clastic Dikes Averaged

Interval: 1272.94-1284.87

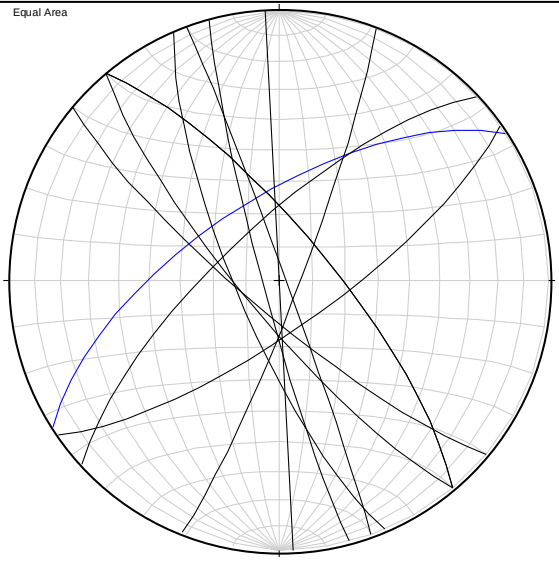

Nd=10 Np=1

Veins

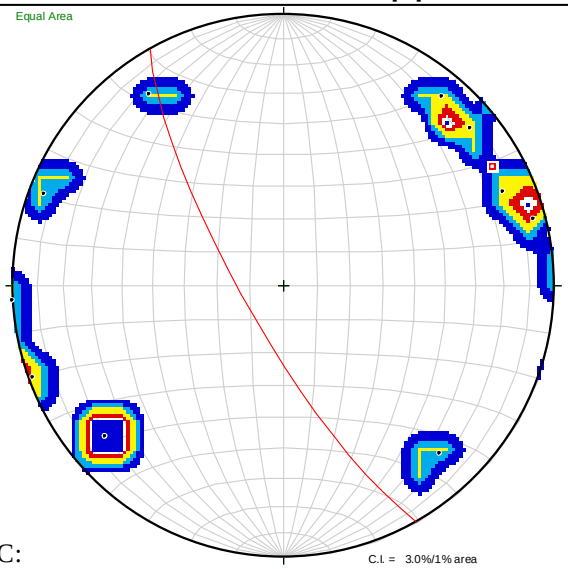

PGC:
150°, 78° W

Veins Averaged

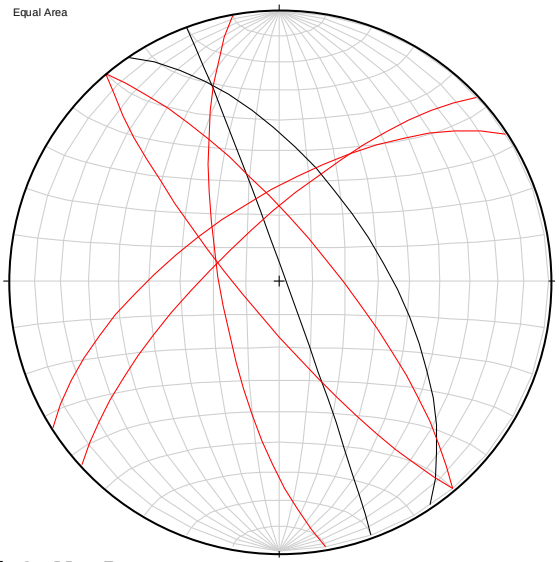

Nd=2 Np=5

Faults

Faults Averaged

Clastic Dikes

Clastic Dikes Averaged

Appendix C:

Stereoplots of natural fractures measured from CoreBase®. Definite fractures are labeled as Nd, whereas possible fracture types are labeled Np. All definite fractures are plotted in black. Possible veins are plotted in blue, possible faults are plotted in red, and possible clastic dikes are plotted in green

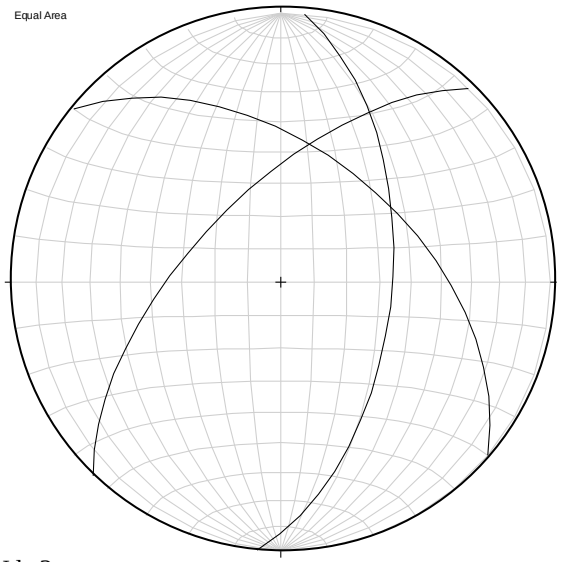

Nd=3

Veins

Veins Averaged

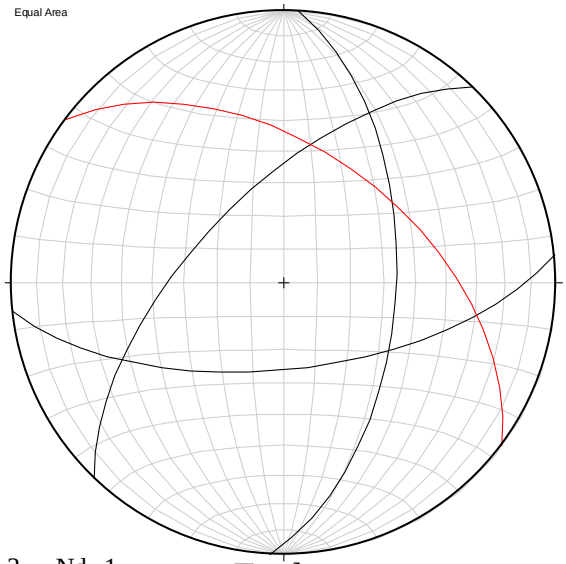

Nd=3 Nd=1

Faults

Faults Averaged

Clastic Dikes

Clastic Dikes Averaged

Veins

Veins Averaged

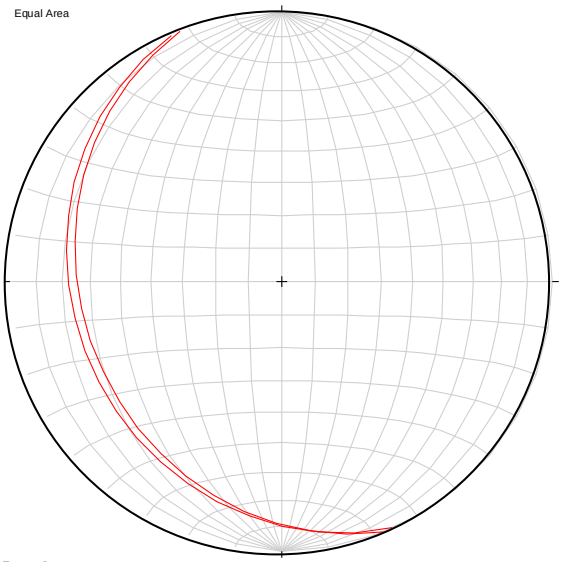

Np=2

Faults

Faults Averaged

Clastic Dikes

Clastic Dikes Averaged

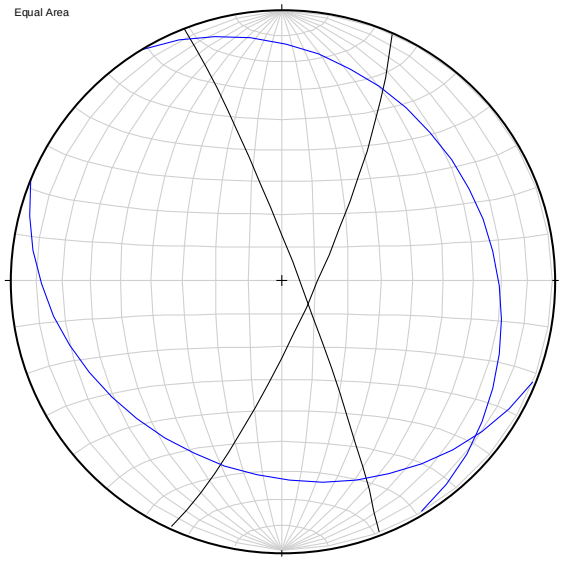

Nd=2 Np=2 Veins

Veins Averaged

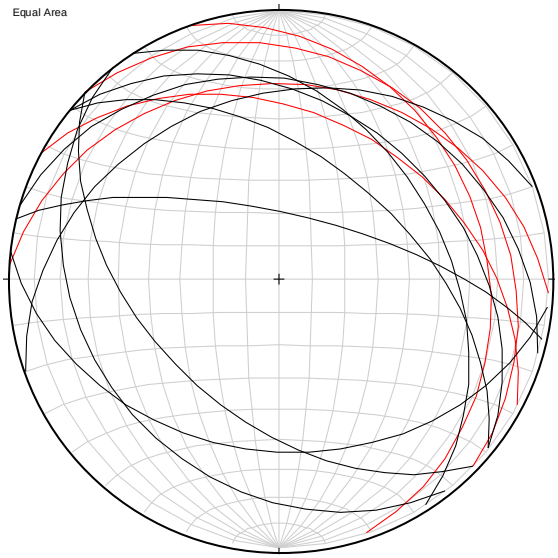

Nd=9 Np=4 Faults

Faults Averaged

Clastic Dikes

Clastic Dikes Averaged

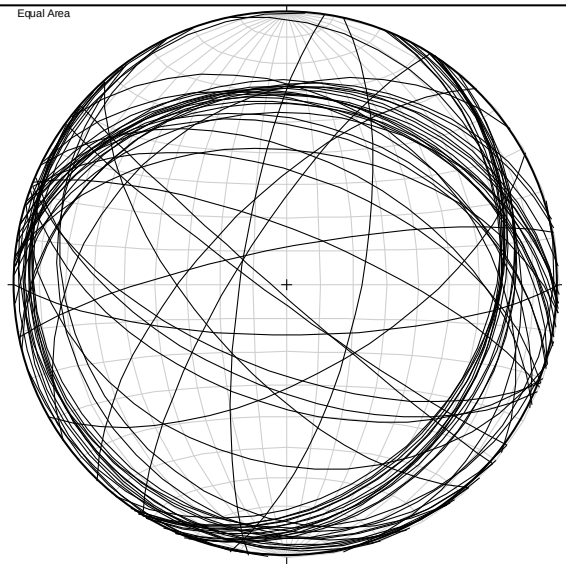

Nd=65

Veins

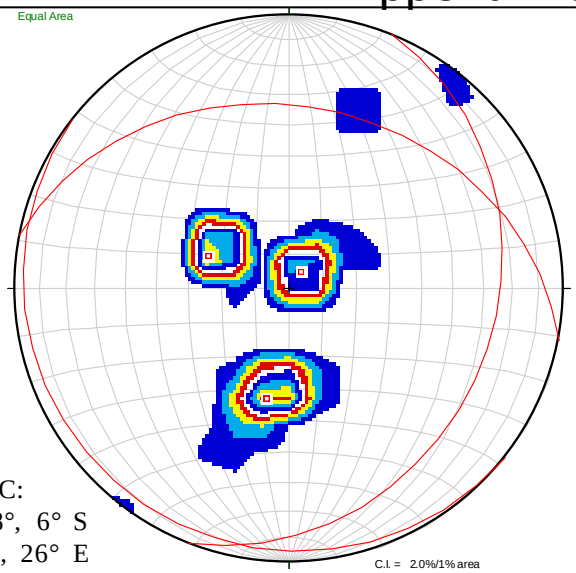

PGC:
128°, 6° S
22°, 26° E
281°, 34° N

Veins Averaged

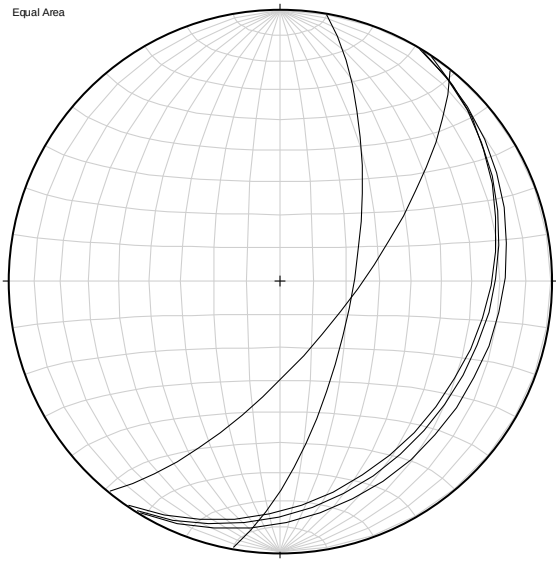

Nd=5

Faults

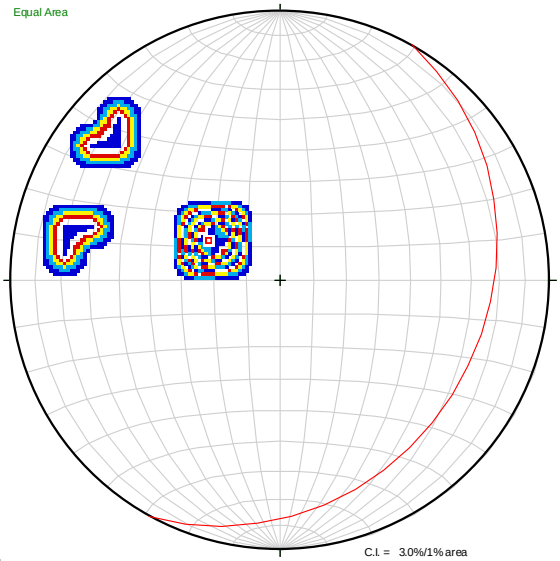

PGC:
29°, 24° E

Faults Averaged

Clastic Dikes

Clastic Dikes Averaged

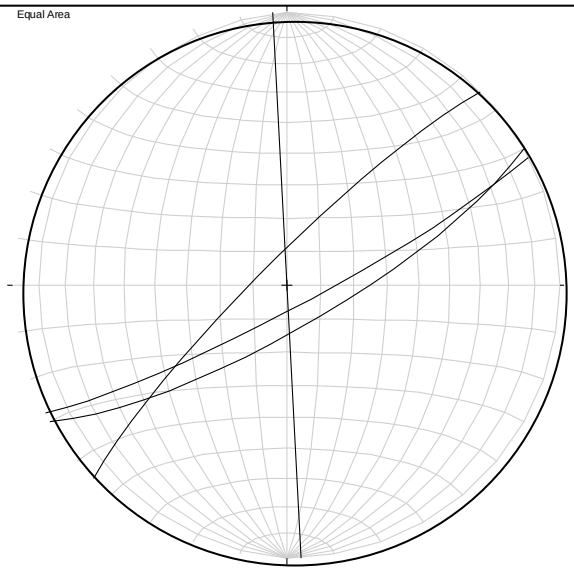

Nd=4

Veins

Veins Averaged

Faults

Faults Averaged

Clastic Dikes

Clastic Dikes Averaged

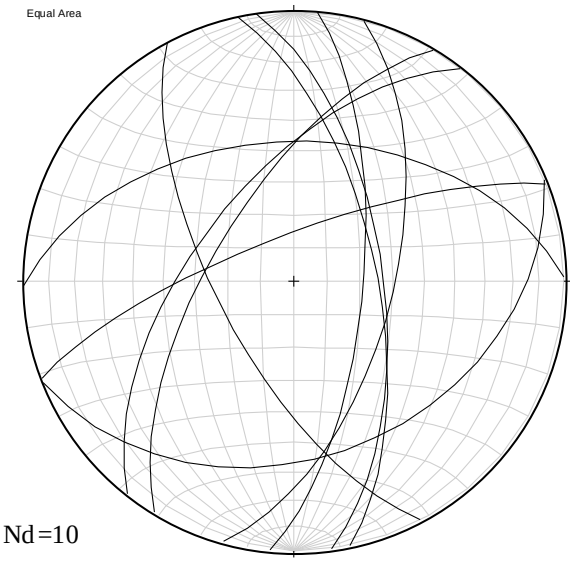

Nd=10

Veins

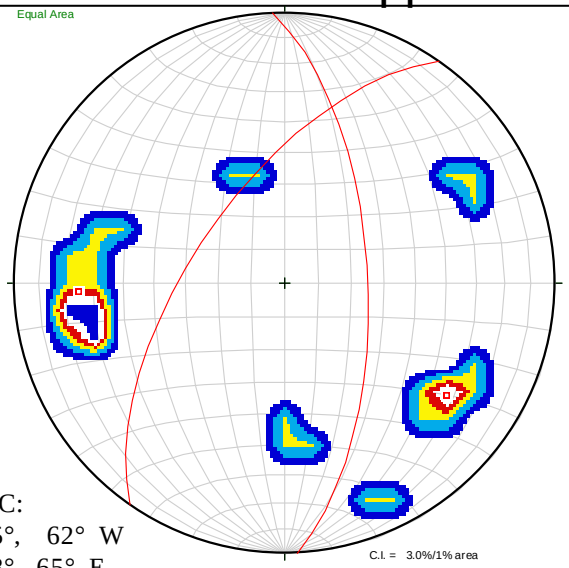

PGC:
215°, 62° W
358°, 65° E

Veins Averaged

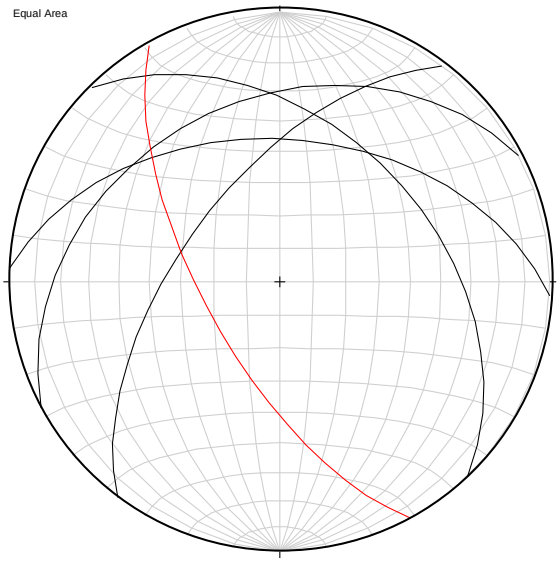

Nd=4 Np=1

Faults

Faults Averaged

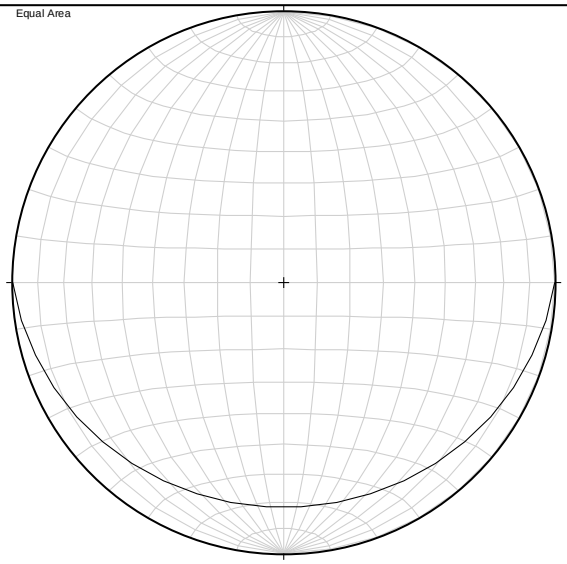

Nd=1

Clastic Dikes

Clastic Dikes Averaged

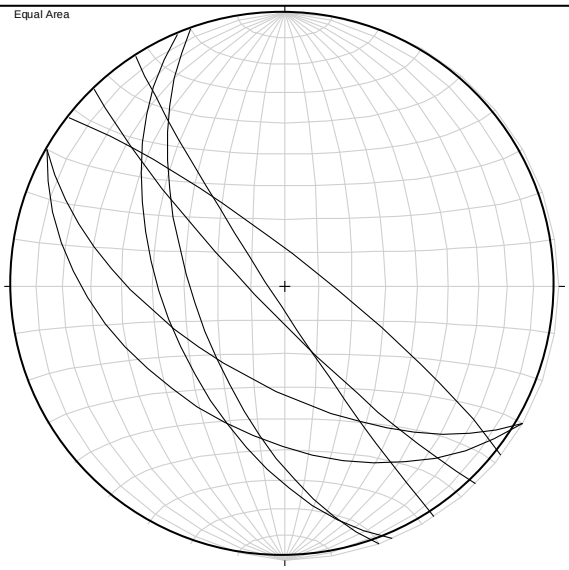

Nd=8

Veins

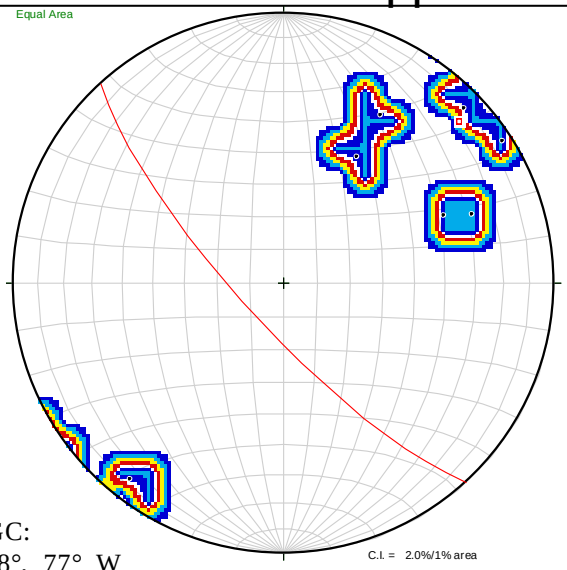

PGC:
138°, 77° W

Veins Averaged

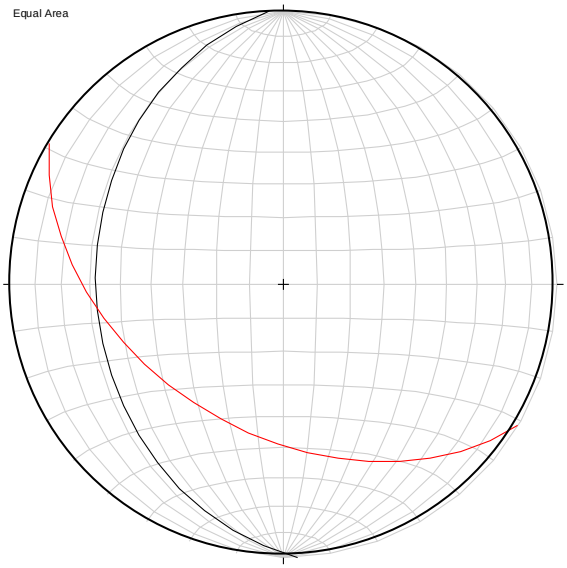

Nd=1 Np=1

Faults

Faults Averaged

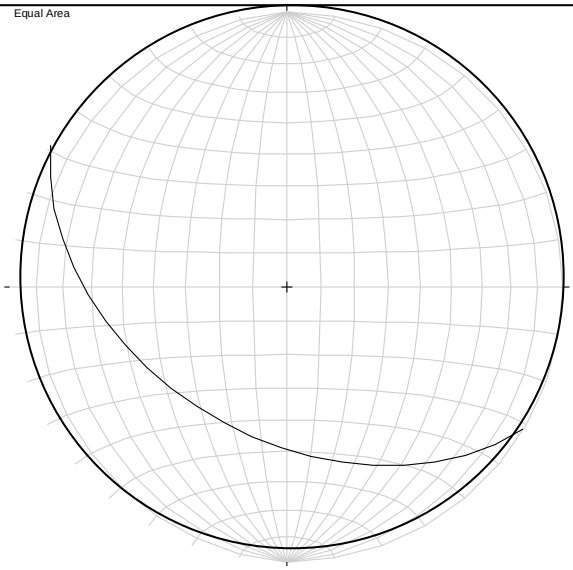

Nd=1

Clastic Dikes

Clastic Dikes Averaged

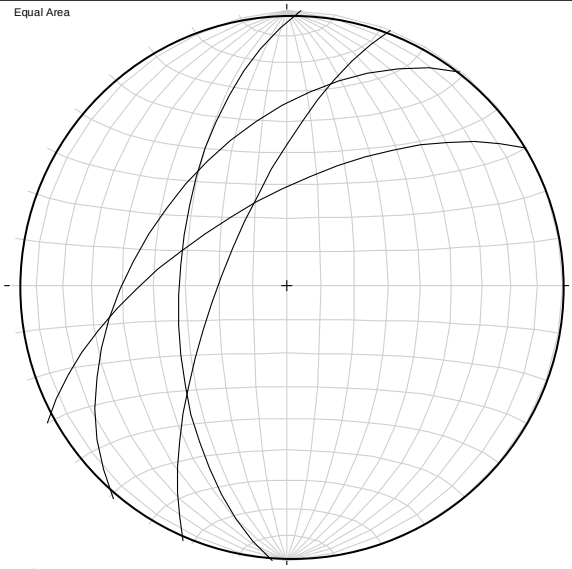

Nd=4

Veins

Veins Averaged

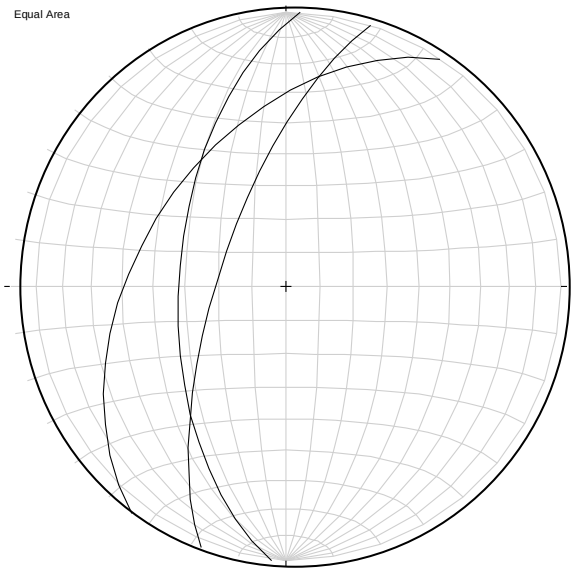

Nd=3

Faults

Faults Averaged

Clastic Dikes

Clastic Dikes Averaged

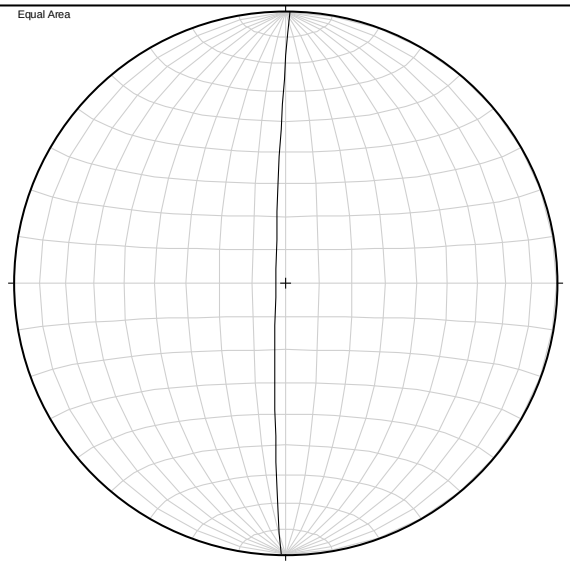

Nd=1

Veins

Veins Averaged

Faults

Faults Averaged

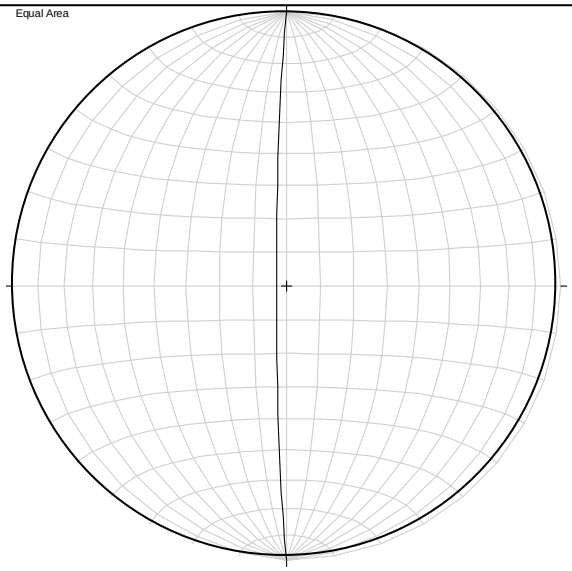

Nd=1

Clastic Dikes

Clastic Dikes Averaged

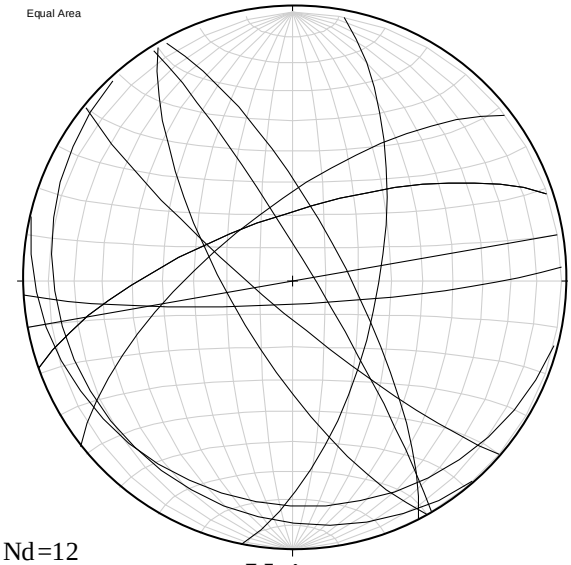

Nd=12

Veins

Veins Averaged

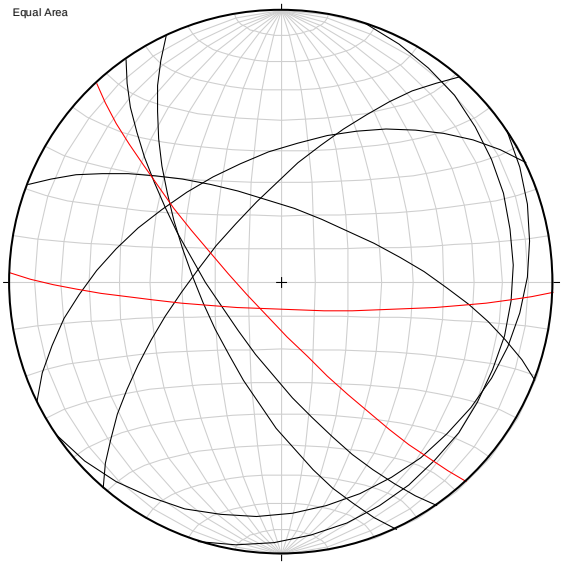

Nd=7 Np=2

Faults

Faults Averaged

Clastic Dikes

Clastic Dikes Averaged

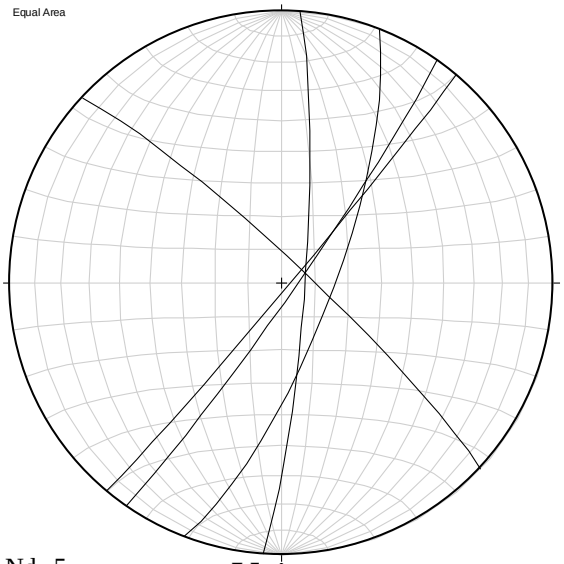

Veins

Veins Averaged

Faults

Faults Averaged

Clastic Dikes

Clastic Dikes Averaged

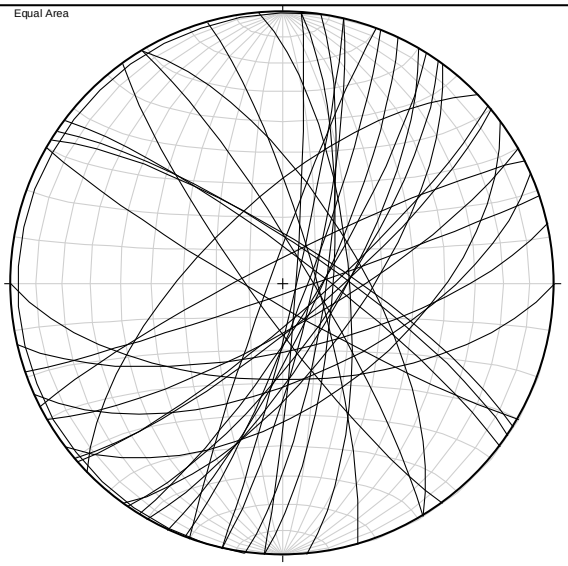

Nd=32

Veins

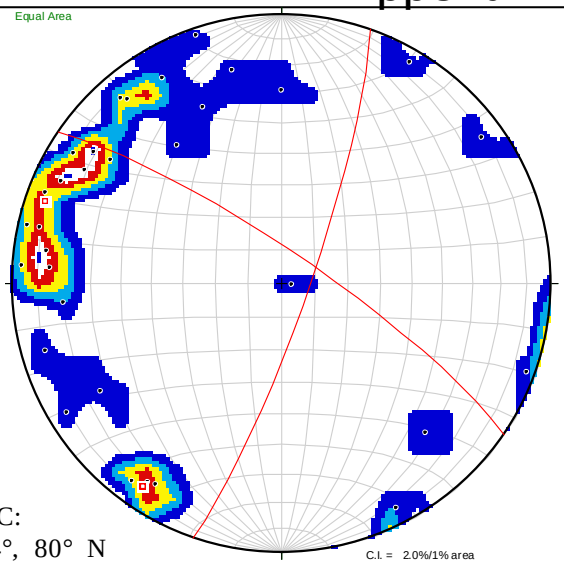

PGC:
304°, 80° N
19°, 82° E

Veins Averaged

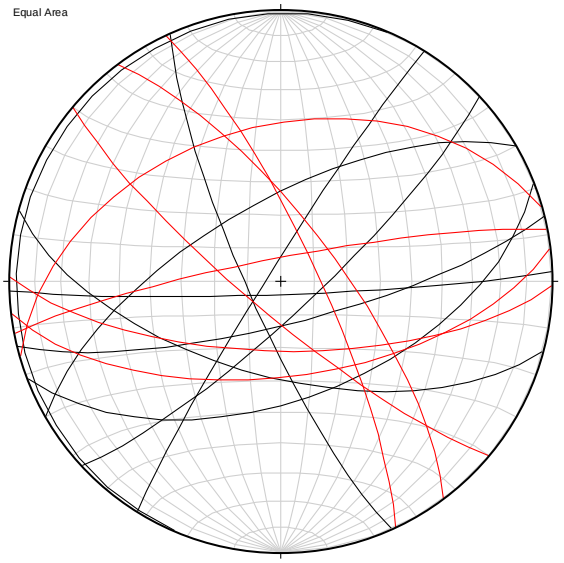

Nd=9 Np=7

Faults

Faults Averaged

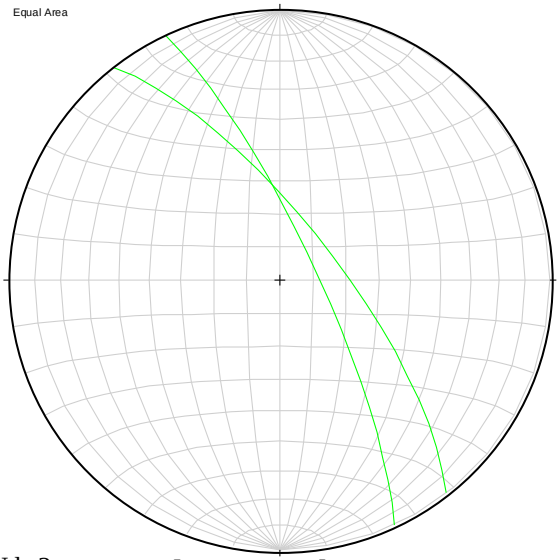

Nd=2

Clastic Dikes

Clastic Dikes Averaged

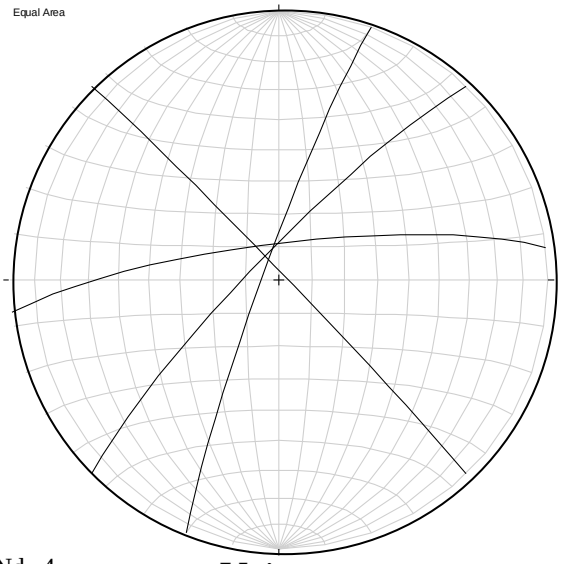

Nd=4

Veins

Veins Averaged

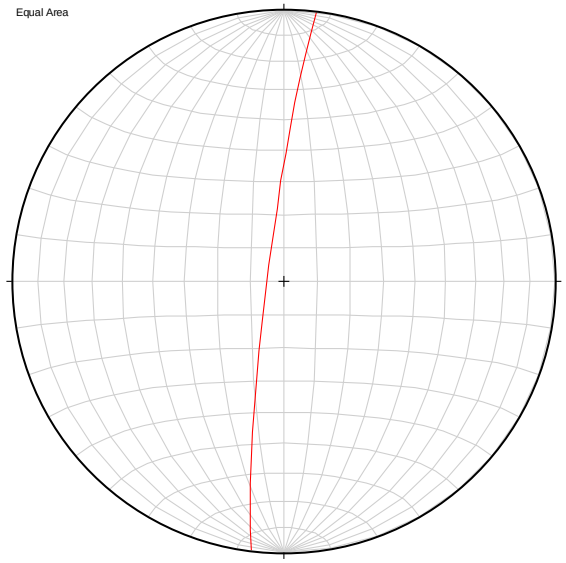

Np=1

Faults

Faults Averaged

Clastic Dikes

Clastic Dikes Averaged

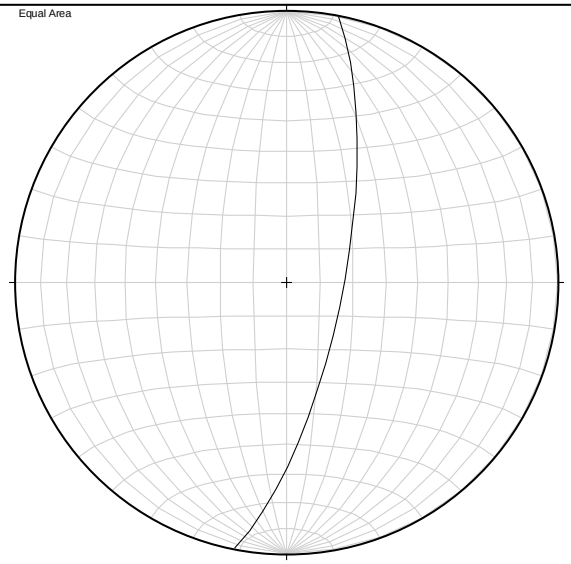

Nd=1

Veins

Veins Averaged

Faults

Faults Averaged

Clastic Dikes

Clastic Dikes Averaged

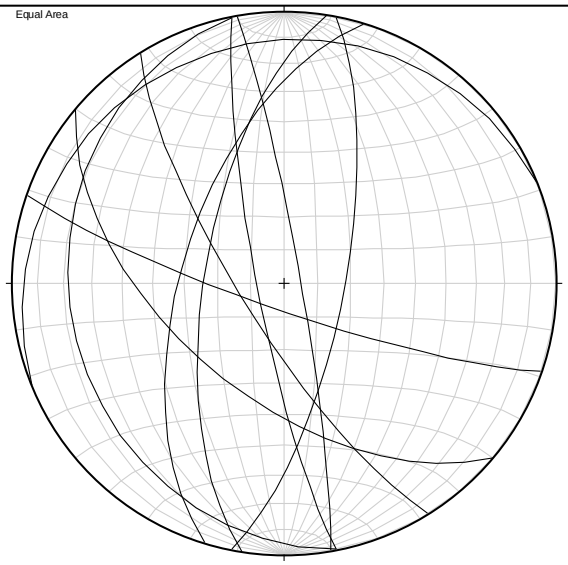

Nd=10

Veins

Veins Averaged

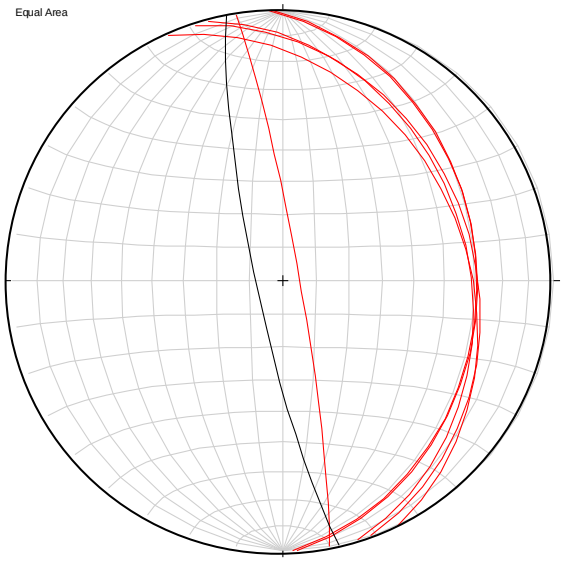

Nd=1 Np=6

Faults

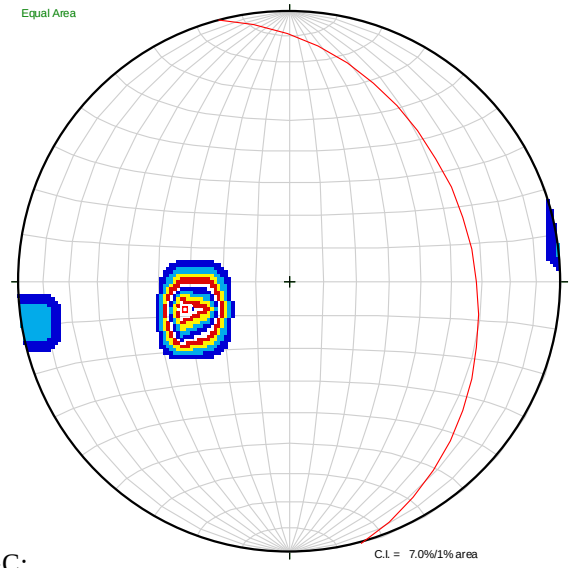

PGC:
345°, 33° E

Faults Averaged

Clastic Dikes

Clastic Dikes Averaged

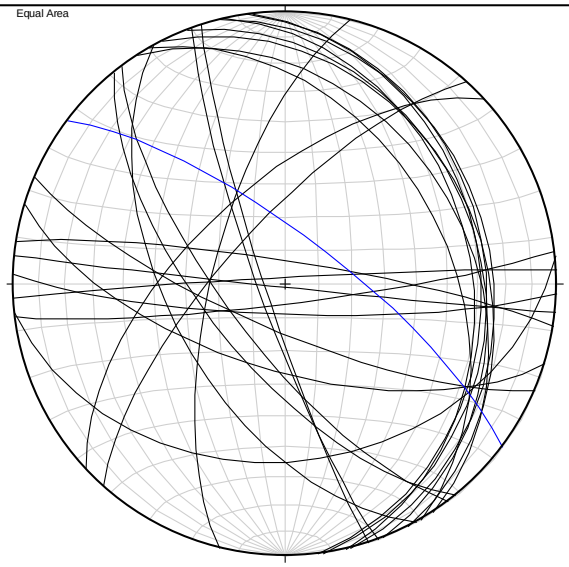

Nd=24 Np=1

Veins

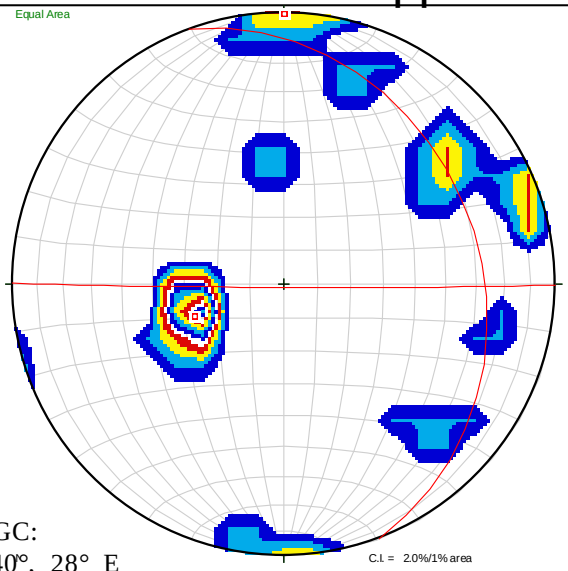

PGC:
340°, 28° E
90°, 89° S

Veins Averaged

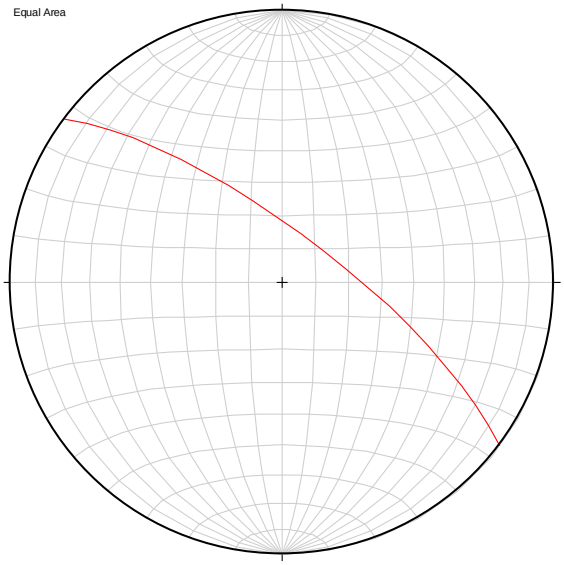

Np=1

Faults

Faults Averaged

Np=1

Clastic Dikes

Clastic Dikes Averaged

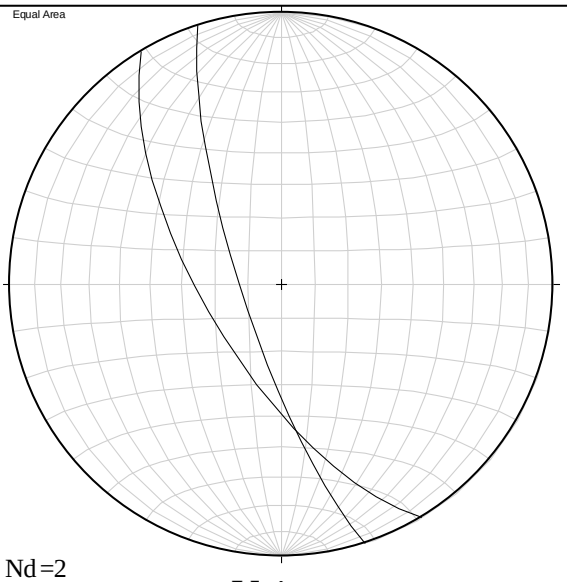

Nd=2

Veins

Veins Averaged

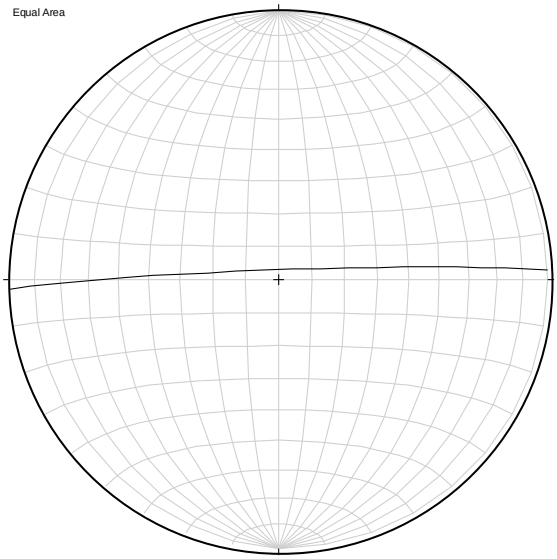

Nd=1

Faults

Faults Averaged

Np=1

Clastic Dikes

Clastic Dikes Averaged

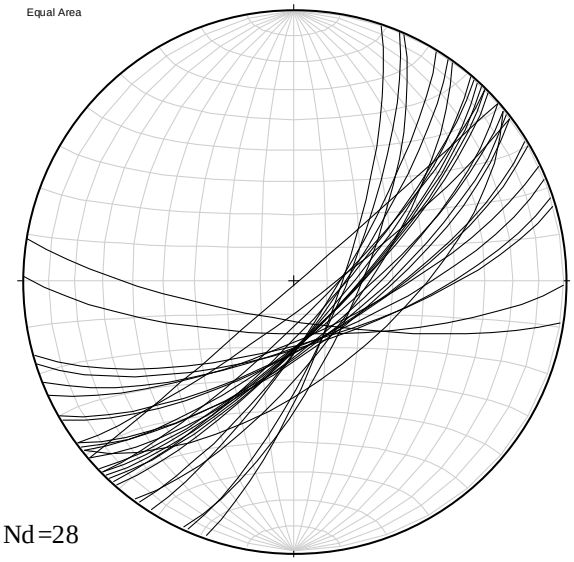

Nd=28

Veins

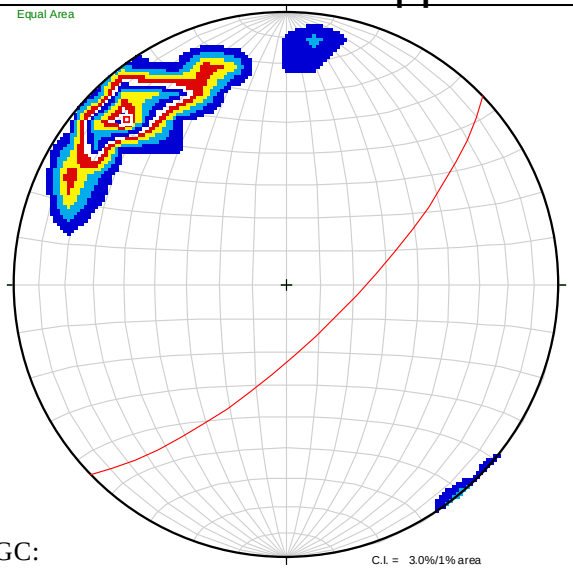

PGC:
46°, 73° S

Veins Averaged

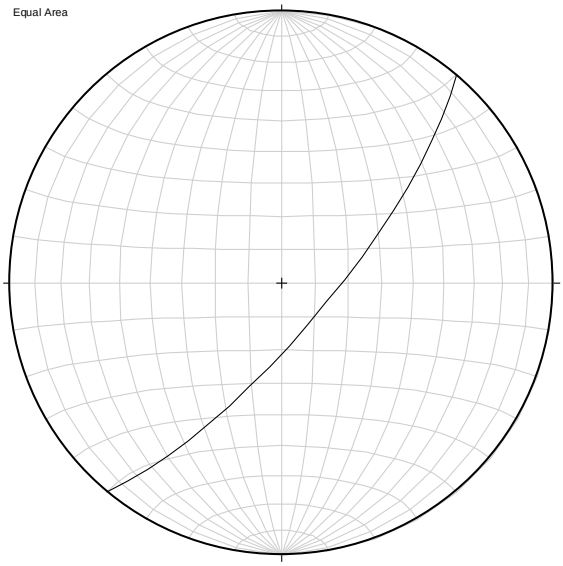

Nd=1

Faults

Faults Averaged

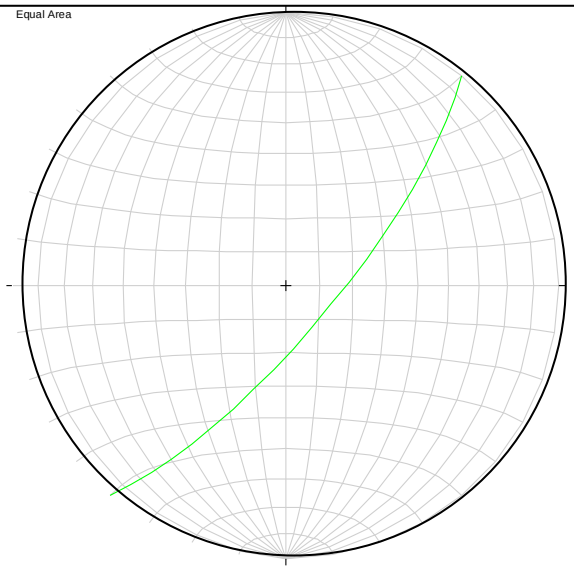

Np=1

Clastic Dikes

Clastic Dikes Averaged

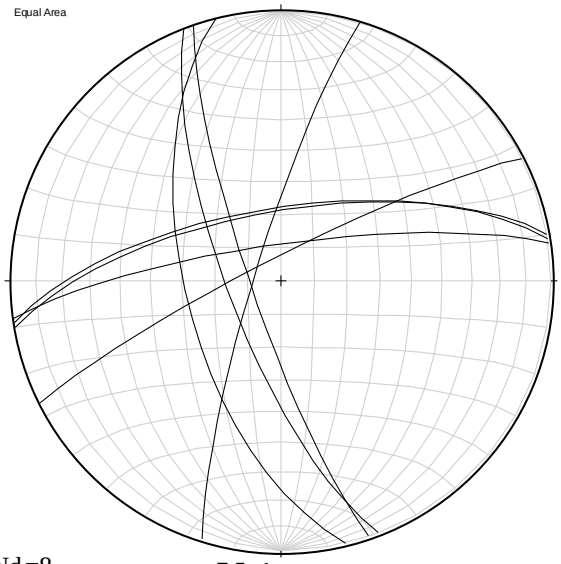

Nd=8

Veins

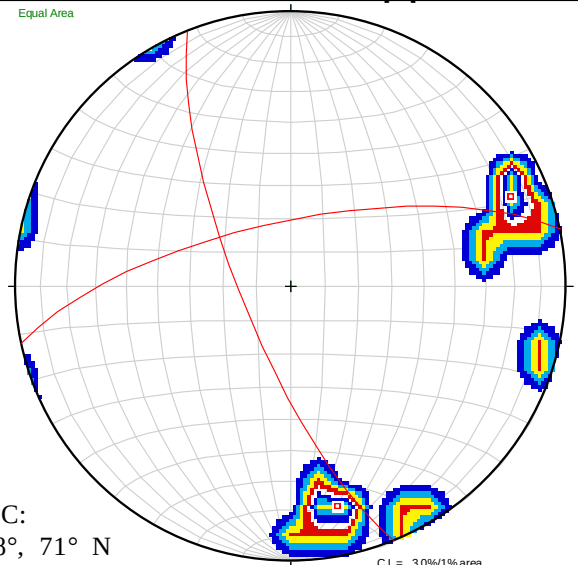

PGC:
258°, 71° N
158°, 75° W

Veins Averaged

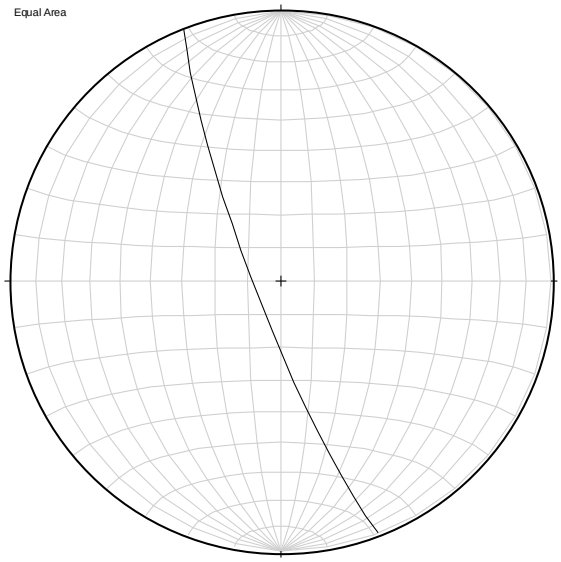

Nd=1

Faults

Faults Averaged

Clastic Dikes

Clastic Dikes Averaged

Interval:1255.84-1264.14

Appendix C

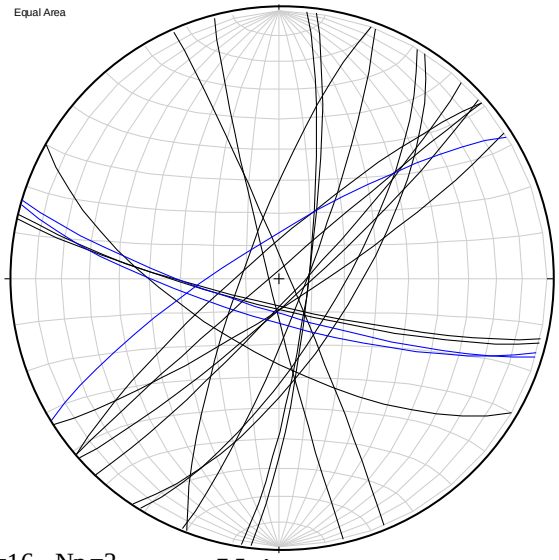

Nd=16 Np=3

Veins

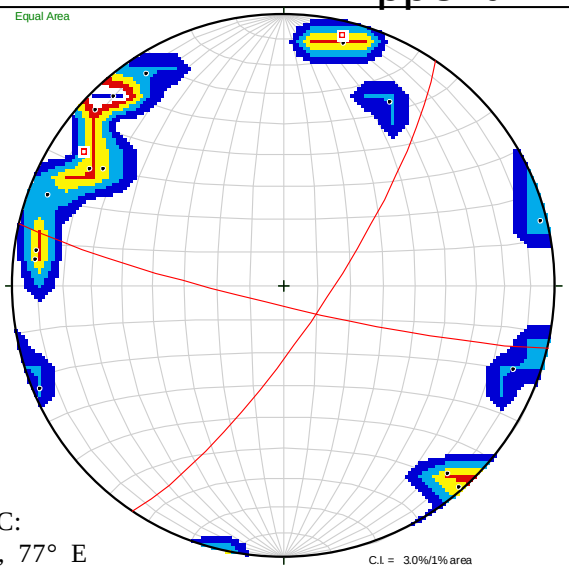

PGC:
34°, 77° E
103°, 84° S

Veins Averaged

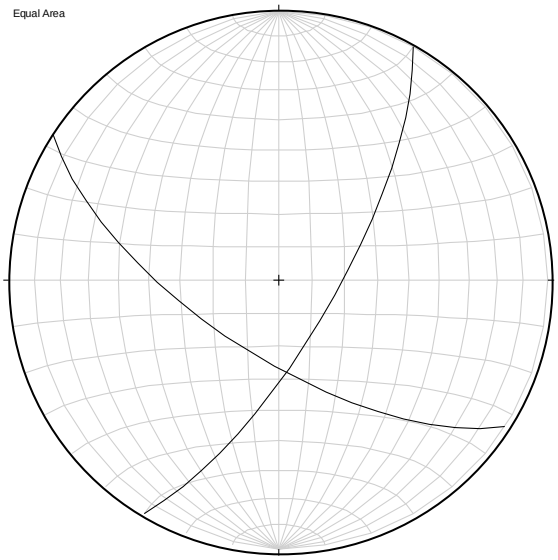

Nd=2

Faults

Faults Averaged

Clastic Dikes

Clastic Dikes Averaged

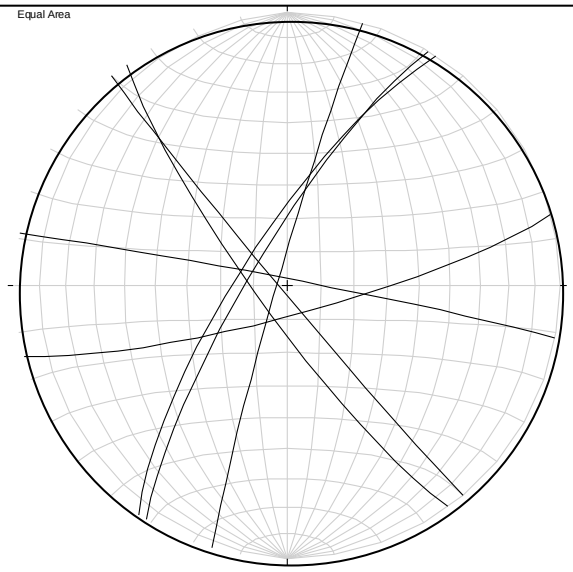

Nd=6

Veins

Veins Averaged

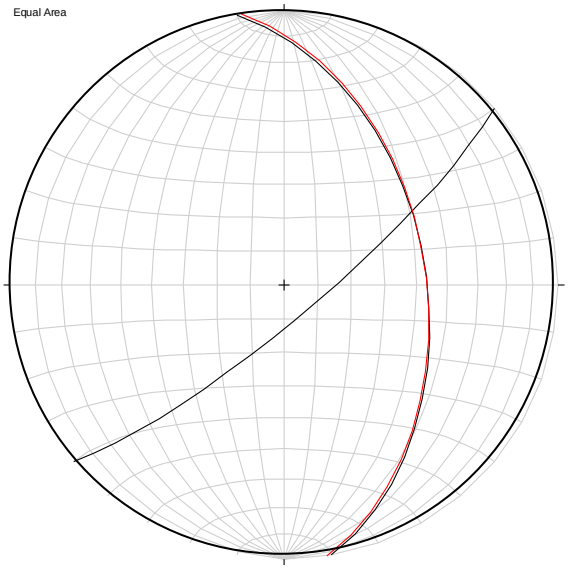

Nd=2 Np=1

Faults

Faults Averaged

Clastic Dikes

Clastic Dikes Averaged

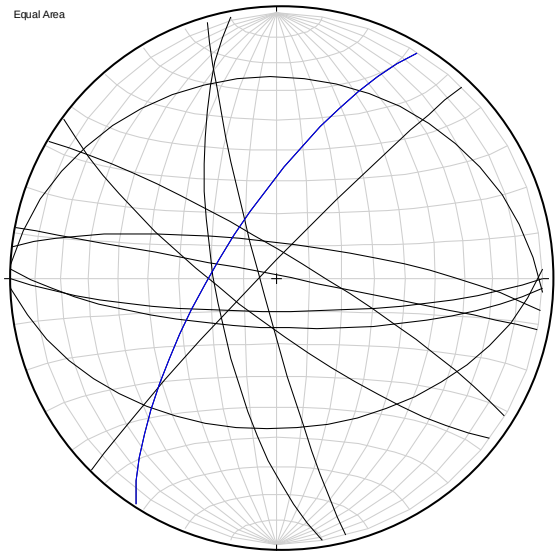

Nd=11 Np=1 Veins

Veins Averaged

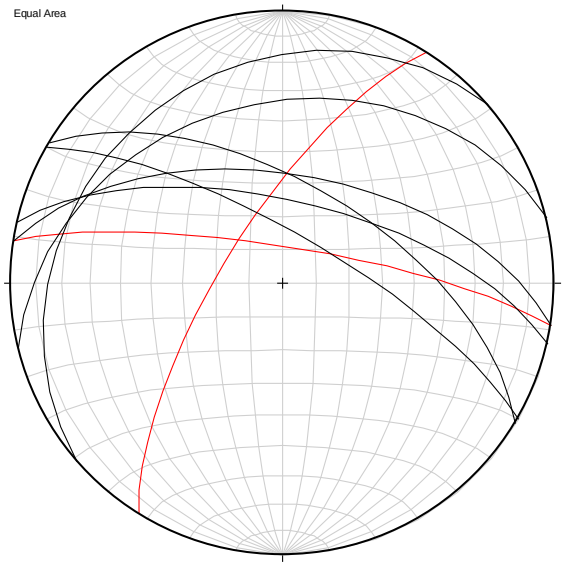

Nd=6 Np=2 Faults

Faults Averaged

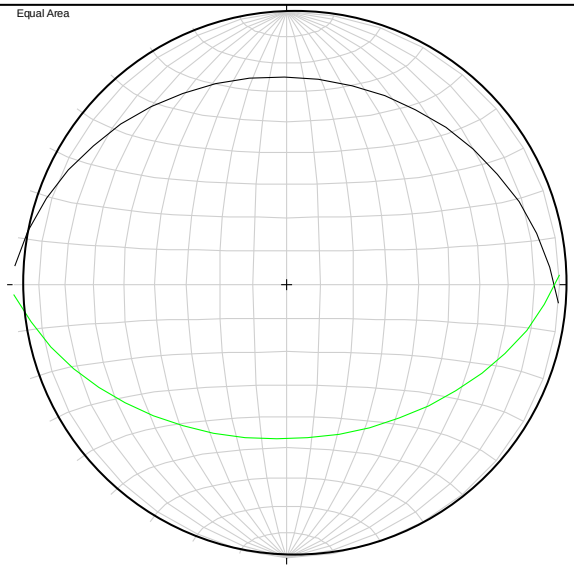

Nd=1 Np=1 Clastic Dikes

Clastic Dikes Averaged

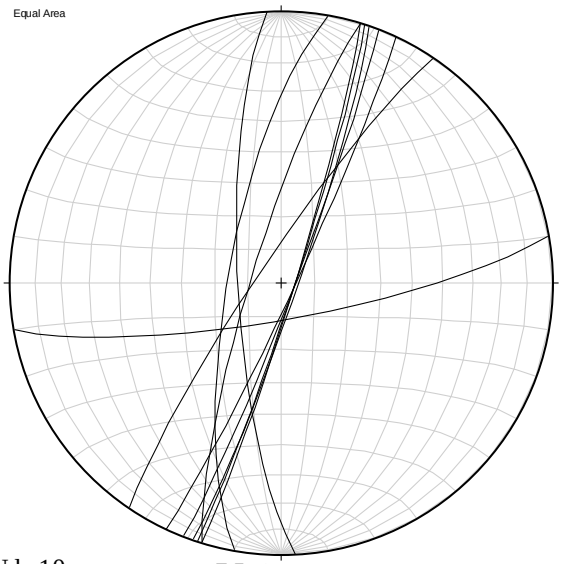

Nd=10

Veins

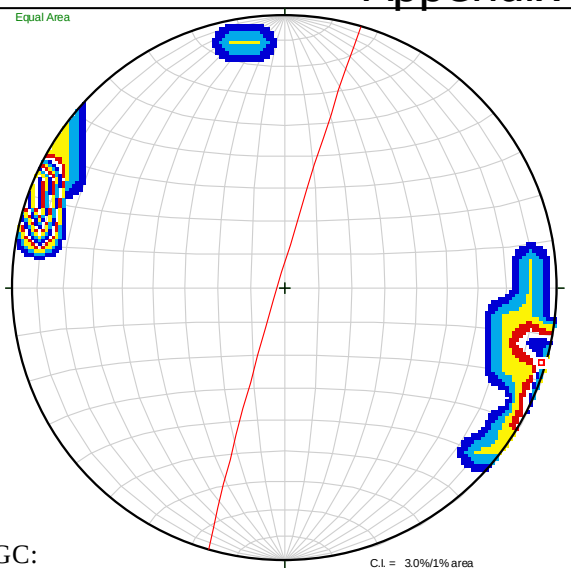

PGC:
196°, 88° W

Veins Averaged

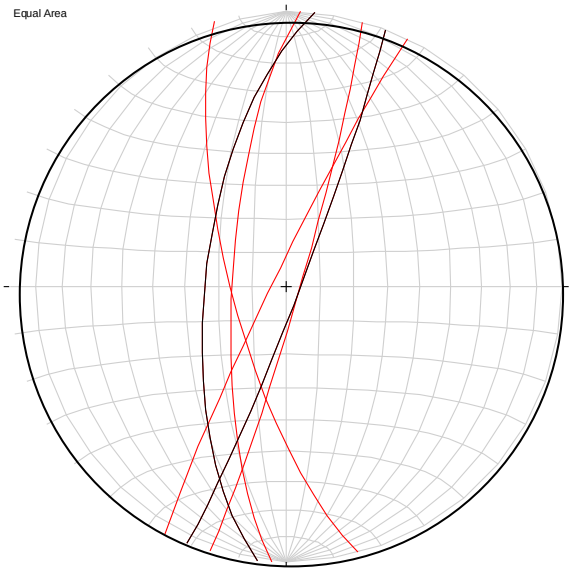

Nd=2 Np=4

Faults

Faults Averaged

Clastic Dikes

Clastic Dikes Averaged

Appendix D:
Stereoplots of bedding measured from CoreBase®. Definite bedding is labeled as Nd, whereas possible bedding is labeled as Np. All definite bedding planes are plotted in black. Possible bedding planes are plotted in fuchsia

Interval: 516.49-522.55

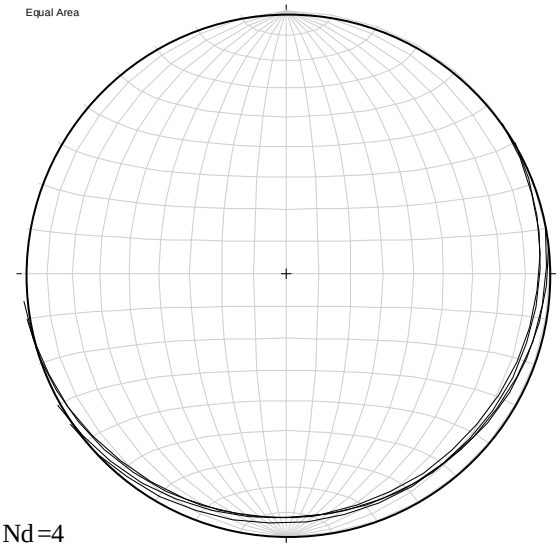

Nd =4

Bedding

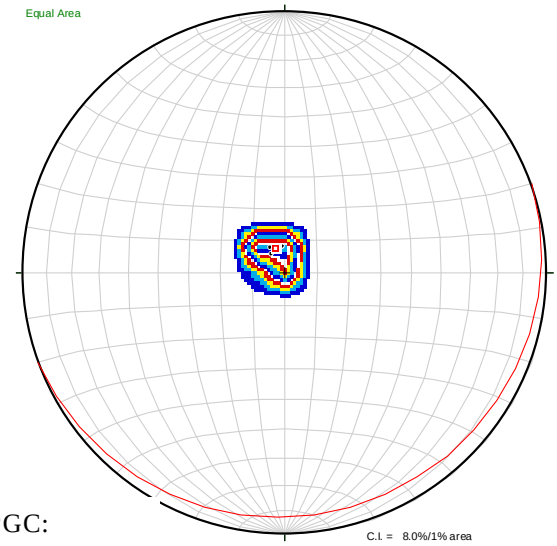

PGC:
70°, 8° S

Bedding Averaged

Interval:535.56-540.55

Oriented

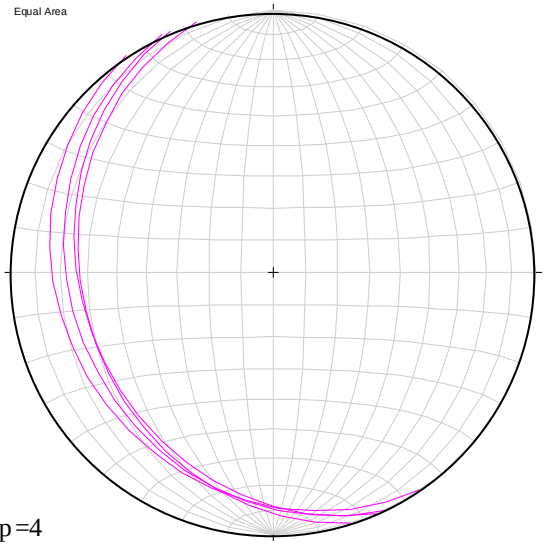

Np =4

Bedding

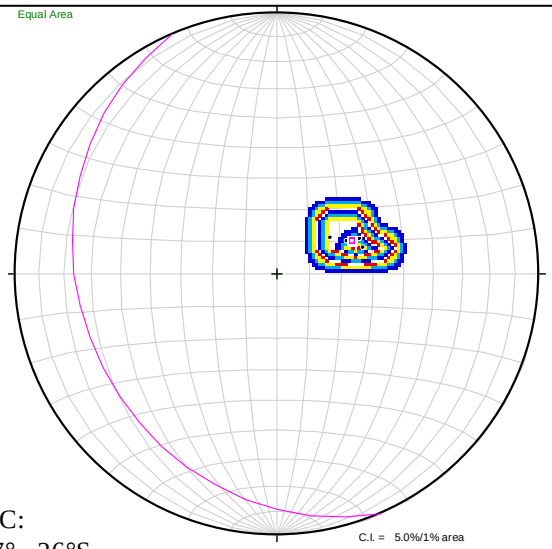

PGC:
157°, 26°S

Bedding Averaged

Interval:614.71-638.95

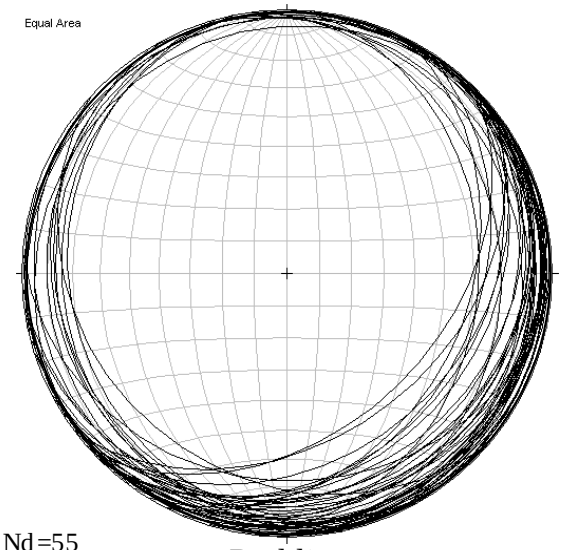

Nd =55

Bedding

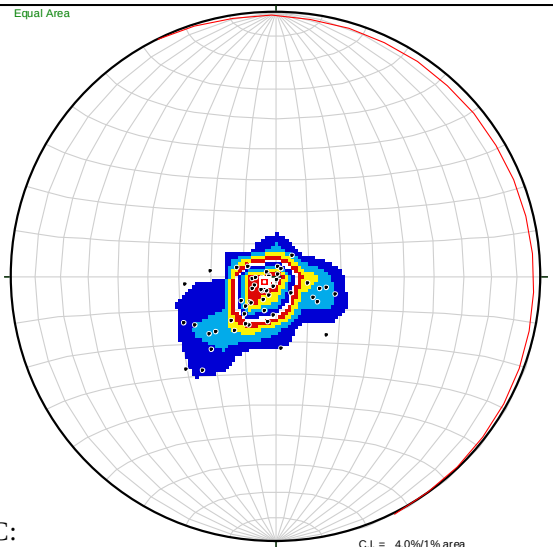

PGC:
333°, 4° E

Bedding Averaged

Interval: 644.47-650.47

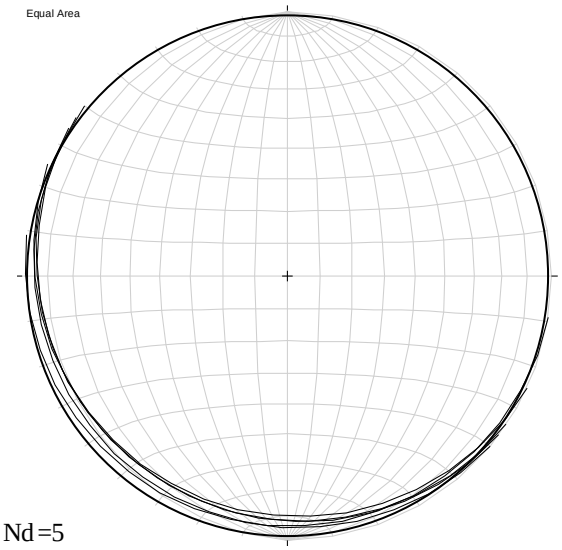

Nd=5

Bedding

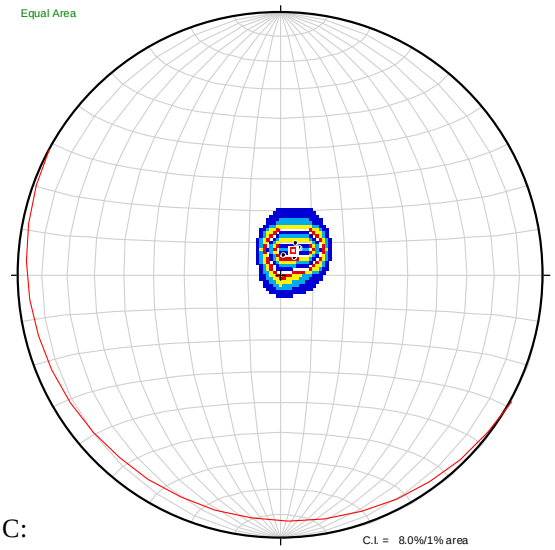

PGC:
119°, 6° S

Bedding Averaged

Oriented

Interval: 874.74-876.28

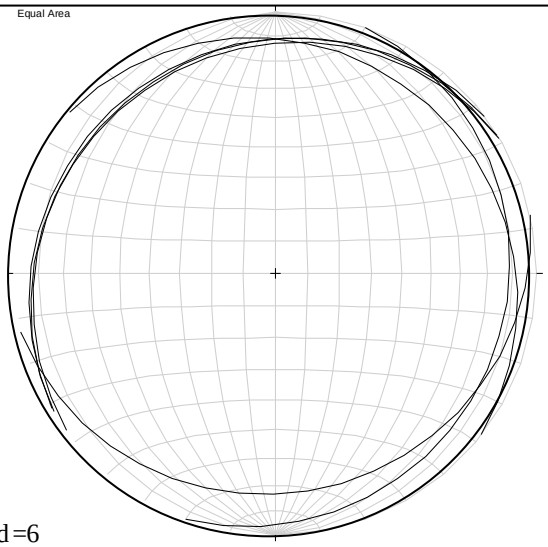

Nd=6

Bedding

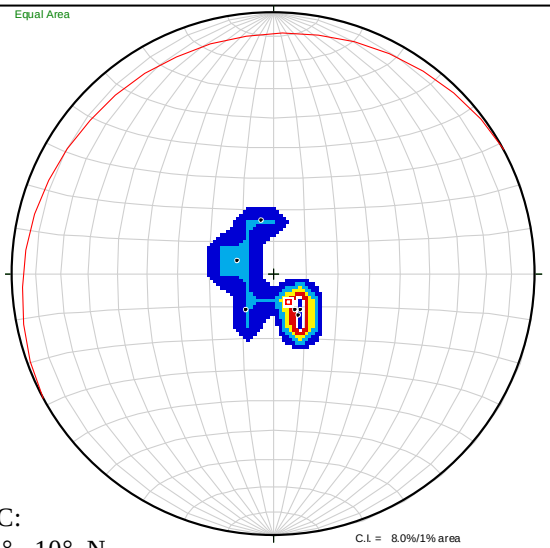

PGC:
242°, 10° N

Bedding Averaged

Oriented

Interval: 900.8-906.44

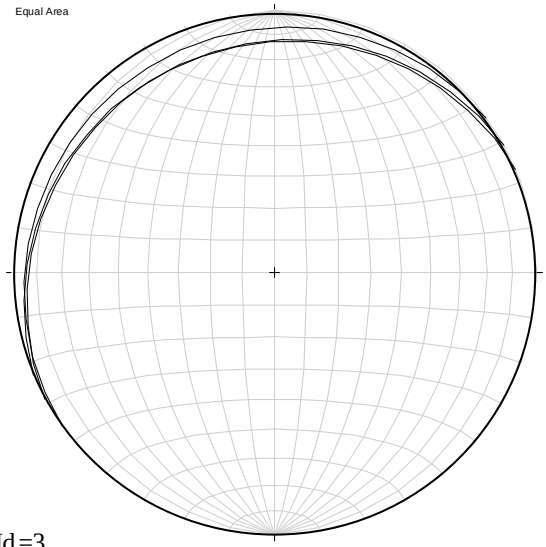

Nd=3

Bedding

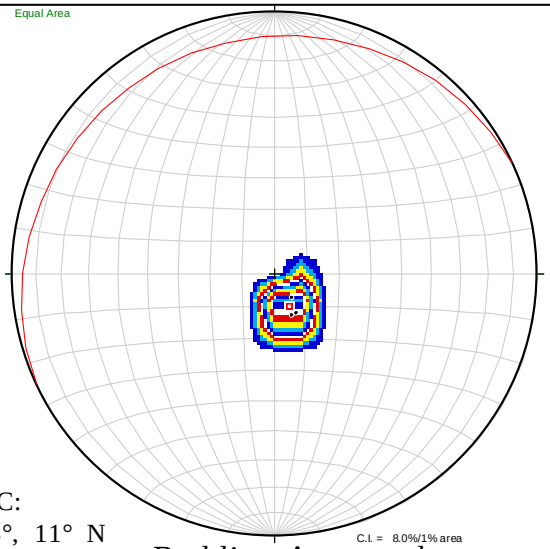

PGC:
245°, 11° N

Bedding Averaged

Interval: 1047.01-1052.15

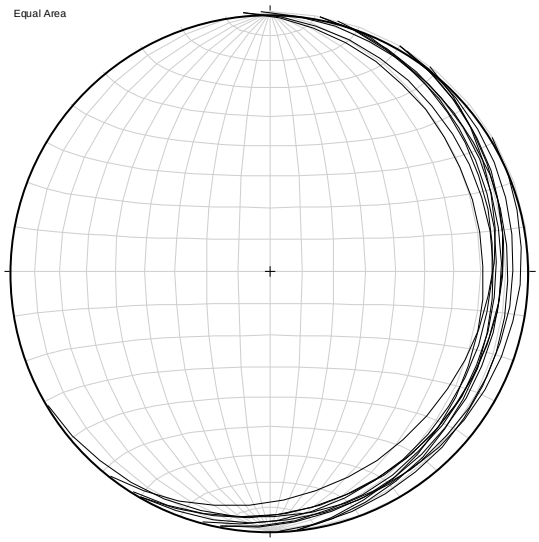

Nd=11

Bedding

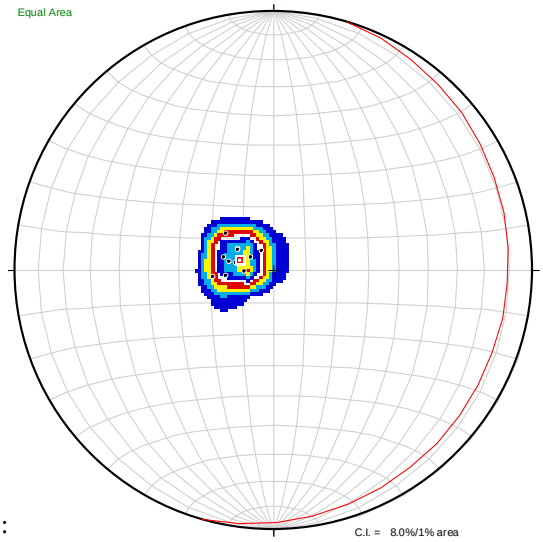

PGC:
16°, 11° E

Bedding Averaged

Oriented

Interval: 1138.33-1192.71

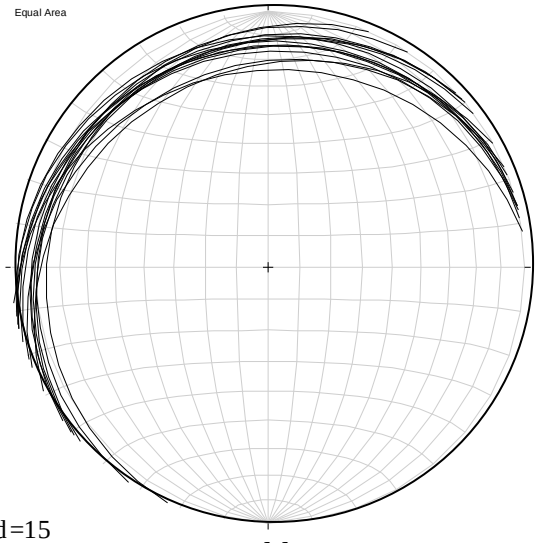

Nd=15

Bedding

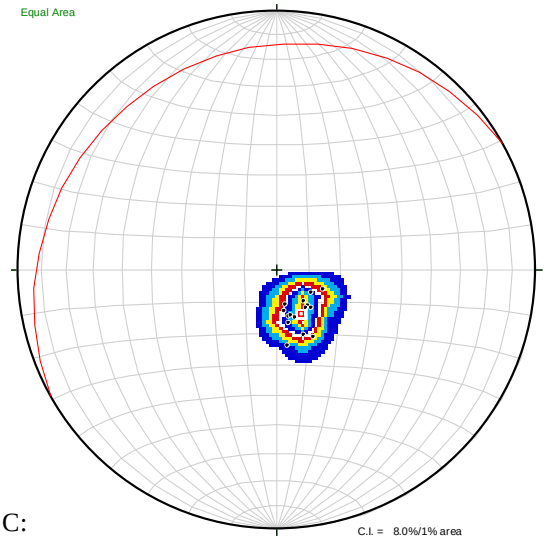

PGC:
241°, 16° N

Bedding Averaged

Interval:1203.36-1217.66

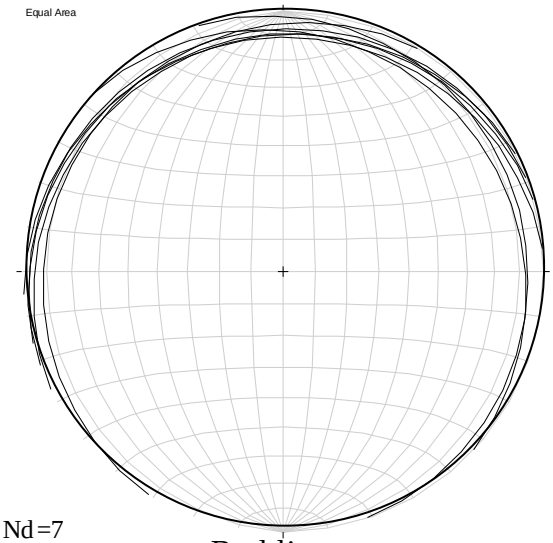

Nd=7

Bedding

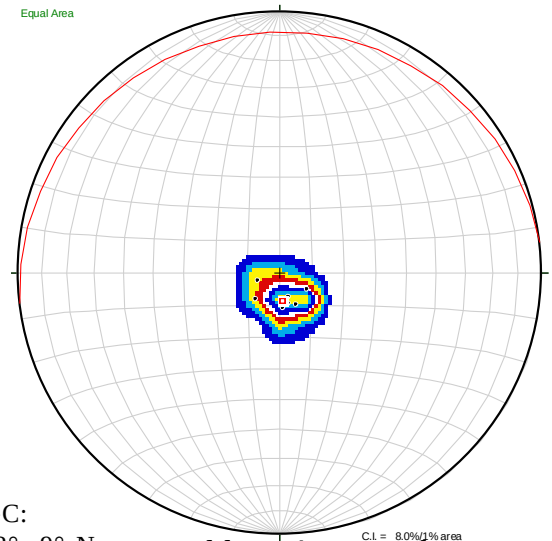

PGC:
263°, 9° N

Bedding Averaged

Interval: 1233.46-1236.83

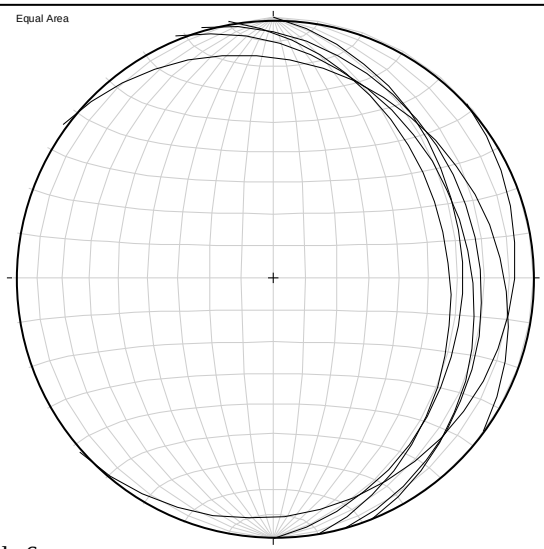

Nd=6

Bedding

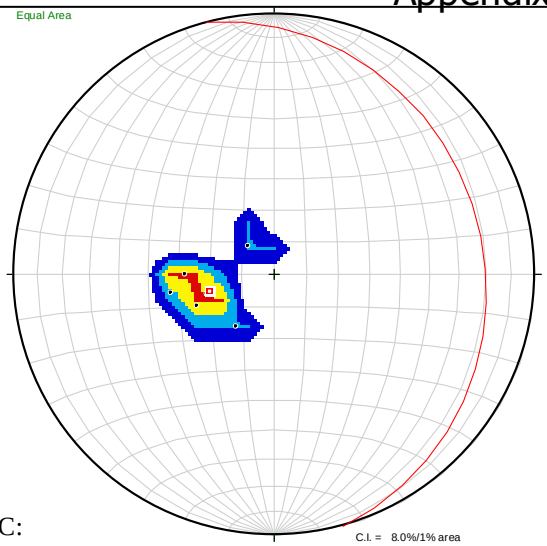

PGC:
345°, 21° E

Bedding Averaged

Interval: 1237.05-1239.34

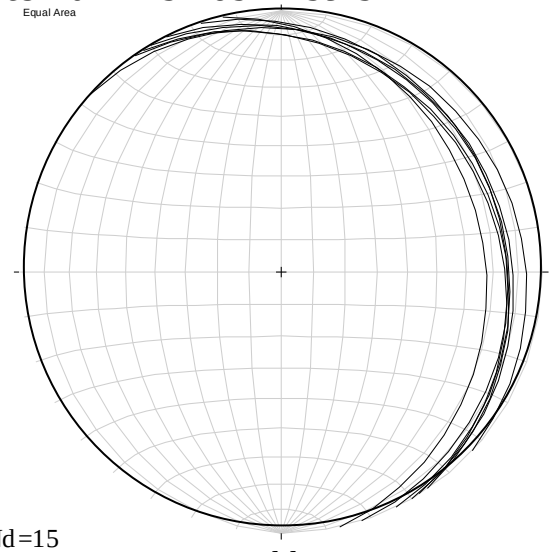

Nd=15

Bedding

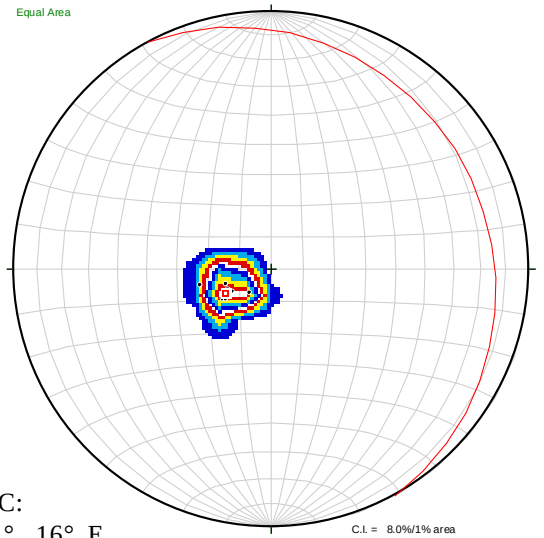

PGC:
331°, 16° E

Bedding Averaged

Interval: 1239.34-1245.24

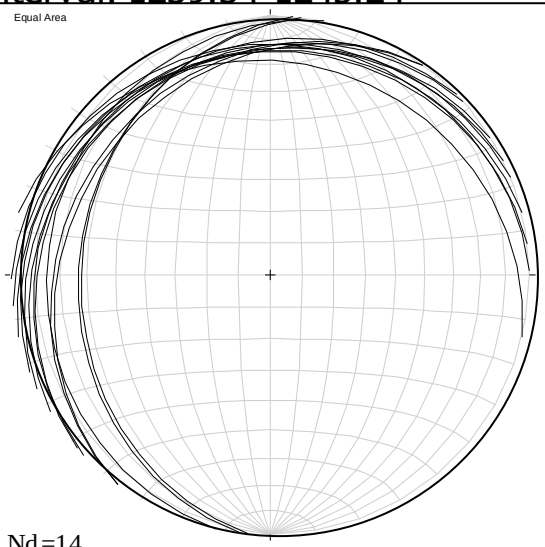

Nd=14

Bedding

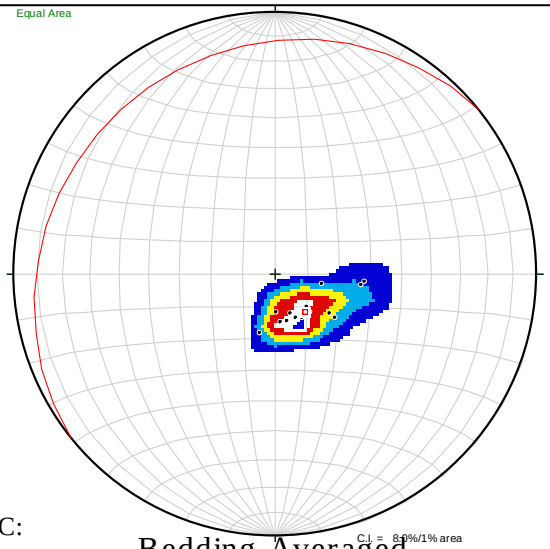

PGC:
231°, 15° N

Bedding Averaged

Interval:1255.84-1264.14

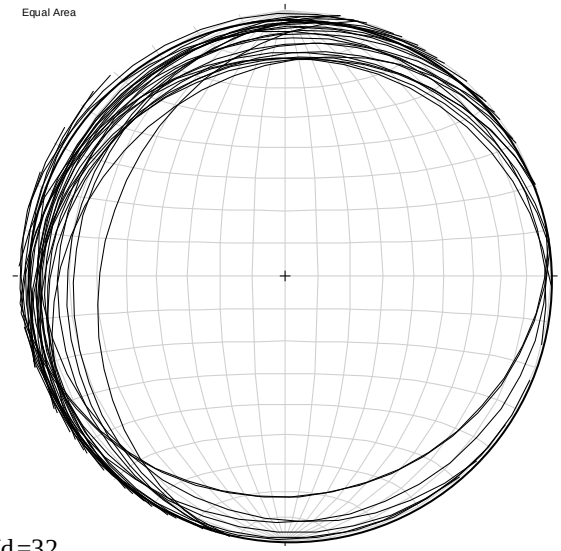

Nd=32

Bedding

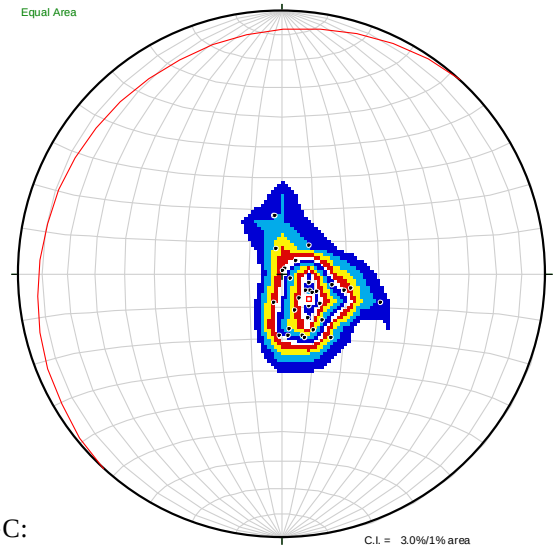

PGC:
223°, 12° W

Bedding Averaged

Interval: 1264.63-1267.25

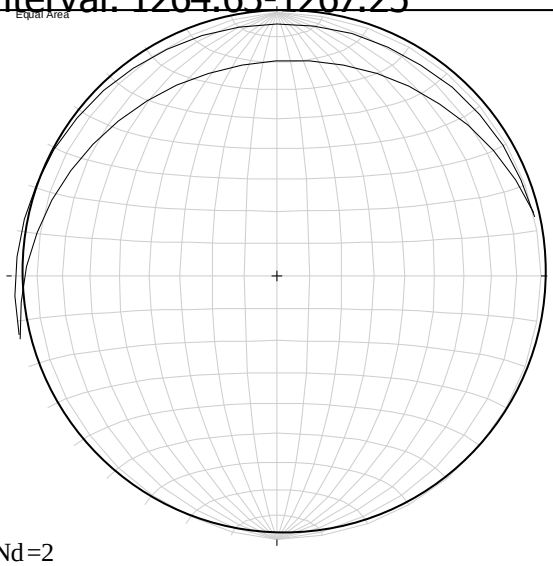

Nd=2

Bedding

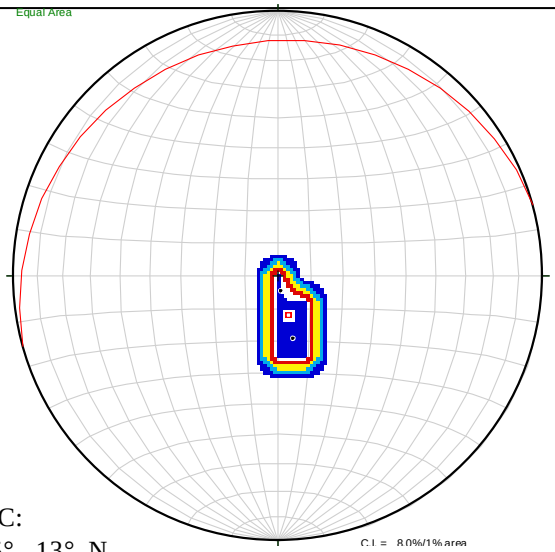

PGC:
255°, 13° N

Bedding Averaged

Interval:1267.63-1272.77

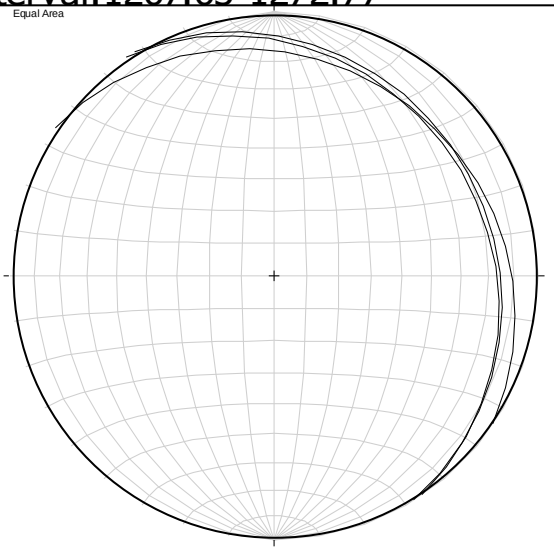

Nd=3

Bedding

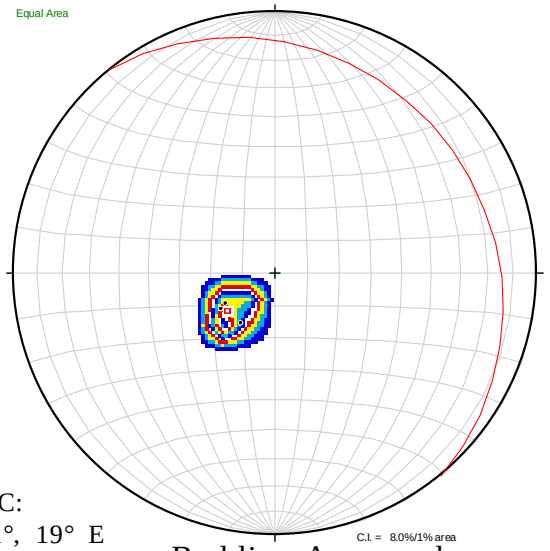

PGC:
321°, 19° E

Bedding Averaged

Interval: 1272.94-1284.87

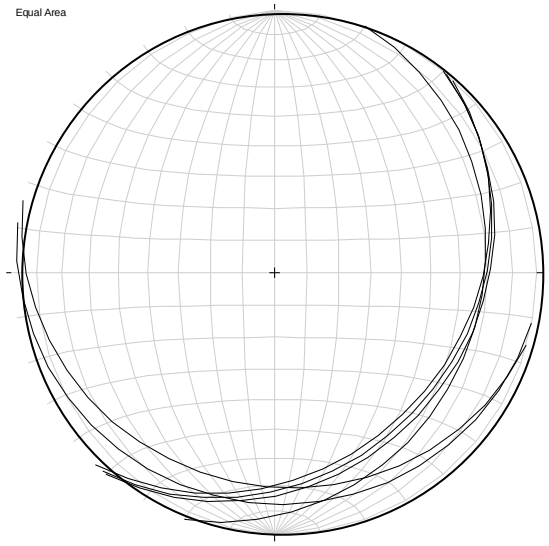

Nd=6

Bedding

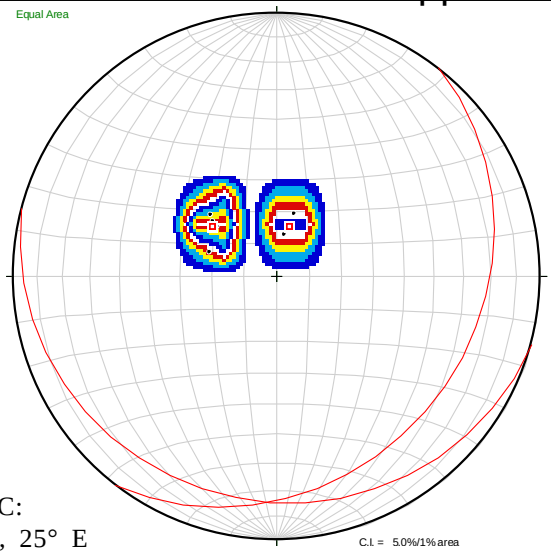

PGC:
38°, 25° E
105°, 16° S

Bedding Averaged